DESIGN AND CONTROL OF STEWART PLATFORM

by

ÖZER ULUCAY

Submitted to the Graduate School of Engineering and Natural Sciences
in partial fulfillment of
the requirements for the degree of
Master of Science

Sabancı University
June 2006

DESIGN AND CONTROL OF STEWART PLATFORM

APPROVED BY:

Assoc. Prof. Dr. Mahmut AKŞİT
    (Thesis Advisor)
....

Prof. Dr. Asif ŞABANOVİÇ
    (Thesis Co-Advisor)
....
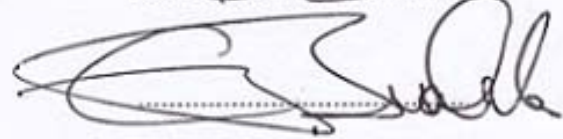
Assist. Prof. Dr. Kemalettin ERBATUR
....

Assist. Prof. Dr. Güllü Kızıltaş ŞENDUR
....

Assoc. Prof. Dr. Erhan BUDAK

DATE OF APPROVAL: 27.06.2006

To my family for their everlasting motivation and support…

ACKNOWLEDGMENTS

DESIGN AND CONTROL OF STEWART PLATFORM

Özer ULUCAY

EECS, MS Thesis, 2006

Thesis Advisor: Assoc. Prof. Dr. Mahmut F. Akşit

Keywords: Parallel Manipulators, Stewart Platform, Micro/Nano Positioning
Sliding Mode Control, Flexure Joints

Abstract

Demand on high precision motion has been increasing in recent years. Since performance of today's many mechanical systems requires high stiffness and accurate positioning capability, parallel manipulators gained popularity. Their superior architecture provides better load capacity and positioning accuracy over the serial ones. In this work, a popular parallel manipulator, Stewart Platform, has been studied. Stewart Platform is a positioning system that consists of a top plate (moving platform), a bottom plate (fixed base), and six extensible legs connecting the top plate to the bottom plate. This work includes design, analysis, control and testing of a complete positioning system. In order to achieve better accuracy over commonly used universal joints, magnets and spherical joints have been employed in the architecture. Flexure joints have been also analyzed to achieve higher precision levels. Because they eliminate friction and backlash, flexure joints would give better results than universal and spherical joints. Therefore, a parametric study for optimum hyperbolic flexure joints has been also presented. Desired performance of the proposed platform is six degrees of freedom with 500 nm minimum incremental motion. System uncertainties and inherent nonlinearities have been eliminated using sliding mode control. This type of control methodology allows stability in the presence of parametric uncertainties and external disturbances. Although analyses indicate system capability of less than 1 nm resolution, real performance is typically lower due to manufacturing imperfections and measurements errors. The proposed model has been analyzed and tested through simulations, and verified via experiments on a designed and constructed sample Stewart Platform. Laser measurements have been used to measure positional accuracy. System has demonstrated positional accuracy better than the desired 500 nm target performance value.

STEWART PLATFORM TASARIM VE KONTROLÜ

Özer ULUCAY

EMBB, Yüksek Lisans Tezi, 2006

Tez Danışmanı: Doçent Dr. Mahmut F. Akşit

Anahtar kelimeler: Paralel Manipülatörler, Stewart Platform, Mikro/Nano Konumlama
Kayan Kipli Kontrol, Esneme Mafsalları

Özet

Son yıllarda yüksek hassasiyetli hareketli sistemlere olan talep hızla artmaktadır. Bugünkü birçok mekanik sistemin performansı yüksek katılık ve hassas konumlama yeterliği gerektirdiğinden paralel manipülatörler popülerlik kazanmıştır. Paralel manipülatörler seri manipülatörlere göre daha sağlam ve hassas konumlama kabiliyetine sahiptir. Bu çalışmada popüler paralel manipülatörlerden biri olan Stewart Platform ele alınmaktadır. Stewart Platform üst plaka (hareket eden platform), alt plaka (sabit taban) ve üst plakayı temele bağlayan ve uzayıp kısalabilen altı bacaktan oluşan bir konumlama sistemidir. Bu çalışmada bütün bir sistemin tasarımı ve analizi yapılmış, kontrol yöntemi geliştirilmiş ve sistem kurulup test edilerek doğrulanmıştır. Daha hassas bir performans elde etmek için yaygın olan kardan mafsalı yerine tasarlanan platformun yapısında mıknatıs ve küresel mafsallar kullanılmıştır. Daha yüksek performans sağlamak için ayrıca esneme mafsalları da çalışılmıştır. Sürtünme, geri tepme ve mafsal boşlukları olmadığından esneme mafsalları kardan ve küresel mafsallardan daha iyi sonuçlar vermektedir. Bu nedenle en uygun hiperbolik esneme mafsalı parametrelerinin bulunması için parametrik bir çalışma da sunulmuştur. Bu çalışmada minimum 500 nm çözünürlüklü hareket sağlayan ve altı serbestlik derecesine sahip bir Stewart Platform kurulması hedeflenmiştir. Sistem belirsizlikleri, doğrusal olmayan davranışlar, parametrik belirsizlikler ve dış etkenlerin olduğu durumlarda kararlılık sağlayabilen kayan kipli kontrol kullanılarak ortadan kaldırılmıştır. Yapılan analiz sonuçları 1 nm'den daha iyi bir hassasiyetin mümkün olduğunu gösterse de, genellikle üretim problemleri ve ölçüm hataları nedeniyle gerçek sistemlerde performansın daha düşük olacağı açıktır. Önerilen model, simülasyonlar ve tasarlanan Stewart Platform üzerinde yapılan deneyler ile doğrulanmıştır. Konumlama hassasiyetinin ölçümü için lazer sistemi kullanılmıştır. Yapılan doğrulama deneyleri sonunda tasarlanan sistemin hedeflenen 500 nm'den daha iyi bir hassasiyet değerini başardığı gösterilmiştir.

TABLE OF CONTENTS

LIST OF TABLES

LIST OF FIGURES

LIST OF SYMBOLS

Inverse Kinematics

$\left(x_w, y_w, z_w\right)$	World (base) coordinate frame
$\left(u_p, v_p, w_p\right)$	Platform coordinate frame
$\vec{A}_i$	Base position vector
$\vec{B}_i$	Platform position vector
$^L\mathrm{R}_U$	Rotation matrix that describes the moving platform to the fixed base
$\vec{p}$	Position of centre of moving platform in world coordinate frame
d_i	Leg lengths

Forward Kinematics (Newton-Raphson Method)

b	Base points in the lower plate
p	Platform points in the upper plate
R_b	Base radius
R_p	Platform radius
$offset\_base$	Base connection offset angles
$offset\_platform$	Platform connection offset angles
$base\_angles$	Base connection points' angles without offset
$platform\_angles$	Platform connection points' angles without offset
$Lambda_b$	Base connection points' angles
$Lambda_p$	Platform connection points' angles
ψ	Angle in x axis (yaw)
θ	Angle in y axis (pitch)
ϕ	Angle in z axis (roll)
Leg_actual	Actual leg lengths' vectors calculated from inverse kinematics

leg_estimated	Estimated leg lengths' vectors
Hactual	Actual transformation matrix
Hestimated	Estimated transformation matrix
xyzeuler	Translation and rotation parameters
est_leglength	Leg lengths obtained from estimated transformation matrix
estleglength	Norms of the estimated leg lengths
H	General transformation matrix
dq	dH / d xyzeuler
dR	Homogeneous matrix (H) derivative with respect to xyzeuler
tolerance	Permissible error value
transEuler_H	Function that converts translation/rotation to a transformation matrix
Hderiv	Function is used which returns derivative of a transformation matrix with respect to translation and roll-pitch-yaw angles
G	$d\mathrm{X} / dxyzeuler$

Forward Kinematics (Constructive Predictor-Corrector Algorithm)

B_i	Base points
P_i	Platform points
$\underset{\sim}{b_i}$	Position vectors of base points in base frame
$\underset{\sim}{p_i}$	Position vectors of platform points in platform frame
$\underset{\sim}{p_i}'$	Position vectors of platform points in base frame
$\underset{\sim}{S_i}$	Leg vectors
S_i	Leg lengths
$\underset{\sim}{d_i}$	Unit vectors along the legs
d_{1x}, d_{1y}, d_{1z}	Direction cosines of the leg vectors
$\Im, \Im'$	Triads for defining rotations to find platform points
θ_1	Angle of rotation about first triad z axis
θ_2	Angle of rotation about second triad z axis

Dynamic Analysis

b_i	Position vector of the i_{th} base point with respect to the reference frame
f_i	Driving force generated by the i_{th} actuator
$(f_p)_i$	Constraint force at the joint at the top of the i_{th} leg
g	Acceleration due to gravity
I	Unit matrix with appropriate dimensions
$(I_t)_i$	Inertia with respect to the center of gravity of the upper moving part of the i_{th} actuator
$(I_b)_i$	Length between the lower gimbals point and the center of gravity of the lower rotating part of the i_{th} actuator
l_i	i_{th} leg length vector with respect to the reference frame
l_i	Length of the i_{th} leg
$(l_t)_i$	Length between the upper gimbals point and the center of gravity of the upper moving part of the i_{th} actuator
$(m_b)_i$	Mass of the lower rotating part of the i_{th} actuator
m_p	Mass of platform including the payload
$(m_t)_i$	Mass of the upper moving part of the i_{th} actuator
n	Unit vector along the leg
p_i	Position vector of the i_{th} upper gimbal point with respect to the platform frame
$(q_p)_i$	Position vector of the i_{th} upper gimbal point with respect to reference frame
$(\dot{q}_p)_i$	Velocity vector of the i_{th} upper gimbal point with respect to reference frame
$(\ddot{q}_p)_i$	Acceleration vector of the i_{th} upper gimbal point with respect to reference frame
Q	Generalized forces projected along the variation of the coordinates q_p
$(Q_f)_i$	Generalized force due to the driving force generated by the i_{th} actuator
$(Q_{m_b g})_i$	Generalized force due to the gravitational force $(mbg)_i$
$(Q_{m_t g})_i$	Generalized force due to the gravitational force $(mtg)_i$
R	Rotation matrix that maps a vector in platform frame into reference frame

t	Translation vector of the origin of platform frame in the reference frame
T	Kinetic energy
$(v_b)_i$	Velocity of the rotating part center of gravity of the i_{th} actuator
$(v_t)_i$	Velocity of the moving part center of gravity of the i_{th} actuator
$\delta(.)$	Virtual displacement of (.)
w	Angular velocity vector of the moving platform with respect to the reference frame
$(w_1)_i$	Angular velocity of the i_{th} leg

Flexure Joint Analysis and Optimization

a	The point where hyperbola intersects x axis
e	Eccentricity
c	Foci of the hyperbola
b	Semi minor axis
A	Length of the flexure
t	Thickness of the flexure

Sliding Mode Control

$\sigma(x)$	Vector of sliding functions
S	Sliding surface
$V(\sigma)$	Lyapunov function
D	Positive definite matrix
u_{eq}	Equivalent control
$\hat{u}_{eq}$	Estimate of equivalent control
K	Positive diagonal matrix
T_s	Sampling time

ABBREVIATIONS

SP   Stewart Platform

SPS   Spherical-Prismatic-Spherical

DOF   Degree of Freedom

PID   Proportional-Integral-Derivative

FEA   Finite Element Analysis

VSC   Variable Structure Control

SMC   Sliding Mode Control

CAD   Computer Aided Design

GA   Genetic Algorithm

1   INTRODUCTION

Stewart Platform is one of the most popular parallel manipulators. It is a six degrees-of-freedom positioning system that consists of a top plate, a bottom plate, and six extensible legs connecting the top plate to the bottom plate. A general Stewart Platform is shown in Figure 1.1.
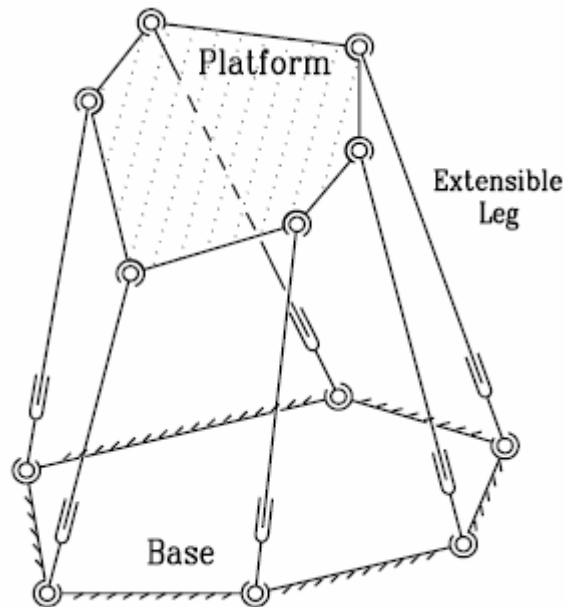
Figure 1.1. General Stewart Platform

The Stewart Platform was originally proposed and presented to academia in 1965 as a flight simulator by Stewart [1]. This structure consisted of three linear actuators in parallel. Gough [2] had earlier suggested a structure similar to Stewart's model as a tire-testing machine. In his system there are six actuators in parallel resulting in a fully parallel actuated mechanism as shown in Figure 1.3. Gough was the first one realizing benefits of this kind of a manipulating structure; however, research on this subject began with Stewart's paper. Therefore, it is a tradition to call the structure as Stewart Platform, or sometimes it is also referred as Stewart-Gough Platform [3].
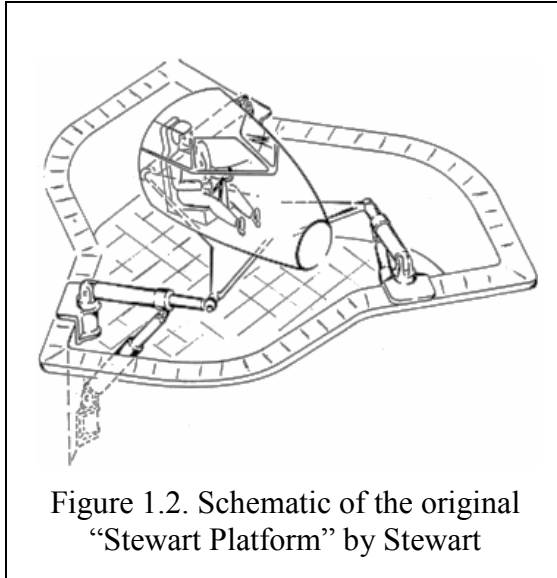
Figure 1.2. Schematic of the original "Stewart Platform" by Stewart	Figure 1.3. The first octahedral hexapod or the original Gough platform
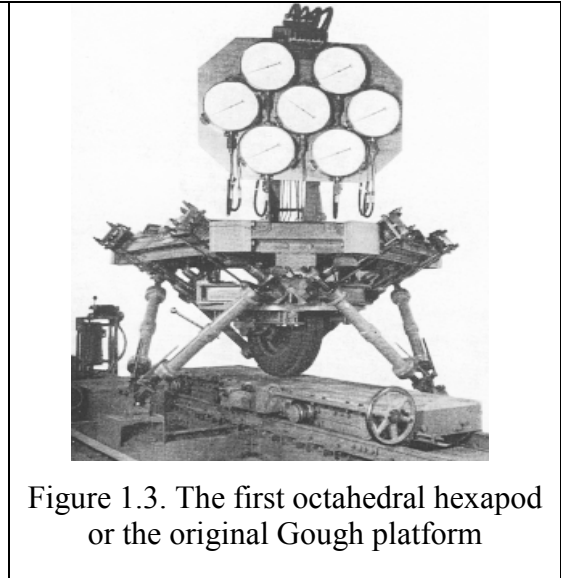
From the time it was proposed, there had been no interest to this mechanism for about 15 years until Hunt stated the advantages of using parallel manipulators. After 1983 researchers acknowledged its high load capacity and precise positioning capabilities, and started to make detailed analysis of the structure. Today's popular parallel manipulator known as Stewart Platform reached its generalized form which consists of six linear actuators that are connected to the base with spherical or universal joints and to the moving platform with spherical joints [4]. From 1980's onward, Stewart Platform, gained popularity mainly because of the advantages offered by parallel manipulators over the serial ones [3].
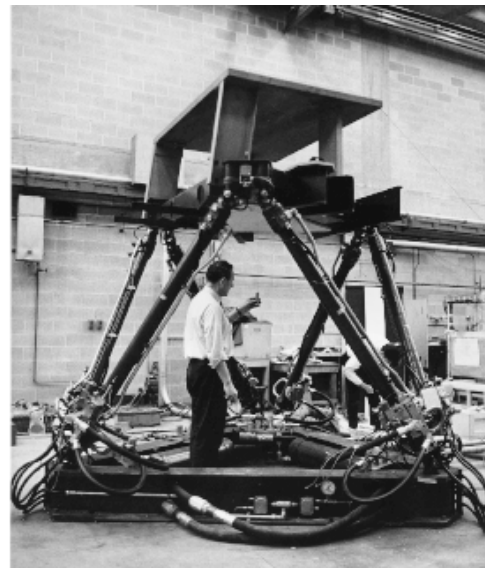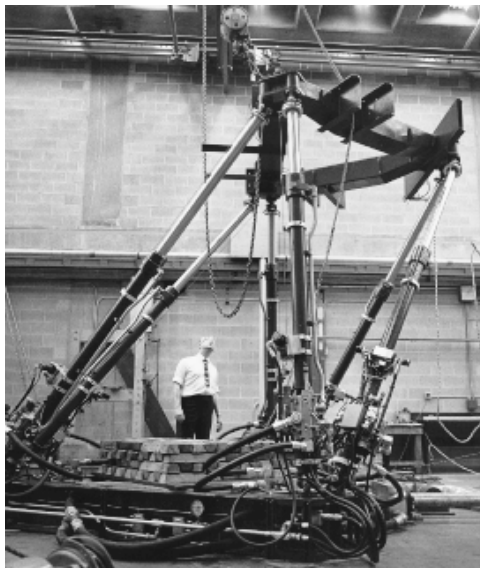
Figure 1.4. The first flight simulator based on an octahedral hexapod in mid 1960s
(courtesy of Klaus Cappel)

Parallel manipulators have been used since 1980's when high load carrying and precise positioning capability is needed. Since the time it was proposed, it has been used as a flight simulator. Besides, a wide variety of applications have benefited from this design. A few of the industries using Stewart Platform design include aerospace and defense, automotive, transportation, machine tool technology, and recently the platform is used in medical applications for its precise positioning capability.

1.1   Objective

The Stewart Platform is a widely accepted design as a motion control device. This is largely because of the system's high load capacity and accurate positioning capability. Stewart Platform provides a large amount of rigidity that enables the system to provide a significant source of positional certainty.

This work aims to develop a Stewart Platform mechanism with the following capabilities:

- Six degrees of freedom

- Working in any orientation

- No moving cables, ease of setup and reduced friction

- Load capacity of 200 gr.

- Repeatability of ±0.5 μm

- Significantly smaller and stiffer package

1.2   Parallel versus Serial Manipulators

With developments in mechanical design and robotics area, researchers first tend to build structures that can perform human tasks. Serial manipulators, open loop serial chains, originated from this idea. Serial manipulators have advantages such as large workspace and high maneuverability as human arm. However, they suffer from similar

disadvantages as the human arm as well. Human arm can not carry high loads since it has a cantilever structure. It does not provide precise motion as a result of its large workspace, bends under heavy load and vibrates at high speeds. Therefore, for high load and precise motion tasks one had to look for another solution. Parallel manipulators, which can also be observed in the nature, provide this solution. Load carrying animals with multiple legs are more stable compared to human bi-ped structure. Since end-effector is connected to the ground with multiple actuators in parallel, these structures provide high rigidity, and used for high load carrying and precise positioning tasks [3].

Parallel manipulators may have serial manipulators in their parallel chains. Stewart Platform has given a central status among parallel manipulators because it clearly shows the duality with the serial manipulators. Having 6 DOF with simple serial chains in parallel makes generalized Stewart Platform a popular parallel manipulator.

1.3   Kinematics

For serial manipulators typically direct kinematics problem is straightforward, but inverse kinematics is challenging. On the contrary, for parallel manipulators reverse is true. For the inverse kinematics problem, the position vector and the rotation matrix are given, and the link lengths are to be solved. Since position of the connection points, orientation and position of the moving platform are known; it is easy to find link lengths of the platform. On the other hand, for the direct kinematics problem, the link lengths are given, and the position vector and the rotation matrix of the moving platform are to be determined. Direct kinematics of Stewart Platform is a challenging problem since it requires solution of a series of non-linear equations. There are at least 8 real solutions. In this thesis both direct and inverse kinematics solutions are presented.

1.4   Design Issues

1.4.1   Considerations for the Design

Parallel manipulators have some advantages and disadvantages over serial manipulators. Parallel manipulators have high stiffness, and load capacity because load is supported by all the legs. Because the load is only in axial direction there is no bending stress in the legs. Because positioning error of the platform does not exceed average of the position errors for the legs, positioning accuracy is high. Besides, they are easily scalable. Platform can be used as a flight simulator or as a positioning device that performs motion in the scale of nanometers. Nevertheless, they have smaller workspace, and there are singular positions in their workspace. For the design of the Stewart Platform, one has to consider drawbacks of the structure. Short link lengths provide stiffness and small positioning error, but large workspace requires long links. Platform has to have large base to provide stability; however, in order to avoid singularities due to rotation about a horizontal axis, the platform must have small base. Having these design matters in mind, a small size platform is designed and constructed.

1.4.2   Flexure Analysis and Optimization

The flexure joints are frequently used in micro-motion mechanisms because of their significant advantages. The monolithic characteristics of the flexure joints help avoid manufacturing errors. These characteristics result in an easy manufacturing process, and yield a very compact design. Besides, the flexure joints have less friction loss, and do not require lubrication. Because of these advantages, this work includes a parametric study of flexure joints for optimum design parameters for the Stewart Platform in consideration. Analyses also verified that flexure joints can provide better accuracy. Construction and testing of a Stewart Platform with flexure joints are suggested as a future work to this thesis.

1.5   Dynamic Analysis

A dynamic model can be used for any system without the need of the real system to test various specified tasks. For the development of control strategies, it is possible to achieve higher performance by incorporating more structural system information. Accounting for the parallel configuration of the Stewart Platform, and the advantages of both Newton–Euler method and Lagrange formulation, an explicit compact closed-form dynamic equation set for the Stewart Platform can be derived. This work presents detailed dynamic analyses of Stewart Platform as well as an ADAMS simulation to illustrate the forces acting on the system.

1.6   Simulation

MATLAB visualization environment and SimMechanics are used to simulate the designed platform. SimMechanics is a powerful commercially available tool used for modeling and simulation of mechanical systems. This model is integrated with MathWorks control design and code generation products [5]. The code for the simulation of the Stewart Platform creates the geometry and dynamic information for the platform in the home configuration. The platform consists of a top plate, a bottom plate, and six extendable legs/links. These links are composed of two bodies with two spherical joints and a prismatic joint connecting the two parts [6].

The entire model consists of link trajectory, controller and plant subsystems. Trajectories can be given with a Magellan Space Mouse or with MATLAB source blocks. Link trajectory subsystem computes link lengths of the platform for a given trajectory reference. The output of the controller is fed through joint actuators as forces for each link. Positions and velocities are sensed by joint sensors. Connections and mates are defined with joints in SimMechanics. Top plate, base, links and their dynamics are modeled in SimMechanics using a CAD translator which exports CAD assemblies from SolidWorks design package.

1.7   Control

System uncertainties and inherent nonlinearities like uncertainty in friction parameters due to time-varying friction characteristics, operating condition changes, load changes, etc., make control a challenging problem. It is highly desired that with nominal control settings, control specifications can be achieved. Therefore, it is necessary to find a methodology that produces a robust controller which can be designed by considering only nominal process parameters. This can be achieved with variable structure control (VSC), which is frequently known as sliding mode control (SMC). This work includes a detailed discussion on controller design for the Stewart Platform using sliding mode control.

2 LITERATURE SURVEY

2.1 Forward Kinematics

The most challenging problem concerning the Stewart problem has been the forward kinematics analysis since late 1980's. The problem is to determine the assembly configurations when base points, platform geometry and link lengths are given. In other words, it is the problem of solving the following kinematics relation

$$\| t + R * p_i - b_i \|^2 = L_i^2 \quad \forall \ i \ = \ 1 \ to \ 6 \tag{2.1}$$

where b_i denotes the i_{th} base point, p_i the i_{th} platform point, R the rotation, $\bar{t}$ the translation matrices for the given link lengths, L_i. Analytical solution for the general case is quite difficult due to highly nonlinear equations with multiple solutions. Therefore, researchers constructed Stewart Platforms with special geometries to simplify the problem.

2.1.1 Analytical Solutions for Special Cases

Merging of base connection points and/or platform connection points can lead to more simplified kinematics equations for a forward kinematics analysis. The platforms with special geometries are characterized by their m base points and n platform points. A 6-6 Stewart Platform is the general case, and 3-3 one is the simplest case.

Although 3-3 is the simplest case, the approach which is based on solution of the input-output relations for the spherical joints makes the problem more difficult [7-9]. Another approach uses the idea that if the joint centers of the pairs of the adjacent limbs are coincident, the hexagonal structure of the platform will be reduced to a triangle and the platform can be put into a form which is isomorphic with those of triple arm

mechanism [10-16]. A third approach converts the platform to an equivalent serial mechanism, and the constraints on the joint angles are utilized to derive the remaining equations for the forward kinematics [17-20]. These approaches on specialized platforms enabled closed form solutions for the simple 3-3 case and for more complicated 5-5 and 6-4 cases. Beside the coincident connection points, some researchers [21-23] proposed the use of angular constraints between six pairs of points, lines, and/or planes in the base and the moving platform to obtain the solution of the problem in closed form.

Apart from the above-mentioned approaches, a decomposition scheme was proposed by Nair and Maddocks [24] for the forward kinematics problem. A linear dependent part and a nonlinear independent part were suggested. Faugere and Lazard [25] classified all the m-n cases according to the combinations of connection points, and found out the existence of 35 different classes.

2.1.2 Numerical Schemes

As discussed above, a closed form solution of the problem is very difficult due to highly nonlinear equations with multiple solutions. It is more advantageous to use computational techniques for practical cases which need only a solution and if a good initial estimate is available from a neighbor position [26-27]. Numerical approaches use some algebraic and geometric elimination methods to simplify the kinematics equations to obtain all the real solutions [28-30]. In order to find all the real roots, Innocenti and Parenti-Castelli [31] used the analytical result of the 5-5 case by a unidimensional search over the value of the removed fictitious leg length to obtain a numerical solution for the 5-5 case. Dasgupta and Mruthyunjaya suggested an efficient 3 dimensional search and verification algorithm based on pure geometric constraints [32].

Although numerical methods have computational advantages and can be utilized to find the real solutions, they are not useful to predict total number of the roots in the complex domain. Raghavan [33] was able to find all distinct solutions in a complex domain by tracking 960 paths which suggest the upper bound for the number of configurations for the Stewart Platform to be 40.

2.1.3 Analytical Methods for General 6-6 Case

In order to reduce the total degree of the final polynomial system to 64, linearization of some equations, which include quadratic terms (that are obtained from (2.7) by using a direction cosine matrix instead of Euler angles) is utilized [34-38]. However, the results which were published by Raghavan [33] contradict the validity of this approach. Assuming the base plate as planar, the fundamental equations are reduced to 40 degree univariate polynomial which is stated by Wen and Liang [39].

Geometry based analytical methods have some drawbacks. They cannot be applied to obtain all real and complex solutions, and to determine the number of solutions available for 6-6 Stewart Platform. Despite the fact that the closed form relation based on geometrical considerations can provide some solutions, no analytical solution is constructed for the general case. Hunt and Primrose [40] give geometrical arguments to find the number of possible configurations in special cases. Possible configurations for the general case were foreseen to be 40, 48, 54 or 64. The idea suggested by Hunt and Primrose is expected to provide valuable insight for general solution of the platform. Wampler [41] and Husty [42] utilized Euler angles, and studied parameters to obtain a mapping of spatial kinematics to eight quadratic equations in eight dimensional image space. The possible positions of the platform can be represented as intersections of six constraint manifolds and the quadratic equations which ultimately lead to 40th univariate polynomial. However, this approach cannot constitute an answer to the number of solutions yet.

2.1.4 Other Approaches

The aforementioned methods are not suitable to obtain a real-time, reliable and fast forward kinematics solution. A reliable and fast approach should satisfy the question of selecting the actual one among all the obtained results, and whether the solution is fast enough for the real time applications. In order to satisfy both needs, Baron and Angeles [43-45] suggested a redundant sensing method to make the resulting procedure fast and robust to measurement noise. This method produces estimates with about the same accuracy as a nonlinear procedure. In this approach, the projection of the

motion of hip-attachment points onto their subspaces enables conversion of the underlying direct kinematics to a linear algebraic system to resolve the ambiguity. The linearization procedure, a polar least square estimate, leads to a fast computation. Implementation of neural networks by Geng and Haynes [46] constitutes yet another research effort for the forward kinematics problem.

2.2 Dynamic Analysis

Dynamic analysis and derivation of dynamic formulation are quite complicated due to the closed-loop structure and kinematics constraints of the Stewart Platform manipulators. However, development and analysis of dynamic models are the important trends in various study fields on Stewart Platform. The importance of the dynamic model can be illustrated in several different ways. A dynamic model can be used for computer simulation of a robotic system without the need of a real system to test various specified tasks. It is possible to achieve higher performance by incorporating more structural system information for the development of control strategies. Revealing all the joint reaction forces and moments through the dynamic analysis is also necessary for sizing the links, bearings, and actuators [47].

Several different methods have been studied to model the dynamics of the Stewart Platform as a multi-body system, such as Newton–Euler method, the Lagrange formulation, the principle of virtual work, and Kane's method. Dasgupta and Mruthyunjaya [48] derived the complete dynamic equations for the Stewart Platform through the pure Newton–Euler approach. Nguyen and Pooran [49] and Lebret et al. [50] developed Lagrange equations of motion, and the latter gave some insight into the structure and properties of these equations. Lee and Geng [51] studied the dynamics of a flexible Stewart Platform manipulator using Lagrange formulation assuming platform to be rigid. The dynamic formulation was established by a combination of screw theory with the principle of virtual work by Gallardo et al [52].

Principle of virtual work formulation is based on the computation of the energy of the whole system with the adoption of a generalized coordinate framework [52]. To simplify this approach, theory of screws, which is a way to express velocities and forces in three dimensional space, combining both rotational and translational parts, was used.

Wang and Gosselin [53] and Tsai [47] also used the principle of virtual work to perform the dynamic analysis of the spatial six DOF parallel manipulators with prismatic actuators.

Koekebakker et al. [54] provided the dynamic formulation of the Stewart Platform through Kane's method. As Liu et al. [55] mentioned, Kane's equation analyses the dynamics of a multibody system with N bodies using the relation

$$F + F^* = 0 \tag{2.2}$$

where F denotes the generalized active force, and F* is projection of active and inertial forces on the generalized velocities. The calculation of accelerations, partial velocities of mass centers, and partial angular velocities of all links are required to apply the method.

Nguyen's equations, Lebret's model, and Koekebakker's formulation all assume that origin of the coordinate system on the moving platform to be the centre of mass of the moving platform. Furthermore, the mass moment of inertia matrix is assumed to be diagonal. Liu et al. [55] also derived a dynamic analysis with constraint equations based on Kane's method. These constraints constitute a set of differential algebraic equations which result in many numerical computational problems [56]. Additionally, Ji [57] studied the effect of leg inertia on the dynamics of the Stewart Platform.

The application of Newton–Euler approach is straightforward. However, this approach needs computation of all constraint forces and moments at all joints. In addition, sometimes these computations are not necessary for the simulation and control of the manipulator. Lagrange formulation provides an orderly structure which can be expressed in closed form. However, derivation becomes quite tedious due to large amount of symbolic computations needed. Principle of virtual work is an efficient approach for dynamic analysis of a Stewart Platform manipulator. However, dynamic structure formulation is not explicit [58]. In general, deriving the equations of motion for a parallel manipulator results in a set of differential algebraic equations as mentioned in [55]. In simulation and control, this formulation can cause difficulties. Choosing the appropriate modeling method makes the dependent variables be explicit functions of the integrable differential equations to avoid the difficulties mentioned earlier. Accounting for the parallel configuration of the Stewart Platform, and combining the advantages of both Newton–Euler method and Lagrange formulation, the explicit compact closed-form dynamic equations of Stewart Platform can be derived in the task space [58].

2.3   Flexure Joints

In order to further improve accuracy of the system, rather than using spherical joints, interactions at joints should be improved to provide the necessary motion in nanometer accuracy. There are several ways to achieve this accuracy. One of them is to prevent the backlash and friction in the joints. Flexure hinges is the best way to prevent backlash and friction due to their characteristics. Today, flexure hinges are used in many areas such as in accelerometers, gyroscopes, translation micro-positioning stages, motion guides, piezoelectric actuators and motors, high-accuracy alignment devices for optical fibers, high- precision cameras and robotic micro-displacement mechanisms.

Mechanically assembled joints such as universal or ball joints reduce the accuracy due to manufacturing errors. The monolithic characteristics of the flexure joints help avoid manufacturing errors. This characteristic brings easy manufacturing process and implies a very compact design that can be used in the micro-assembly workstation presented in [59-60]. From operation point of view, flexure joints clearly reduce frictional losses. Therefore, they do not require lubrication, and inaccuracies due to lubrication would be eliminated.

Flexure joints must be designed extremely carefully due to their very sensitive force-displacement relationship. Because of this, high dimensional accuracy during the fabrication and calibration after fabrication process are needed. Flexure may also be sensitive to the working temperature [61].

Young et al. [61] presented a new design tool and analysis for parallel kinematics manipulator with flexure joints. The main difference between flexure mechanisms and conventional joints is the consideration of kinematics stability and the design issue.

Wei et al. [62] stated that the flexure hinges have a lot of advantages compared to the others such as ball joints or universal ones. Because of the fact that they are manufactured monolithically, they are very compact in structurally. Besides, they have a lot of advantages like having no backlash, no friction, no lubrication and no error due to lubrication. However, they have a limited range of motion as they have to flex without sustaining any plastic deformation at the joints.
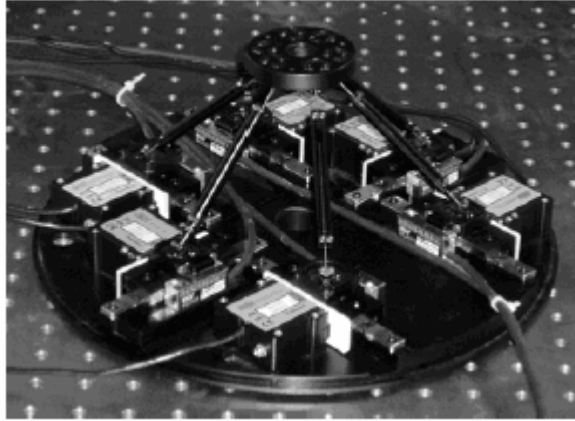
Figure 2.1. Wide range flexure-hinge based parallel manipulator

2.3.1   Hybrid Flexure Hinges

Flexure hinges with single-axis can be divided into two main categories: leaf and notch type hinges [63]. Due to relative low rotation precision and stress concentration, leaf type hinge is seldomly adopted. In 1965, Paros and Weisbord [64] introduced the first notch hinge and circular flexure hinge. The common feature of these two types is ease of manufacture. Therefore, researchers turned their attention to other configurations that could provide precision rotation in an even larger angular range.

Smith et al. [65] presented a flexure hinge of elliptic cross-section, the geometry of which is determined by ratio of the major and minor axes. Likewise, Lobontiu et al. [66] introduced an analytical model for corner-filleted flexure hinges that are incorporated into planar amplification mechanisms. Later, they also introduced the parabolic and hyperbolic hinges configurations [67]. Closed-form equations are formulated to characterize their compliance both for the active rotation and all other in and out-of-plane motions.

To sum up, Gui-Min et al. [63] represented the compliance model of the right circular hybrid flexure hinges. The close-form solutions were provided to characterize the flexibility and precision of rotation. The precision model with stress considerations were verified with the finite element analysis. Their results show that the most suitable solutions for large displacements and high accuracy are reached with the right circular hybrid flexure hinges (Figure 2.2) rather than the right circular ones and corner filleted hinges.
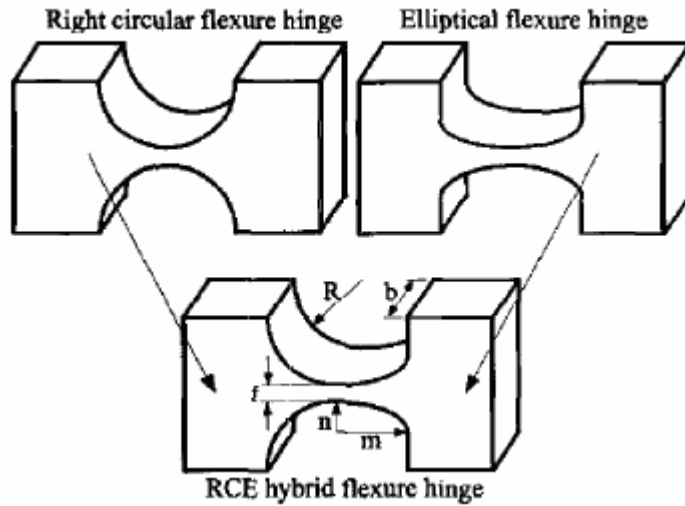
Figure 2.2. Right circular hybrid flexure hinge

2.3.2 Two Axis Flexure Hinges with Axially Collocated Notches

According to Lobontiu and Garcia [68], the flexure needs to be compliant in the bending direction and rigid for all other axes and deformations. Constructively, a flexure hinge may have several (multiple) sensitive axes. These sensitive axes define the rotations and motions. The flexure hinges configurations were defined in [68] with their compliant/sensitive axis as illustrated in Figure 2.3.
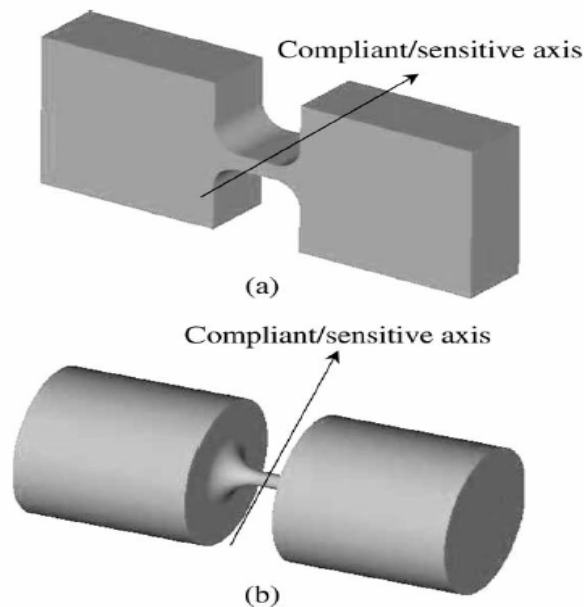
Figure 2.3. Flexure hinges' configurations with their compliant/sensitive axis

Apart from these, Paros and Weisbord [64] presented two-axis circular flexure hinges which are designed in serial configuration.
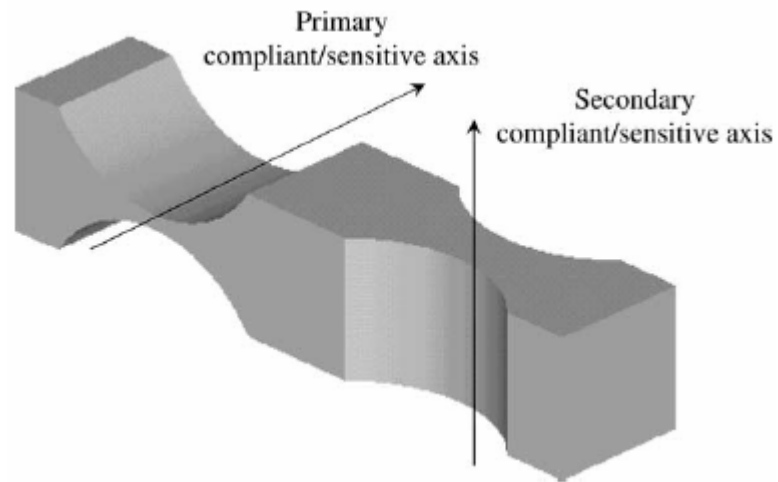
Figure 2.4. Two-axis circular flexure hinges designed in serial configuration

The serial design preserves the convenience of having each flexure hinge designed according to the standard single-axis geometry. However, it also requires the extra-length that is necessary to locate the two flexures in a serial manner.

Two-axis flexure hinges with symmetric and axially-collocated notches are presented in [68]. The compliance based formulation is solved with an emphasis on the capacity of rotation. Stress, precision of rotation and efficiency in terms of strain energy are calculated. Later, all the calculations are performed again for the two axis flexure hinges with parabolic notches. The parabolic-profiled two-axis flexure is also compared with its constant rectangular cross-section counterpart in terms of several performance criteria. Based on the analytical model the results show that parabolic-profiled two-axis flexures give better performance than their rectangular cross-section counterparts.

2.3.3 Design of Symmetric Conic-Section Flexure Hinges Based on Closed-form Compliance Equations

The most widely used formulation for flexure hinge design was proposed by Lobontiu et al. [69]. They derived closed form equations of compliance for conic section (circular, elliptic, parabolic and hyperbolic) flexure hinges.

16
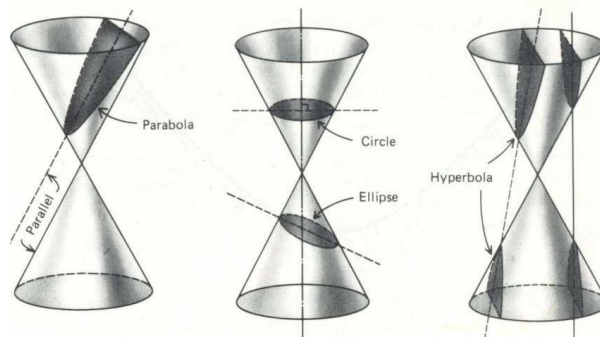
Figure 2.5. Conic section flexure hinges

The analysis was performed in terms of two non dimensional parameters. This allows performance comparison of elliptic, parabolic and hyperbolic flexure hinges relative to circular flexure hinges. The elliptic, parabolic and hyperbolic flexure hinges are more compliant (in stated order) than the circular ones for large length to thickness ratios. Hyperbolic flexures perform best in terms of preserving the center of rotation position.

2.4   Workspace and Singularity Analysis

The aspect of the parallel manipulators make Stewart Platforms superior compared to the serial manipulators due to their rigidity. However, mechanism's number of degrees of freedom instantaneously changes at some configurations which are referred as singularities in kinematics. For parallel manipulators, one or more degrees of freedom are gained at singular configurations. This causes loss in the rigidity of the structure, and the mechanism cannot support force or movement in certain directions [70]. Therefore, singularities must be avoided or excluded from the workspace in order to improve the performance. There has been ongoing research to find the singularities of Stewart Platform, and many different solutions have been proposed.

When Hunt stated the advantages of such parallel manipulators in 1978, he also mentioned a singular configuration when the moving plate rotates about a line intersected by all six legs [71]. In 1986, Fitcher [72] found another singular configuration which occurs when the moving plate is kept parallel to the base, and rotated 90 degrees about z-axis. In 1988, Merlet [73] used Grassmann Geometry to find

17

possible singular configurations. He found other possible singular configurations in addition to the ones stated by Hunt and Fichter. All of these approaches use geometric information; however, it is hard to provide a unified relation this way. Singular configurations can be found case by case if a modified or new Stewart Platform is designed. A singularity equation is needed to create a unified relation [74]. In 1993, Sefrioui and Gosselin [75] derived an analytic expression of the singularity loci for a planar three DOF parallel manipulator. Until 1996 there had not been a deep study on the analytic expression of singular configurations in six DOF parallel manipulators. In 1996, St-Onge and Gosselin [76] derived an analytic equation directly from the property of the determinant, which is a fourth-degree polynomial of the position variables.

In addition to the research on the singular configurations, characteristics of the singular configurations have been studied [74]. In 1990, Gosselin and Angeles [77] classified the singularities of the closed-loop kinematics chain mechanisms into three categories in general form. In 1991, Ma and Angeles [78] suggested another classification of the singular configurations, and derived conditions for the architecture singularity.

Other studies on singularity includes the work by Kim et al. [74] who used extra sensors on Stewart Platform to reduce the complexity of the position kinematics problem, and to find singular configurations. In 1999, they used extra sensors to simplify velocity equation as it was done in the forward position kinematics case, and derived the singularity equation directly from the velocity equation. Singular configurations can also be found by forming the Jacobian symbolically. If determinant of the Jacobian is set equaled to zero, singular configurations can be extracted from this equation. However, since each Jacobian element is quite complicated, Su et al. [79] proposed a simple singularity analysis for Stewart Platform using Genetic Algorithm (GA). In this method, the square of the determinant of Jacobian matrix is selected as the object function, and the minimal value of the objective function is found in the trajectory workspace using GA. If the minimum of this objective function is zero, then there are certain singularities. Otherwise, there is no singularity position for that Stewart Platform.
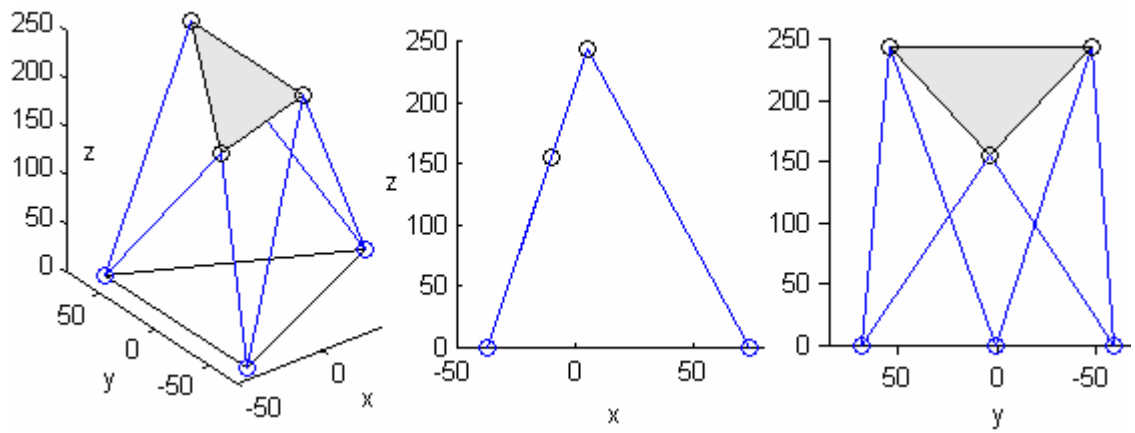
Figure 2.6. Hunt's singular configuration (Legs' vectors cross the same line in space)
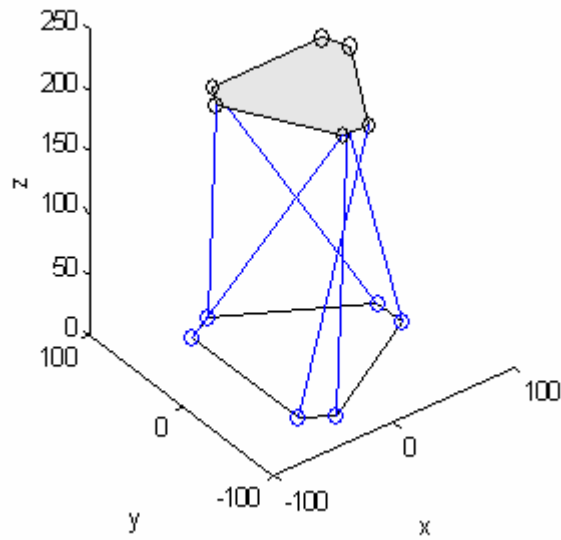
Figure 2.7. Fitcher's singular configuration (rotation ±90˚ in z axis)

3   KINEMATICS OF STEWART PLATFORM

A Stewart Platform has six degrees of freedom, which are controlled by changing the heights of six actuators. The mechanism should be designed so that the joints that connect the actuators, links and the moving platform have enough freedom to achieve the desired motion. A general form of the DOF equation for both planar and spatial mechanism can be written as follows [80]:

$$N = \lambda(l - j - 1) + \sum_{i=1} f_i - I_d \tag{3.1}$$

where N denotes the effective DOF of the mechanism, λ the DOF of the space in which the mechanism operates, l number of links, j number of joints, f_i DOF of the joints, and I_d denotes passive DOF of the mechanism.

The designed platform uses 12 spherical joints and 6 prismatic joints that connect 14 links. Each leg consists of two parts (12 links) that are connected to moving (13th link) and base (14th link) plates with prismatic joints. Besides, spherical joints have 3 DOF and prismatic joints have 1 DOF, and there are 6 passive DOF associated with the six *SPS* legs. Hence the number of DOF of the mechanism is

$$N = 6[14 - 18 - 1] + [6 + (3*12)] - 6 = 6 \tag{3.2}$$

The following sections present inverse and forward kinematics solutions.

3.1   Inverse Kinematics

For the inverse kinematics problem, the position vector and the rotation matrix of the upper plate frame (U) with respect to base frame (L) are given, and the limb lengths are to be found.
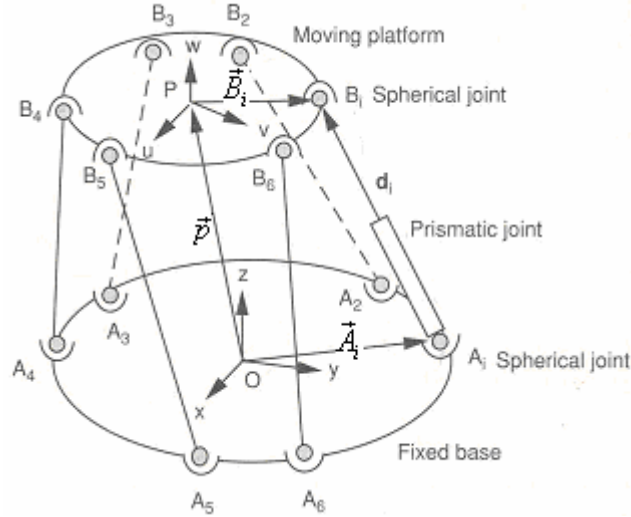
Figure 3.1. Schematic of Stewart Platform

For analyzing the inverse kinematics of the Stewart Platform, it is needed to have two cartesian coordinate systems. As it is shown in the schematic of the platform, base has the coordinate system (x_w, y_w, z_w) which is also the world coordinate system, and moving platform has the coordinate system (u_p, v_p, w_p). To define the place of the moving platform, its coordinates must be transformed into world coordinate frame. Therefore, position vector $\vec{p}$ of the centroid P and the rotation matrix $^L R_U$ are used to describe position and orientation of the moving platform in fixed base frame. Then the

transformation matrix of the platform becomes $^L R_U = \begin{bmatrix} u_x & v_x & w_x \\ u_y & v_y & w_y \\ u_z & v_z & w_z \end{bmatrix}$.

According to Figure 3.1, $\vec{A}_i = [A_{i_x} \quad A_{i_y} \quad A_{i_z}]^T$ and $^U \vec{B}_i = [B_{i_u} \quad B_{i_v} \quad B_{i_w}]^T$ are chosen as the position vectors, and the vector calculation is given by

$$\overline{A_i B_i} = \vec{p} + {}^L R_U \, {}^U \vec{B}_i - \vec{A}_i \tag{3.3}$$

By taking the dot product of the two vectors, leg/link lengths can be calculated from

$$d_i^2 = [\vec{p} + {}^L R_U \, {}^U \vec{B}_i - \vec{A}_i]^T [\vec{p} + {}^L R_U \, {}^U \vec{B}_i - \vec{A}_i] \tag{3.4}$$

21

3.1.1 Inverse Kinematics Solution of Designed Stewart Platform

For inverse kinematics problem, position and orientation of the designed platform is defined by a position vector and a rotation matrix. Using rotation about fixed axis, rotation matrix is constructed as

$$R = R_z(\phi)R_y(\theta)R_x(\psi)$$ (3.5)

$$R = \begin{bmatrix} \cos\phi\cos\theta & -\sin\phi\cos\psi + \cos\phi\sin\theta\sin\psi & \sin\phi\sin\psi + \cos\phi\sin\theta\cos\psi \\ \sin\phi\cos\theta & \cos\phi\cos\psi + \sin\phi\sin\theta\sin\psi & -\cos\phi\sin\psi + \sin\phi\sin\theta\cos\psi \\ -\sin\theta & \cos\theta\sin\psi & \cos\theta\cos\psi \end{bmatrix}$$ (3.6)

As an example, given position vector $p = [17.5\ 17.5\ 231.5156]$ that includes x, y and z positions of the centre of the upper plate in the given order as well as the identity matrix for rotation, the leg lengths of the platform are calculated from (3.4) as

L1 = 2.326466081954836e+002   L2 = 2.374630714334958e+002

L3 = 2.399554919298858e+002   L4 = 2.334214926787315e+002

L5 = 2.402842826444521e+002   L6 = 2.420027176689111e+002

3.1.2 Workspace of the Platform

In order to find maximum position that platform can reach, references in x, y and z axes are given to inverse kinematics code. If for a given desired position, one of the legs can not extend to its reference length, desired position is not recorded. For given range of desired positions $x = 0:0.5:50$, $y = 0:0.5:50$, $z = -10:0.5:15$, workspace of the platform is determined (see

Figure 3.2). From the results, maximum relative position is found as:

$$x:46\ mm\ y:44.5\ mm\ z:\text{-}5.5\ (218.7491)\ mm$$

Therefore, maximum relative distance from home configuration is $6.4237839e+001\ mm$. for the platform design in consideration.

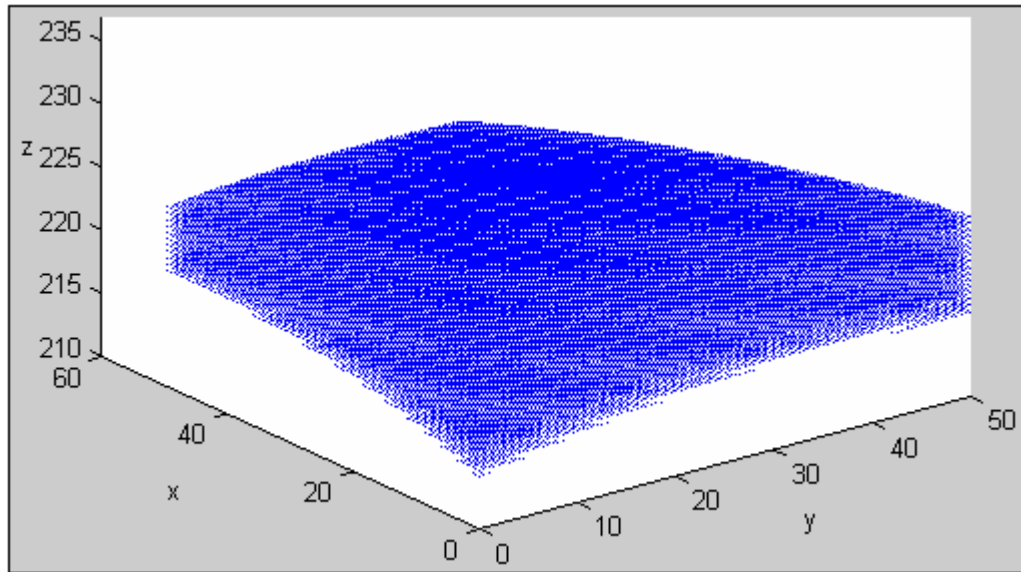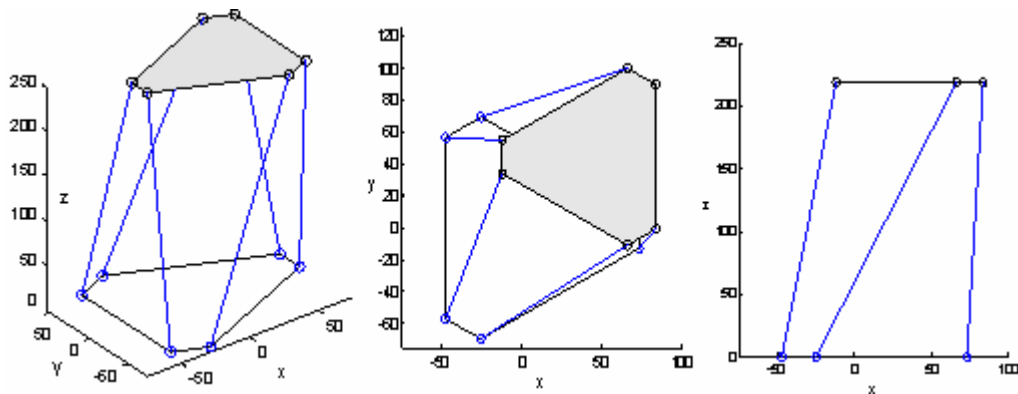Figure 3.2. Workspace of the designed platform

Figure 3.3. Maximum relative distance platform can reach

Apart from translational workspace of the platform, the mechanism's orientation limits are also calculated. The platform can rotate 11 degrees in x direction (ψ), 14.5 degrees in y direction (θ), and 49 degrees in z direction (ϕ).
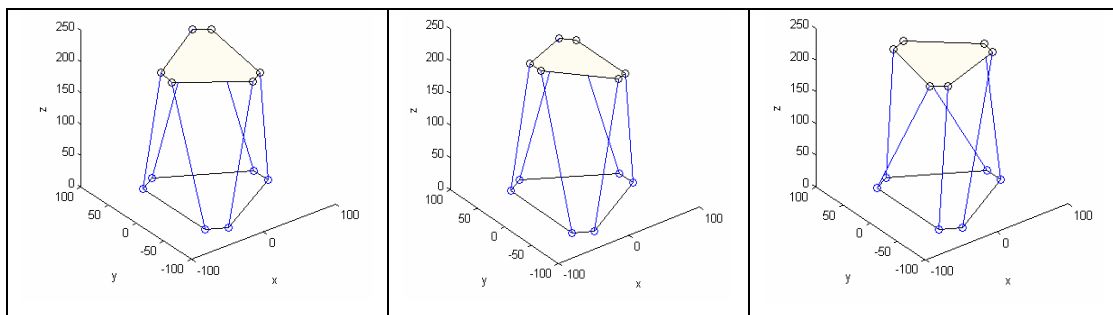
Figure 3.4. Maximum rotations in x, y and z axes

3.2   Forward (Direct) Kinematics

For the direct kinematics problem, the leg lengths are given, position vector and the rotation matrix of the moving platform are to be found. Direct kinematics of Stewart Platform is a difficult problem since position vector contains three scalar unknowns and rotation matrix contains nine scalar unknowns. The forward kinematics problem requires the solution of a set of non-linear equations which has at least 8 real solutions. In this work a general solution is not provided; however, two numerical solutions are presented. The first one uses Newton-Raphson method. Actual position and orientation is obtained from the estimation of position vector and rotation angles. Even though this approach is not suitable for a theoretical investigation aiming at determining all the possible solutions, it is easier to find the actual configuration if a good starting point is available in the form of a neighboring configuration. The second approach uses geometric constraints, and under these constraints all link and joint positions are identified. This approach uses direction cosines of the first leg and an angle as a starting point to determine the position of the second leg upper platform connection point. A search within upper and lower bounds of these parameters gives tentative solutions that satisfy user defined permissible error. After solutions are predicted, correction algorithm is used to correct the errors and all the real closures of the platform are identified [32].

3.2.1   Direct Kinematics Solution Using Newton-Raphson Method

First direct kinematics solution presented in this work is estimate correction with Newton-Raphson method. Using Newton-Raphson method, the error between the estimated and actual leg lengths is decreased to zero iteratively which leads to the actual configuration of the platform. Leg lengths depend on x, y, z translation parameters and Euler angles. A function ' X ' is defined which depends on leg lengths and describes the configuration of the platform. Leg lengths can be estimated by making function $X(leg\_lengths(xyzeuler))$ linear around $xyzeuler$ vector's initial values. The error is $(leg\_lengths - estimated\_leglengths)$ which is determined by given estimated

xyzeuler vector. Therefore, finding function X 's derivative with respect to *xyzeuler* leads to calculation of $\Delta xyzeuler$ [81].

3.2.1.1   Solution for the Designed Platform

Tolerance value for the solution is given as ' tolerance = mean(leg_lengths)/1e7 ' and output of the program is shown in Table 3.1. The first row gives the error of the estimated values. (Translational parameters' units are mm and rotational parameters' units are radian.)

$$
\begin{array}{l}
\textit{Actual translational parameters}: \begin{bmatrix} 18.5 & 12.5 & 231.5156 \\ 10 & 10 & 211.0156 \end{bmatrix} \\
\textit{Estimate values} \qquad\qquad\qquad\quad :
\end{array}
$$

$$
\begin{array}{l}
\textit{Actual Euler angles}: \begin{bmatrix} 174.532925199\text{e-}003 & 174.532925199\text{e-}003 & 174.532925199\text{e-}003 \\ 0.00000000000\text{e-}003 & 0.00000000000\text{e-}003 & 0.00000000000\text{e-}003 \end{bmatrix} \\
\textit{Estimate values} \quad :
\end{array}
$$

$$\text{error} = 32.0235987755983$$

$$
\begin{array}{l}
\text{Actual xyz}: \begin{bmatrix} 18.5000000000\text{e+}000 & 12.5000000000\text{e+}000 & 231.515600000\text{e+}000 \\ 18.5000001036\text{e+}000 & 12.4999999485\text{e+}000 & 231.515600032\text{e+}000 \end{bmatrix} \\
\text{Result xyz}:
\end{array}
$$

$$
\begin{array}{l}
\text{Actual } \phi\theta\psi: \begin{bmatrix} 174.532925199\text{e-}003 & 174.532925199\text{e-}003 & 174.532925199\text{e-}003 \\ 174.532924820\text{e-}003 & 174.532924983\text{e-}003 & 174.532924198\text{e-}003 \end{bmatrix} \\
\text{Result } \phi\theta\psi:
\end{array}
$$

$$\text{error} = 189.151083240802\text{e-}009$$

Table 3.1. Parameters for forward kinematics solution using Newton - Raphson method

The second row of Table 3.1 presents an example with a total error of ~189e-9. When the parameters' errors are acceptable as in this example, the program gives the actual configuration. Detailed information on calculations using this method is given in Appendix B.

3.2.1.2   Home, Estimated and Actual Configurations

In Figure 3.5, the Stewart Platform is shown at its home position. In this configuration, platform's height is 214.0156 mm, and x and y of the centre position of

the moving platform is 0. From the results acquired in the previous section, estimated and actual configurations of the platform are drawn. Figure 3.6 shows the platform with estimated translation and orientation. Actual configuration which is also the result of the solution is shown in Figure 3.7.
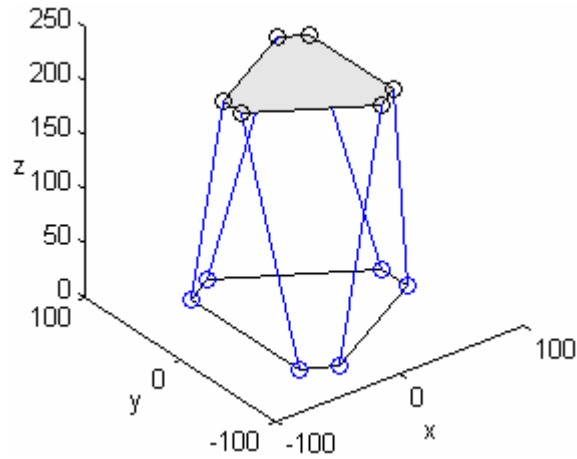
Figure 3.5. Stewart Platform in home configuration
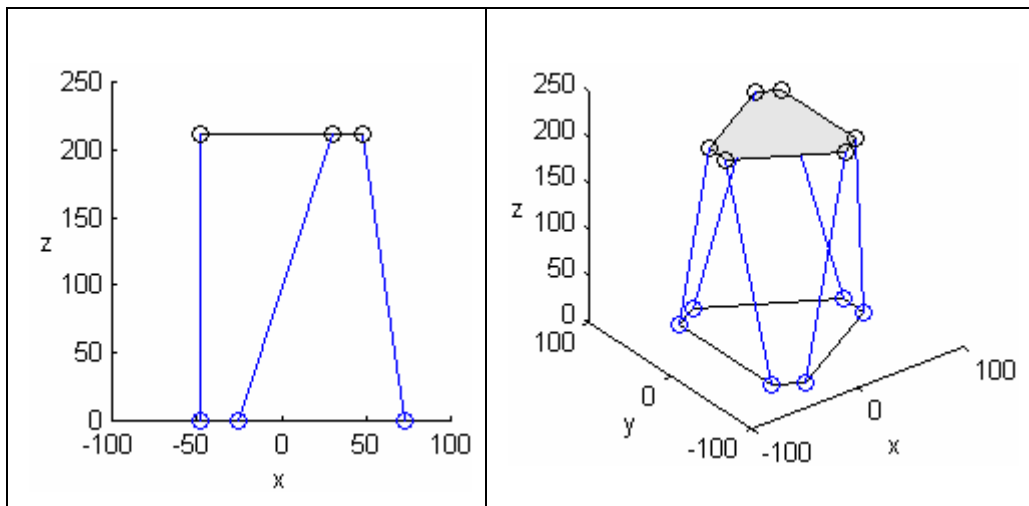
Figure 3.6. Estimated configuration of the platform
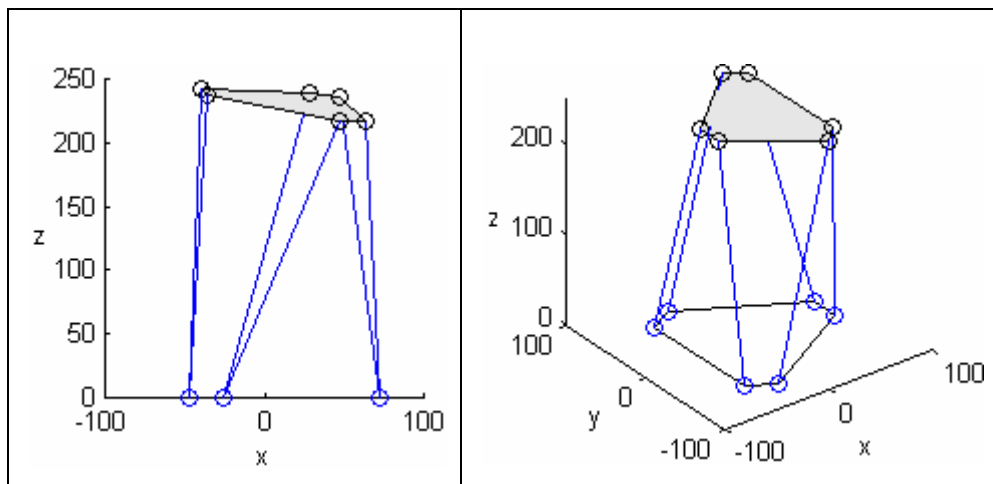
Figure 3.7. Actual configuration of the platform

3.2.2 Numerical Solution Based on Geometric Constraints

Presented solution is an implementation of Dasgupta and Mruthyunjaya's *'constructive predictor-corrector algorithm'* [32]. The direct position kinematics problem is to determine the leg vectors for given leg lengths. For that reason, once the joint variables of the legs are known, the configuration of the platform can be calculated. When two variables of the first leg are determined by a close arbitrary estimate, the second platform connection point is constrained to move in a circle and the third leg can be solved using geometric constraints. Then, the configuration of the system is fully determined, and remaining leg vectors are solved. Once the tentative solutions are close enough, solutions can be predicted by a three dimensional search. The results can be corrected by any locally efficient optimization technique. Newton-Raphson method is used for the optimization technique in the presented solution.

3.2.2.1 Calculations for the Designed Platform

For three dimensional search, x and y direction cosines' values are constrained between -0.15 and 0.15, and theta value is searched for all possible values (0-2*pi). Increment values are 0.005 for direction cosines and 0.002 for theta leading to 2*10^7 iterations. The program finds 7934 tentative solutions for given parameter values. These values converge to 8 real possible configurations of the platform. Histograms of tentative solutions' x, y and z positions are shown in Figures 3.8, 3.9 and 3.10.

Figure 3.8. Histogram of possible solutions for platform's x position
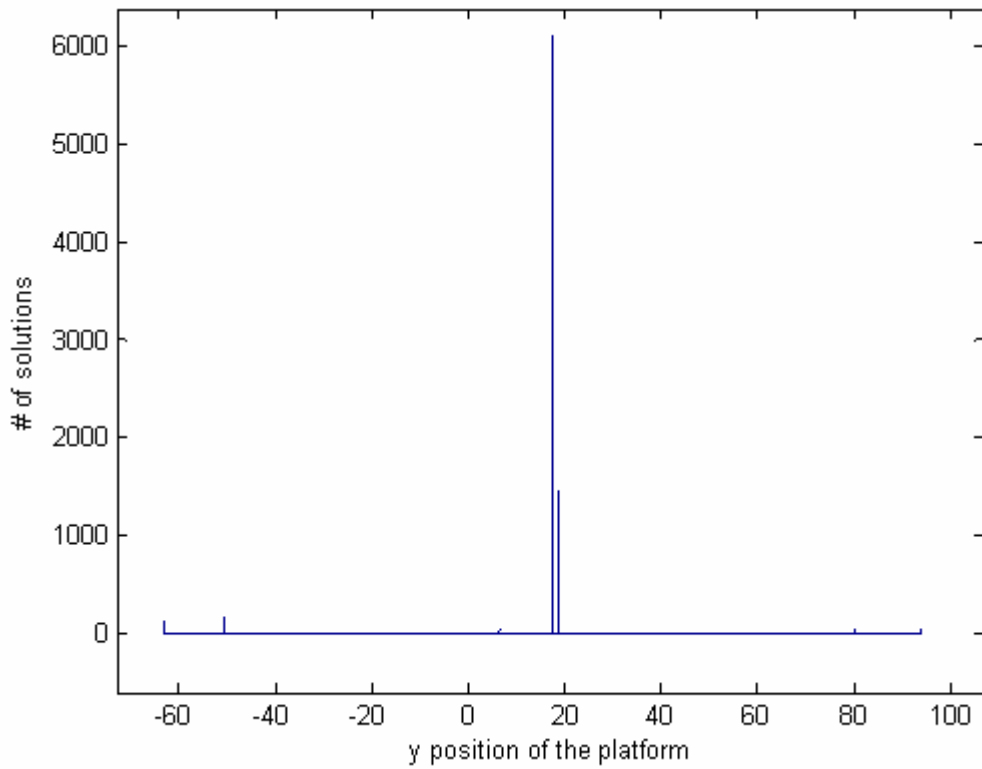
Figure 3.9. Histogram of possible solutions for platform's y position
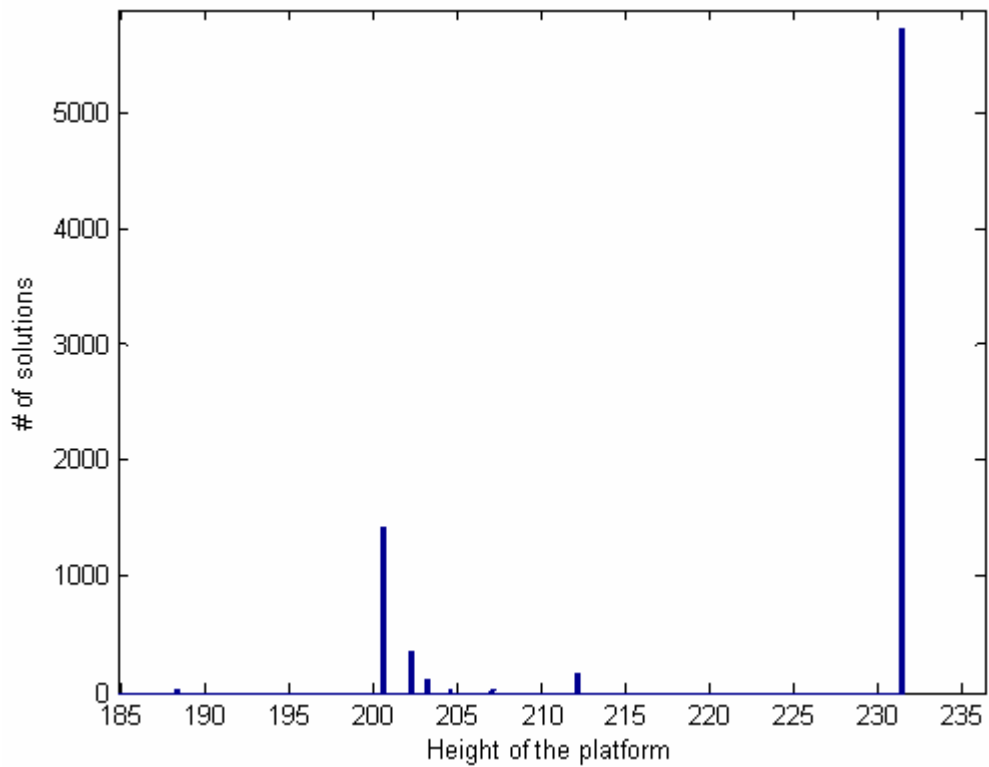
Figure 3.10. Histogram of possible solutions for platform height

$$\begin{bmatrix} -4.6624233\mathrm{e}{-001} & 8.8247205\mathrm{e}{-001} & 6.2138382\mathrm{e}{-002} & 5.7402468\mathrm{e}{+001} \\ 8.8247205\mathrm{e}{-001} & 4.5900837\mathrm{e}{-001} & 1.0273461\mathrm{e}{-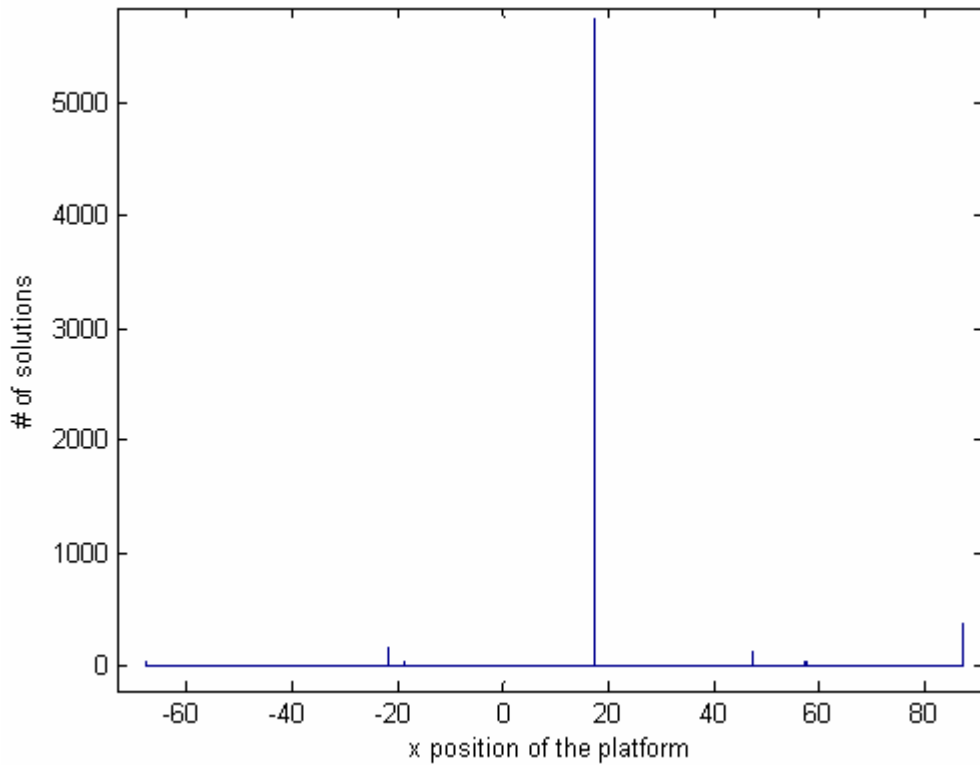001} & 9.3615182\mathrm{e}{+001} \\ 6.2138384\mathrm{e}{-002} & 1.0273461\mathrm{e}{-001} & -9.9276605\mathrm{e}{-001} & 1.8825470\mathrm{e}{+002} \end{bmatrix}$$

$$\begin{bmatrix} -9.8482046\mathrm{e}{-001} & 1.6445677\mathrm{e}{-002} & 1.7279524\mathrm{e}{-001} & 1.7613816\mathrm{e}{+001} \\ 1.6445966\mathrm{e}{-002} & -9.8218226\mathrm{e}{-001} & 1.8720987\mathrm{e}{-001} & 1.8918530\mathrm{e}{+001} \\ 1.7279522\mathrm{e}{-001} & 1.8720990\mathrm{e}{-001} & 9.6700272\mathrm{e}{-001} & 2.0068875\mathrm{e}{+002} \end{bmatrix}$$

$$\begin{bmatrix} -6.1798109\mathrm{e}{-001} & 4.7376212\mathrm{e}{-007} & -7.8619296\mathrm{e}{-001} & 8.7277252\mathrm{e}{+001} \\ 3.8664776\mathrm{e}{-007} & 1.0000000\mathrm{e}{+000} & 2.9868127\mathrm{e}{-007} & 1.7500044\mathrm{e}{+001} \\ 7.8619296\mathrm{e}{-001} & -1.1940037\mathrm{e}{-007} & -6.1798109\mathrm{e}{-001} & 2.0218058\mathrm{e}{+002} \end{bmatrix}$$

$$\begin{bmatrix} -3.4873785\mathrm{e}{-001} & -9.3524663\mathrm{e}{-001} & 6.0791855\mathrm{e}{-002} & 4.7334694\mathrm{e}{+001} \\ -9.3524663\mathrm{e}{-001} & 3.4306326\mathrm{e}{-001} & -8.7300295\mathrm{e}{-002} & -6.3167107\mathrm{e}{+001} \\ 6.0791855\mathrm{e}{-002} & -8.7300295\mathrm{e}{-002} & -9.9432540\mathrm{e}{-001} & 2.0315816\mathrm{e}{+002} \end{bmatrix}$$

$$\begin{bmatrix} 5.8066944\mathrm{e}{-001} & 7.2630182\mathrm{e}{-001} & 3.6784326\mathrm{e}{-001} & -1.8668194\mathrm{e}{+001} \\ 7.2630183\mathrm{e}{-001} & -2.5799164\mathrm{e}{-001} & -6.3712320\mathrm{e}{-001} & 8.0145152\mathrm{e}{+001} \\ -3.6784326\mathrm{e}{-001} & 6.3712320\mathrm{e}{-001} & -6.7732220\mathrm{e}{-001} & 2.0452466\mathrm{e}{+002} \end{bmatrix}$$

$$\begin{bmatrix} 9.8618220\text{e-}001 & -1.2791251\text{e-}001 & -1.0527613\text{e-}001 & -6.7801061\text{e+}001 \\ -1.2791251\text{e-}001 & -9.9176228\text{e-}001 & 6.7799142\text{e-}003 & 6.4672608\text{e+}000 \\ -1.0527613\text{e-}001 & 6.7799027\text{e-}003 & -9.9441992\text{e-}001 & 2.0703961\text{e+}002 \end{bmatrix}$$

$$\begin{bmatrix} 5.4377732\text{e-}001 & -7.9020065\text{e-}001 & 2.8264671\text{e-}001 & -2.1850196\text{e+}001 \\ -7.9020067\text{e-}001 & -3.6866734\text{e-}001 & 4.8955827\text{e-}001 & -5.0656575\text{e+}001 \\ -2.8264665\text{e-}001 & -4.8955830\text{e-}001 & -8.2489002\text{e-}001 & 2.1228523\text{e+}002 \end{bmatrix}$$

$$\begin{bmatrix} 1.0000000\text{e+}000 & -6.7563220\text{e-}014 & -2.7843626\text{e-}013 & 1.7500000\text{e+}001 \\ 6.7563220\text{e-}014 & 1.0000000\text{e+}000 & -5.4251173\text{e-}014 & 1.7500000\text{e+}001 \\ 2.7843626\text{e-}013 & 5.4251173\text{e-}014 & 1.0000000\text{e+}000 & 2.3151560\text{e+}002 \end{bmatrix}$$

Table 3.2. Configurations of the platform from forward kinematics solution

First three columns in Table 3.2 show rotation matrices and fourth columns show position of the platform. For given leg lengths

$L1 = 2.326466065312008\text{e+}002$

$L2 = 2.374630694983699\text{e+}002$

$L3 = 2.399554899469744\text{e+}002$

$L4 = 2.334214905853267\text{e+}002$

$L5 = 2.402842806155509\text{e+}002$

$L6 = 2.420027160063402\text{e+}002$

solutions that are given in Table 3.2 are obtained. To check the solutions, inverse kinematics is used to verify that these solutions give the same leg lengths. (Last configuration found with forward kinematics solution is the example given in Chapter 3 to find the leg lengths with inverse kinematics for $x = 17.5$ $y = 17.5$ $z = 231.5156$ and no rotation). Detailed information on calculations using this method is given in Appendix C.

In Table 3.3, all solutions found from forward kinematics solution are presented in the order given in Table 3.2.
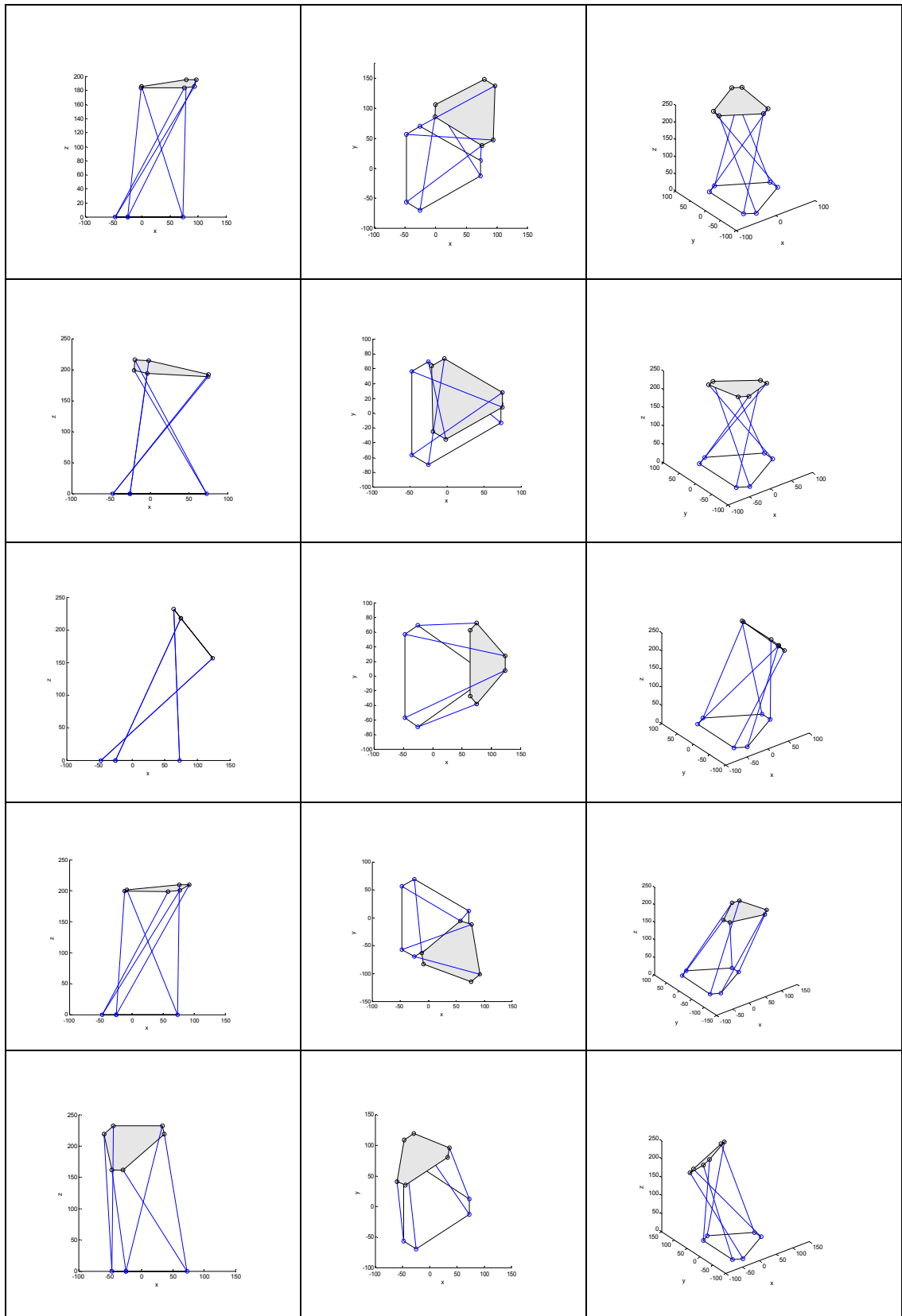
Table 3.3. Example of a forward kinematics solution based on geometrical constraints

3.2.2.2 Remarks

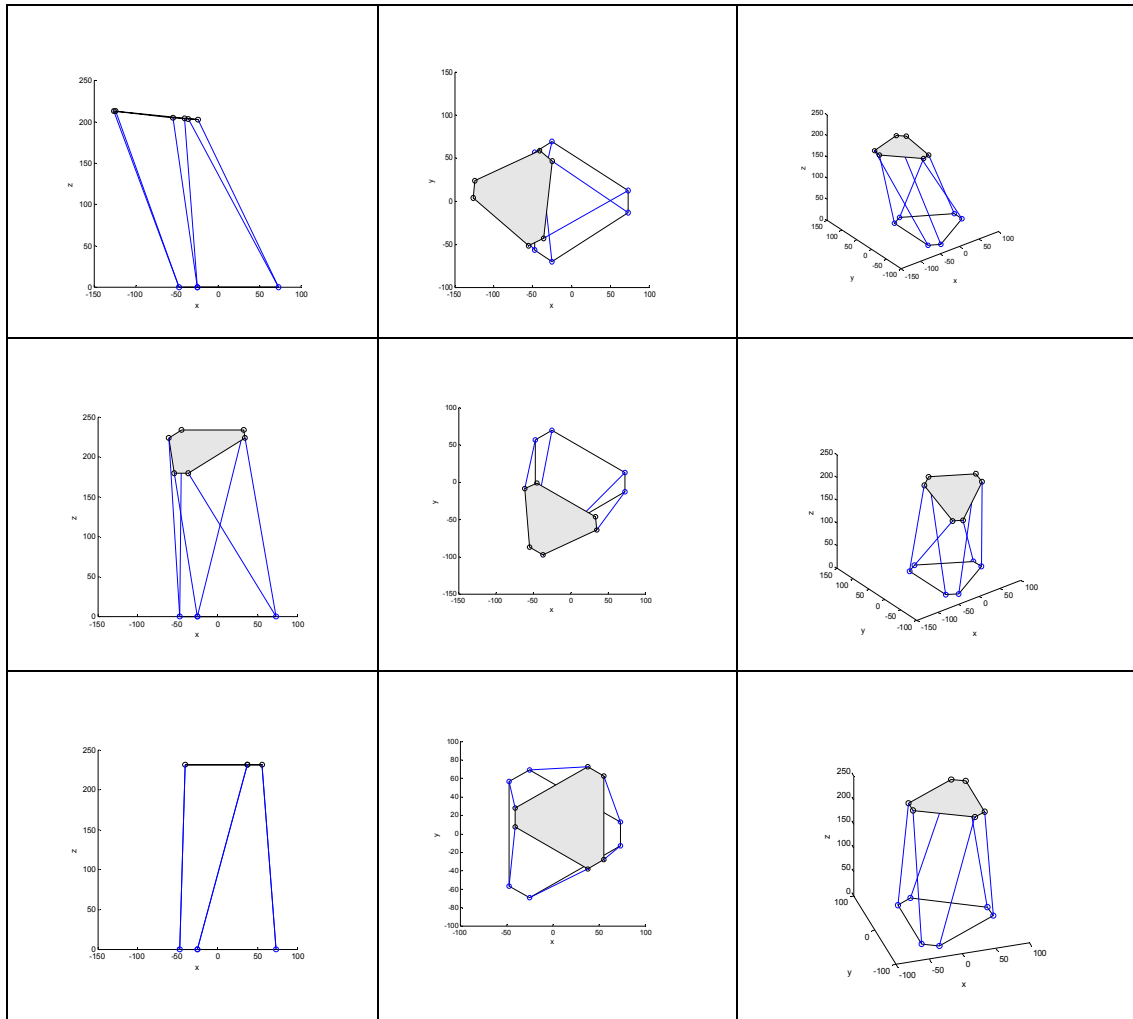This algorithm mainly focuses on predicting tentative solutions for all the real assembly configurations of the Stewart Platform by considering pure geometrical constraints. After the tentative solutions are found, some geometric checks are needed to economize the computation. When the tolerances are very strict, the algorithm works fine by tracing all the neighborhoods of the solution. However, fine adjustments lead to lots of redundant computations in order to find the solutions within permissible tolerance. Because, the values of the increments should be in micro scale for the designed Stewart Platform, obtaining fine solutions requires lots of computation which results in merging large number of predictions to the same configuration. Although this algorithm can not be used for real time applications, it provides high accuracy with reasonable increment values.

4 DYNAMIC ANALYSIS

4.1 Dynamic Equations of the Stewart Platform

Dynamic analysis presented in this section follows from the work by Guo et al. [58]. In order to derive a dynamic model, the system is separated into two parts which are the moving platform (upper plate) and the six actuators with the base platform. The constraint forces f_p at the top plate joints are derived using Lagrange formulation.

| Figure 4.1. Force analysis diagram | Figure 4.2. Position analysis of a leg |
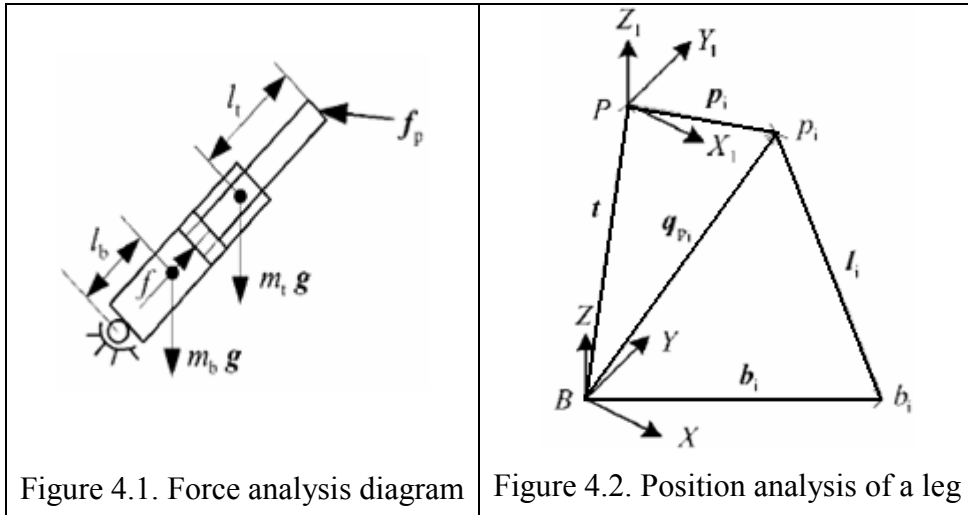
Considering q_p and $\dot{q}_p$ as the corresponding generalized coordinates and velocities with the kinetic energy, T ($q_p, \dot{q}_p$), the Lagrange equations of the system are given by

$$\frac{d}{dt}(\frac{\partial T}{\partial \dot{q}_p}) - \frac{\partial T}{\partial q_p} = Q \tag{4.1}$$

where Q denotes the generalized forces projected along the variation of the generalized coordinates q_p.

The kinetic energy can be given by

$$T = \frac{1}{2} v_t^T m_t v_t + \frac{1}{2} w_l^T (I_t + I_b) w_l$$

$$= \frac{1}{2} \dot{q}_p^T ((I + \frac{l_t \tilde{n}^2}{l})^T m_t (I + \frac{l_t \tilde{n}^2}{l})$$

$$+ (I_t + I_b) \tilde{n}^T \frac{\tilde{n}}{l^2}) \dot{q}_p \qquad (4.2)$$

$$= \frac{1}{2} \dot{q}_p^T (M_1 + M_2) \dot{q}_p$$

where equations

$$w_l = \frac{n \times \dot{q}_p}{l} = \frac{\tilde{n} \dot{q}_p}{l} \qquad (4.3)$$

(angular velocity of the actuator)

$$v_t = \dot{q}_p + w_l \times (-l_t n) = (I + \frac{l_t \tilde{n}^2}{l}) \dot{q}_p \qquad (4.4)$$

and (velocity of the center of gravity for the moving parts of the actuator) have been employed.

$$M_1 = (I + \frac{l_t \tilde{n}^2}{l})^T m_t (I + \frac{l_t \tilde{n}^2}{l})$$

$$M_2 = \frac{(I_t + I_b) \tilde{n}^T \tilde{n}}{l^2} \qquad (4.5)$$

Considering equations (4.1) and (4.2), the following relations can be derived:

$$\frac{d}{dt} (\frac{\partial T}{\partial \dot{q}_p}) = \frac{d}{dt} ((M_1 + M_2) \dot{q}_p)$$

$$= \frac{d(M_1 + M_2)}{dt} \dot{q}_p + (M_1 + M_2) \ddot{q}_p \qquad (4.6)$$

$$\frac{dM_1}{dt} = \frac{2 m_t l_t}{l^2} (n \dot{q}_p^T \tilde{n}^T \tilde{n} + n^T \dot{q}_p \tilde{n}^T \tilde{n} + \tilde{n}^T \tilde{n} \dot{q}_p n^T)$$

$$- \frac{m_t l_t^2}{l^3} (2 n^T \dot{q}_p \tilde{n}^T \tilde{n} + n \dot{q}_p^T \tilde{n}^T \tilde{n} + \tilde{n}^T \tilde{n} \dot{q}_p n^T) \qquad (4.7)$$

$$\frac{dM_2}{dt} = - \frac{I_t + I_b}{l^3} (2 \dot{q}_p^T n \tilde{n}^T \tilde{n} + \tilde{n}^T \tilde{n} \dot{q}_p n^T + n \dot{q}_p^T \tilde{n}^T \tilde{n})$$

$$\frac{\partial T}{\partial q_p} = \frac{\partial}{\partial q_p}(\frac{1}{2}\dot{q}_p{}^T(M_1+M_2)\dot{q}_p)$$

$$= m_t l_t(-\dot{q}_p{}^T\dot{q}_p\frac{\partial}{\partial q_p}(\frac{1}{l})+\frac{\partial}{\partial q_p}(\frac{\dot{q}_p{}^Tl\dot{q}_p{}^Tl}{l^3}))$$

$$+\frac{1}{2}(m_t l_t^2+I_t+I_b)(\dot{q}_p{}^T\dot{q}_p\frac{\partial}{\partial q_p}(\frac{1}{l^2})$$

$$-2\frac{\dot{q}_p{}^Tl}{l^2}\frac{\partial}{\partial q_p}(\frac{\dot{q}_p{}^Tl}{l^2}))$$

(4.8)

To simplify equation (4.8), the following expressions of the partial derivatives are used.

$$\frac{\partial}{\partial q_p}(\frac{1}{l}) = -\frac{n}{l^2}$$

$$\frac{\partial}{\partial q_p}(\frac{1}{l^2}) = -2\frac{n}{l^3}$$

$$\frac{\partial}{\partial q_p}(\frac{\dot{q}_p{}^Tl}{l^2}) = \frac{\dot{q}_p}{l^2} - 2\frac{nn^T\dot{q}_p}{l^2}$$

$$\frac{\partial}{\partial q_p}(\frac{\dot{q}_p{}^Tl\dot{q}_p{}^Tl}{l^3}) = \frac{1}{l^2}(2n^T\dot{q}_p\tilde{n}^T\tilde{n}\dot{q}_p - n\dot{q}_p{}^Tnn^T\dot{q}_p)$$

(4.9)

Then, equation (4.8) can be rewritten as

$$\frac{\partial T}{\partial q_p} = \frac{m_t l_t}{l^2}(n\dot{q}_p{}^T\dot{q}_p + 2n^T\dot{q}_p\dot{q}_p - 3n\dot{q}_p{}^Tnn^T\dot{q}_p)$$

$$-\frac{m_t l_t^2}{l^3}(n\dot{q}_p{}^T\dot{q}_p + \dot{q}_p\dot{q}_p{}^Tn - 2nn^T\dot{q}_p\dot{q}_p{}^Tn)$$

$$-\frac{I_t+I_b}{l^3}(n^T\dot{q}_p\dot{q}_p + n\dot{q}_p{}^T\dot{q}_p - 2n\dot{q}_pnn^T\dot{q}_p)$$

(4.10)

As shown in Figure 4.1, there are several external forces acting on the leg, such as the gravitational forces due to the mass of the actuator (m_t and m_b), the driving force f generated by the actuator, and the constraint force at the upper gimbal acting on the leg. On the basis of the principle of virtual work, two systems of forces are equivalent if they do the same virtual work in dynamics sense. Therefore, the generalized force Q_f which is projected along the variation of the generalized coordinates (q_p) can be derived as follows

$$\delta W = Q_f{}^T \delta q_p = f \delta l = f n^T \delta q_p = (nf)^T \delta q_p \tag{4.11}$$

where equation

$$\dot{l} = n^T \dot{q}_p = \begin{bmatrix} n^T & n^T \tilde{p}_b{}^T \end{bmatrix} \dot{q}$$
$$= [n^T \quad (\tilde{p}_b n)^T] \dot{q} = [n^T \quad (Rp \times n)^T] \dot{q} \tag{4.12}$$

(the velocity of the length of the leg) has been employed.

$$Q_f = nf \tag{4.13}$$

Similarly, the generalized forces due to the gravitational effects can be derived by

$$Q_{m_t g} = (I + \frac{l_t \tilde{n}^2}{l})^T m_t g = (I + \frac{l_t \tilde{n}^2}{l}) m_t g$$
$$Q_{m_b g} = (\frac{l_b \tilde{n}^T \tilde{n}}{l})^T m_b g = (\frac{l_b \tilde{n}^T \tilde{n}}{l}) m_b g \tag{4.14}$$

where equation (5.4) and the equation

$$v_b = w_l \times l_b n = (\frac{l_b \tilde{n}^T \tilde{n}}{l}) \dot{q}_p \tag{4.15}$$

(velocity of the center of gravity for the rotating parts of the actuator) (4.15) have been applied. Therefore, the generalized force projected along the variation of the generalized coordinates q_p can be derived by using equations (4.13) and (4.14) as

$$Q = Q_f + Q_{m_t g} + Q_{m_b g} + f_p . \tag{4.16}$$

Using equations (4.1), (4.6), (4.7), (4.10), and (4.16), the constraint force f_p at a joint at the top of the leg can be given by

$$f_p = (M_1 + M_2)\ddot{q}_p + C_a \dot{q}_p - (Q_f + Q_{m_t g} + Q_{m_b g}) \tag{4.17}$$

where

$$C_a = \frac{m_t l_t}{l^2} (n \dot{q}_p{}^T \tilde{n}^T \tilde{n} + n^T \dot{q}_p \tilde{n}^T \tilde{n} + \tilde{n}^T \tilde{n} \dot{q}_p n^T)$$
$$- \frac{m_t l_t{}^2}{l^3} (n^T \dot{q}_p \tilde{n}^T \tilde{n} + \tilde{n}^T \tilde{n} \dot{q}_p n^T) \tag{4.18}$$
$$- \frac{2(I_t + I_b)}{l^3} (\tilde{n}^T \tilde{n} \dot{q}_p n^T)$$

Equation (4.17) can be rewritten as

$$f_p = (M_1 + M_2)[I \quad R\tilde{p}^T R^T]\ddot{q} + C_a[I \quad R\tilde{p}^T R^T]\dot{q}$$
$$+ (M_1 + M_2)\tilde{w}^2 Rp - (Q_f + Q_{m_t g} + Q_{m_b g}) \tag{4.19}$$

where equations

$$\dot{q}_p = \dot{t} + w \times Rp = \dot{t} + (\tilde{p}_b)^T w = \dot{t} + R\tilde{p}^T R^T w$$

$$= [I \quad R\tilde{p}^T R^T]\begin{bmatrix} \dot{t} \\ w \end{bmatrix} = [I \quad R\tilde{p}^T R^T]\dot{q} \tag{4.20}$$

(velocity of the upper gimbal point q_p) and

$$\ddot{q}_p = [I \quad R\tilde{p}R^T]\ddot{q} + \tilde{w}^2 Rp \tag{4.21}$$

(acceleration of the upper gimbal point q_p) have been used.

4.2 Dynamic Analysis using ADAMS

The reaction forces are derived through dynamic analysis. The basis of derivation of the forces is the equations presented in the proceeding section, In this work commercially available dynamics program, ADAMS, is used to perform the dynamic analysis of the platform.

4.2.1 Simulation Steps in ADAMS

- First, the solid model of the Stewart Platform is generated in SolidWorks.
- Then this model is imported in parasolid format to ADAMS.
- Later, inertia and mass values for each part is entered as part property and center of mass and joint connection markers are attached to each part.
- Fixed joints are attached to the parts which had to be fixed, translational joints are attached to the actuators of the struts, and rotational joints are attached to the spherical joints. Friction is defined for every joint.
- After defining the joints, motion for each joint is defined. Translational joints are constrained to move along leg vectors.
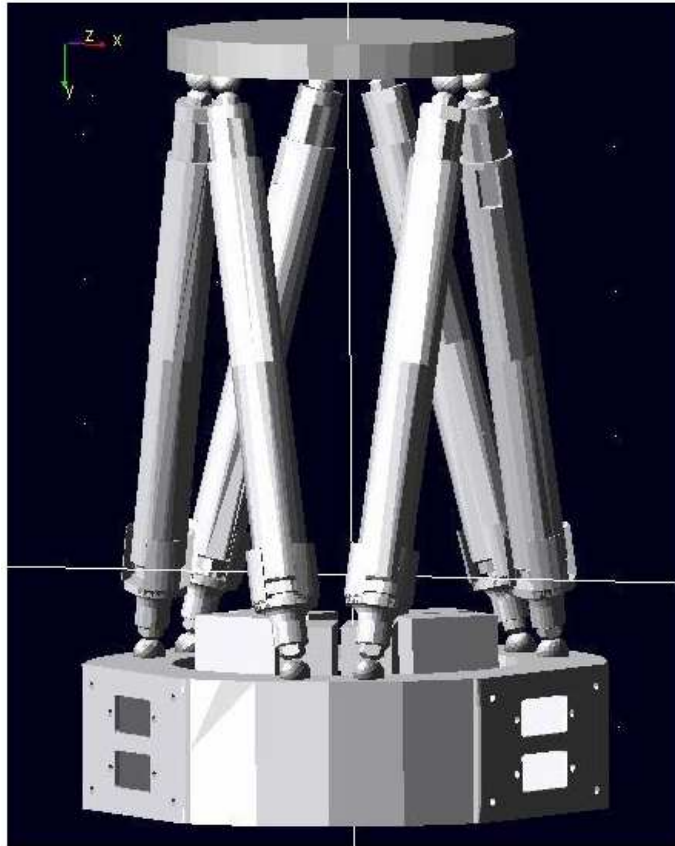
Figure 4.3. Stewart Platform model used in ADAMS

- The step before deriving the forces is to define trajectory for the moving upper plate. Reference trajectory points (see section 4.2.2) are created from output of a C++ code for each translational joint. These points are used to define a cubic spline as the trajectory of the translational joints. These points are the displacement of the translational joints at each step. After defining splines for each translational joint at each strut of the platform, the translational motion for each joint is acquired.

- The last step is the simulation of the platform with defined motion and constraints. After the simulations, the maximum forces at the struts for different trajectories are acquired.

4.2.2 Trajectory Generation for Translational Joints

Trajectory generation code generates required leg lengths of the Stewart Platform at every time increment to move it in desired path. The center of the top plate should

trace the path with desired orientation. During the motion orientation may also be changed. Motion trajectories corresponding to trapezoidal velocity references are generated. However, for given acceleration, motors may not reach maximum velocity and in that case triangular velocity references are applied.
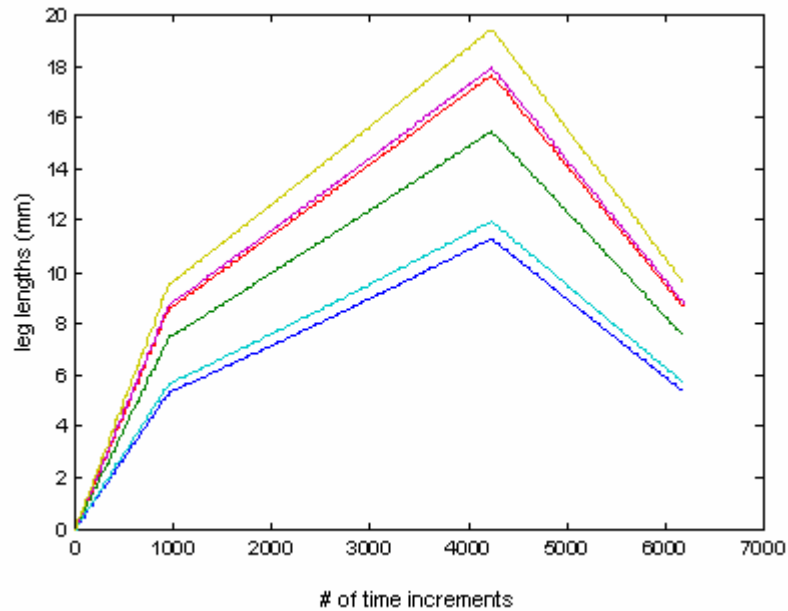

Figure 4.4. Example of legs' motion graphs according to trapezoid velocity reference

4.2.3 Forces at Spherical Joints

Forces at the joints are calculated for different translation and orientation of the platform. In latter subsections, for reference trajectory 20 mm in x axis, 10 mm in y axis and 5 mm in z axis, forces acquired at upper and lower spherical joints are given.

4.2.3.1 Upper Spherical Joints
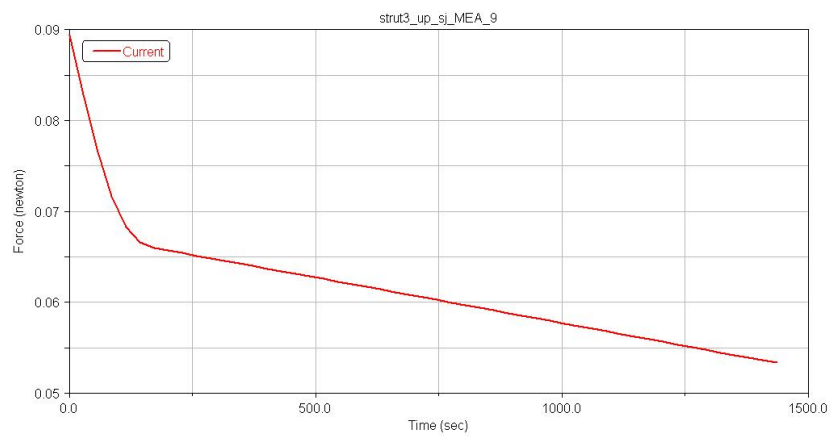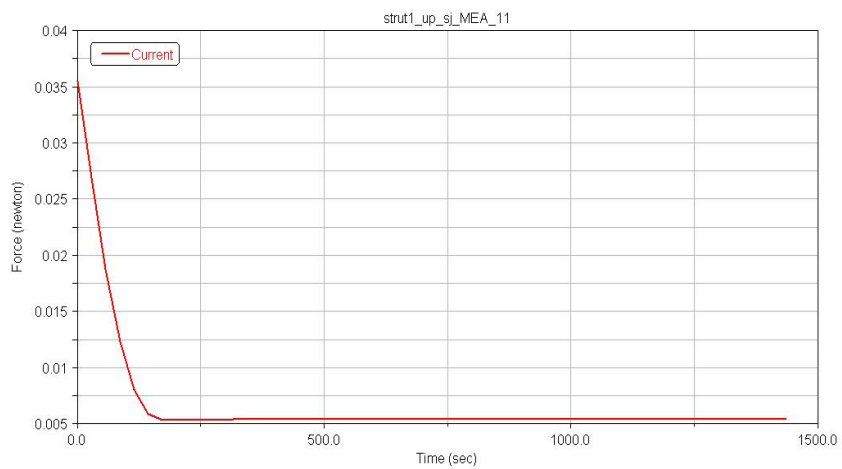
- **X-axis**

- **Y-axis**
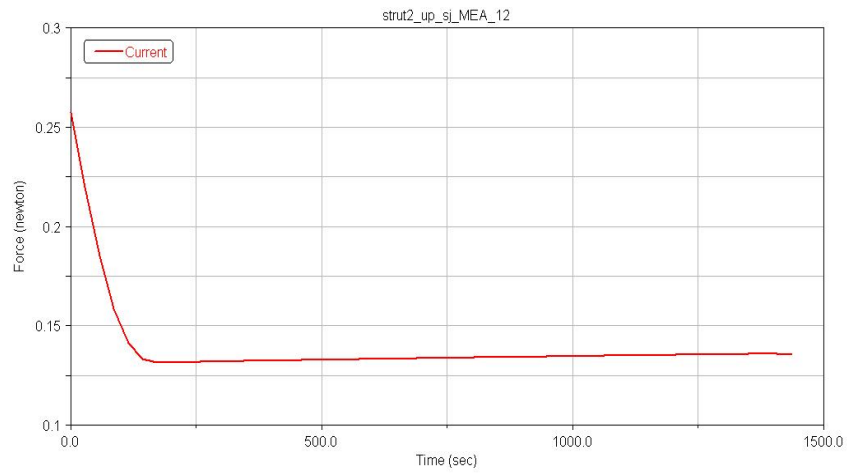
- **Z-axis**

- **Magnitude**

4.2.3.2 Lower Spherical Joints

- **X-axis**
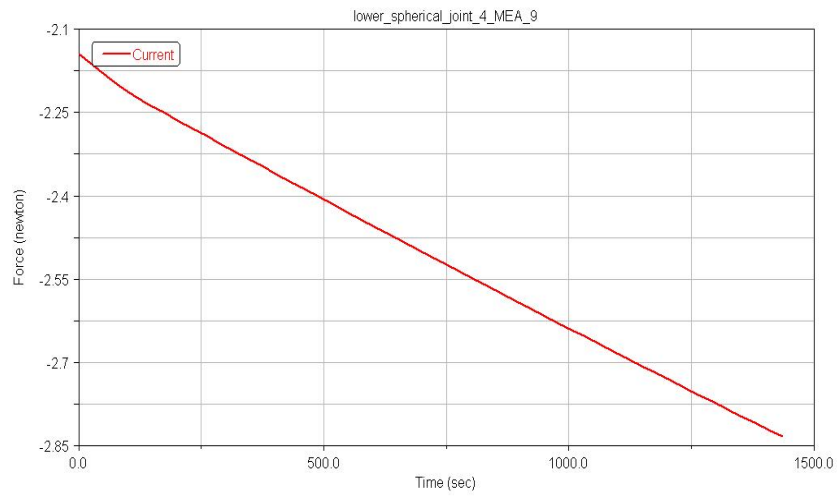
- **Y-axis**
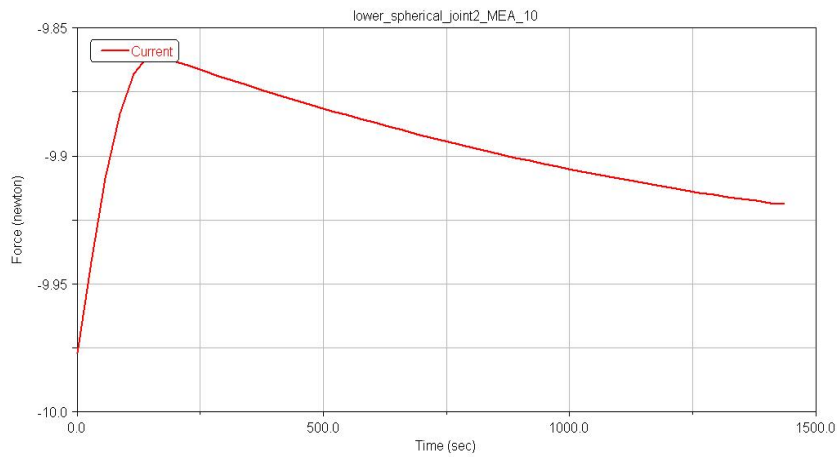
- **Z-axis**
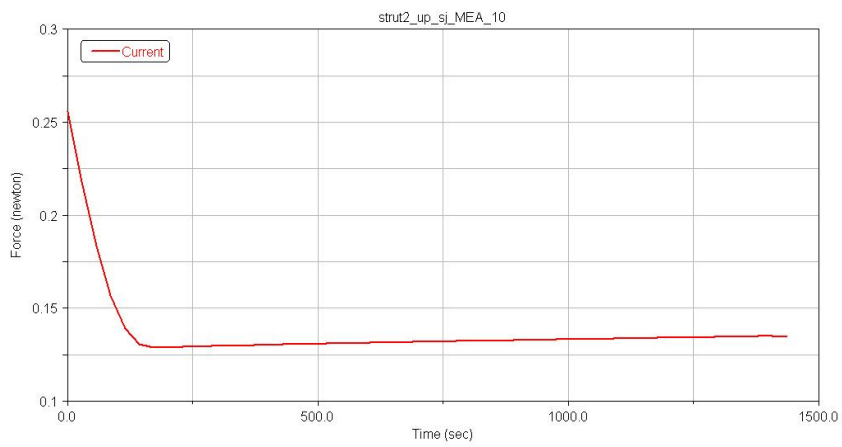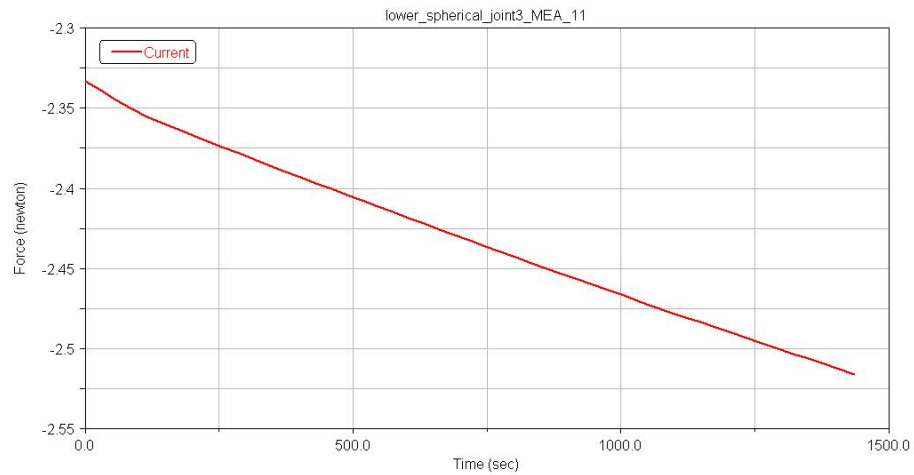

- **Magnitude**
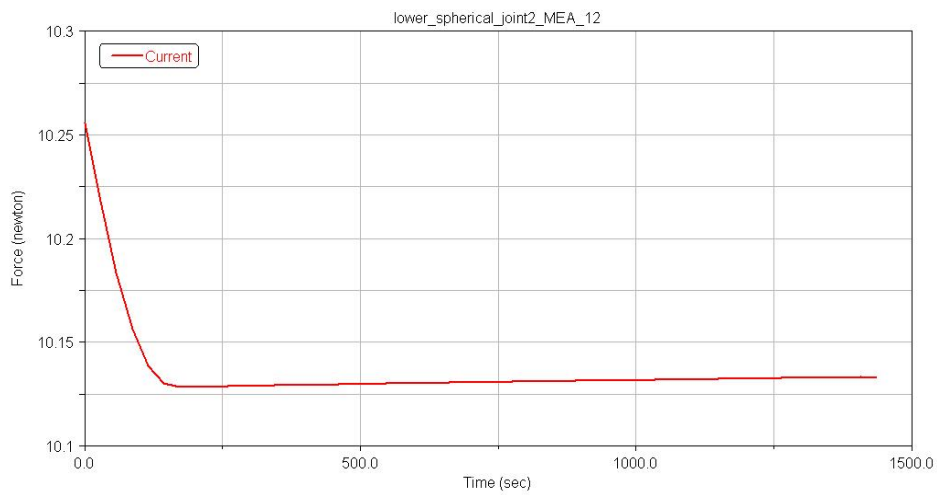
4.2.4 Overview of the Maximum Forces Acquired During Simulations

Upper Spherical Joints	Lower Spherical Joints
• **X-axis:** 0.113 Newton	• **X-axis:** 2.85 Newton
• **Y-axis:** 0.32 Newton	• **Y-axis:** 10.04 Newton
• **Z-axis:** 0.217 Newton	• **Z-axis:** 2.95 Newton
• **Magnitude:** 0.27 Newton	• **Magnitude:** 10.26 Newton

5   SIMULATION

Apart from the kinematics and dynamic analyses presented before, a series of detailed simulation of the platform has been performed. Although computer-aided design (CAD) tools allow modeling of machines as geometric assemblies, they are not suitable to incorporate controllers and to perform dynamic simulations. Commercially available packages Simulink and SimMechanics use a block diagram approach to model control systems and simulate their dynamics. Once the assembly is modeled in a CAD platform, it can be exported into a XML physical modeling file which can be converted into a SimMechanics model in Simulink. For the simulation of the Stewart Platform, the structure is first modeled with SolidWorks, and then the model is translated to SimMechanics model.

5.1   SimMechanics

"SimMechanics is a block diagram modeling environment for the engineering design and simulation of rigid body machines and their motions, using the standard Newtonian dynamics of forces and torques" [5]. In the SimMechanics, it is possible to model and simulate mechanical systems by specifying bodies, their mass properties, their possible motions, kinematics constraints, and coordinate systems. The code allows user to initiate and measure rigid body motions.

SimMechanics provides modeling and simulation of mechanical systems. Distinctively, the code has blocks which directly represent physical components and relations in addition to mathematical operations.

5.2 Characteristics of Stewart Platform

The Stewart Platform contains six linear actuated legs, a stationary rigid base and top plate. The legs are connected to the base and top plates via spherical joints which are defined by coincident central points at the holes and the joints. Each leg has an upper and a lower part connected by a prismatic joint. Therefore, the platform has 13 mobile bodies and 18 joints. The platform model translated from CAD model is modified and corrected with the help of the model created by Smith and Wendlandt [6].

5.3 Modeling Stewart Platform in SimMechanics

The entire model of the Stewart Platform could be divided into five tasks:

1. Modeling Physical Plant
2. Reference Trajectory Generation
3. Controller Design
4. Initialization of the Platform
5. Visualization of the Platform
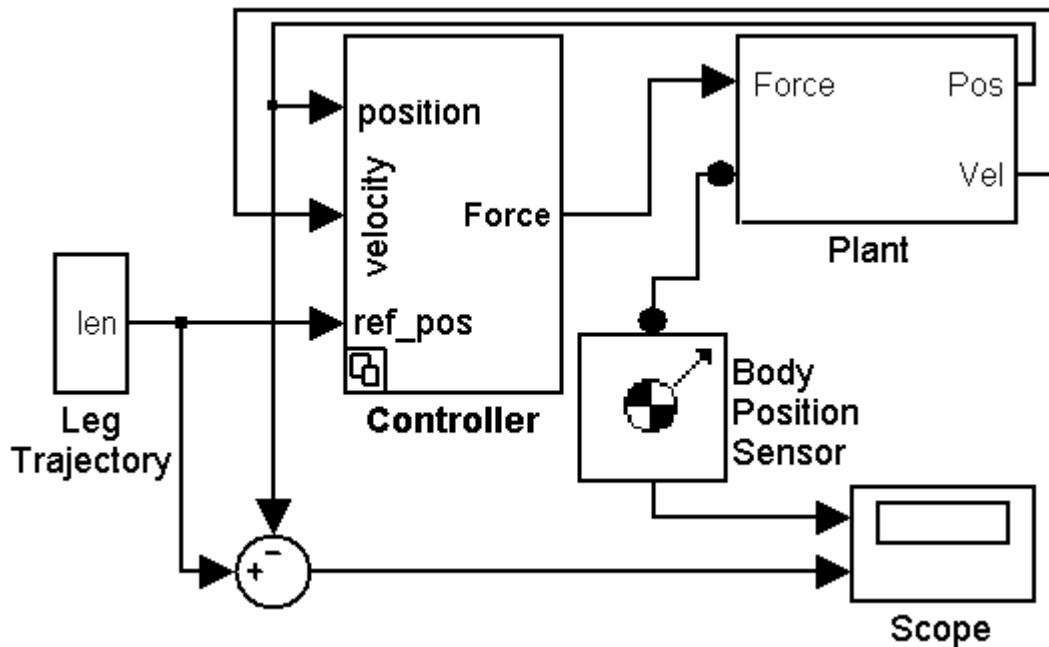
Figure 5.1. Stewart Platform simulation model

5.4   Modeling Physical Plant
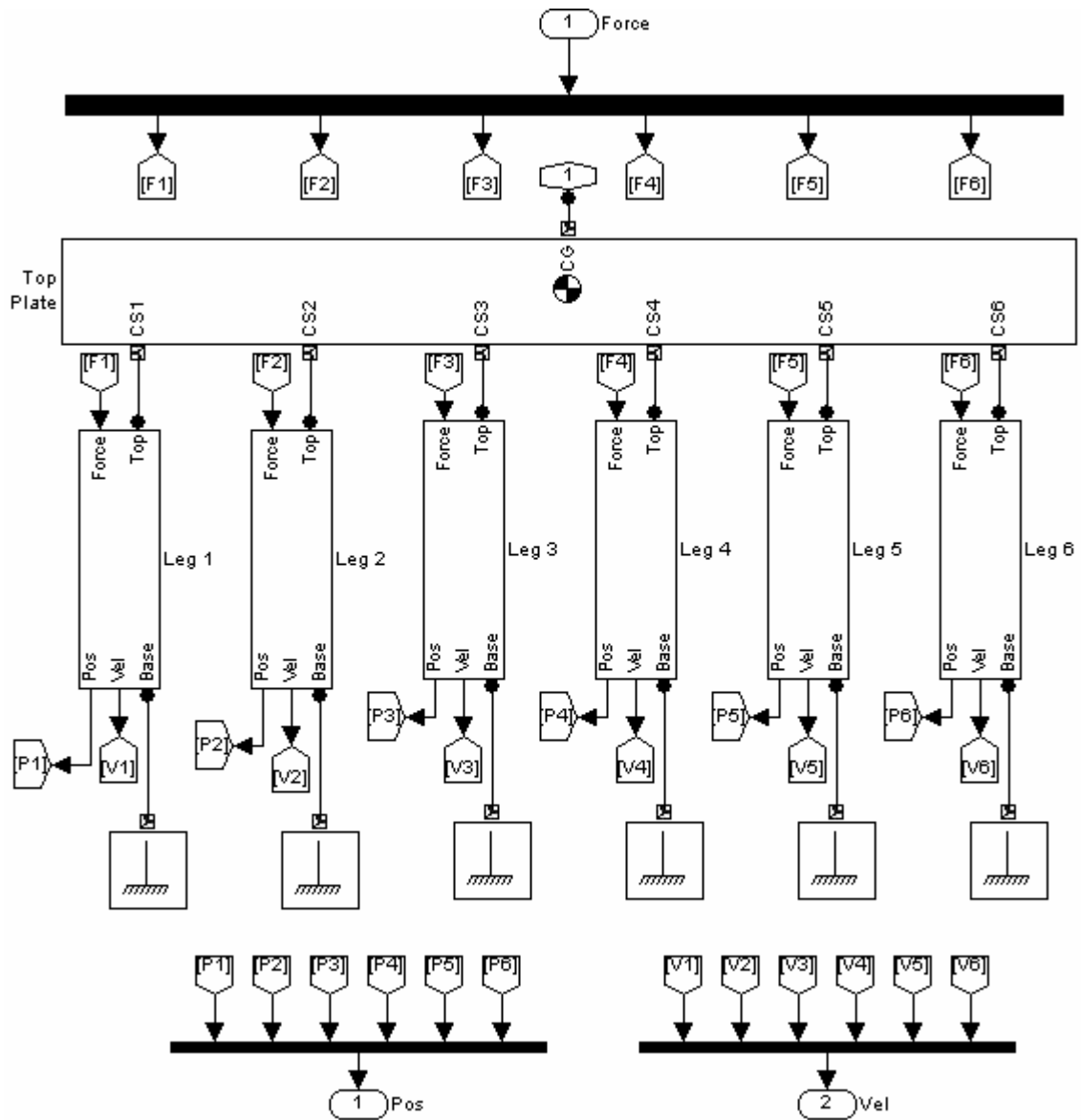
Figure 5.2. SimMechanics plant model of SP

The physical plant subsystem contains six moving legs and top plate. Base is connected to the ground. The points where legs' upper parts and top plates are connected are defined as CS1, CS2, CS3, CS4, CS5, and CS6.
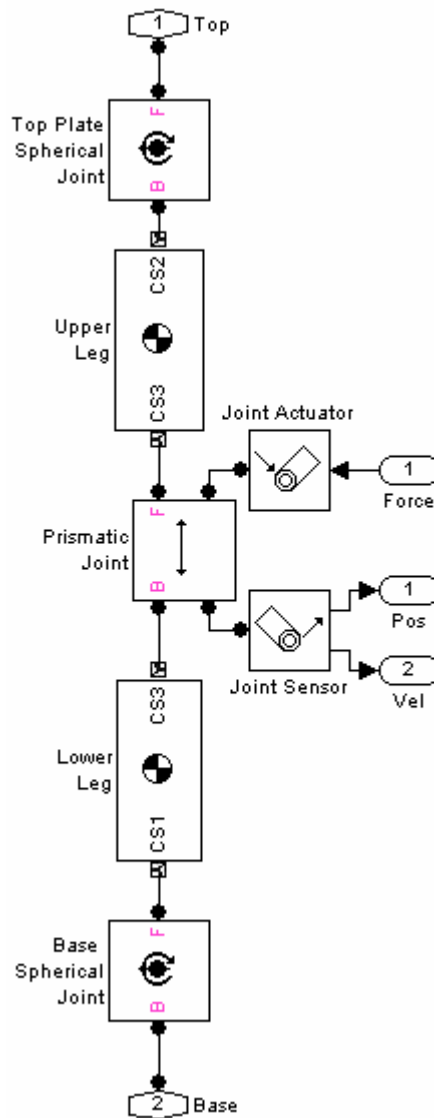
Figure 5.3. Leg subsystem

A leg subsystem is shown in Figure 5.3. The upper and lower parts are connected by a prismatic joint. The prismatic joint is actuated by a given force that is output of the controller. Moreover, in order to observe the errors, a joint sensor is attached to prismatic joint. There are also two spherical joints which connect the leg to the base and top plates.

- The spherical joints connecting legs' lower parts to the base plate impose three constraints:
  - Three positional constraints, requiring two points to be collocated.

- The prismatic joints connecting legs' upper parts to the lower ones impose five constraints:
  - Two positional constraints, allowing the two parts to slide along the leg axis but not translate in the other two directions.
  - Three rotational constraints.
- The spherical joints connecting legs' upper parts to the moving plate impose three constraints:
  - Three positional constraints, requiring two points to be collocated.

For simplicity, the spherical joints which connect lower parts to the base could be replaced with universal joints. Each spherical joint adds three degrees of freedom whereas each universal joint adds only two degrees of freedom. Although there is no mechanism constraining rotation along the leg axis, the legs are unable to rotate in this direction due to the fact that the prismatic joints are actuated only in the leg axis direction. Therefore, universal joints can also be used instead of the spherical joints.

5.5   Reference Trajectory Generation

Before designing a controller for the platform, computation of motion errors, i.e. the difference between the desired and the actual trajectory, is required.
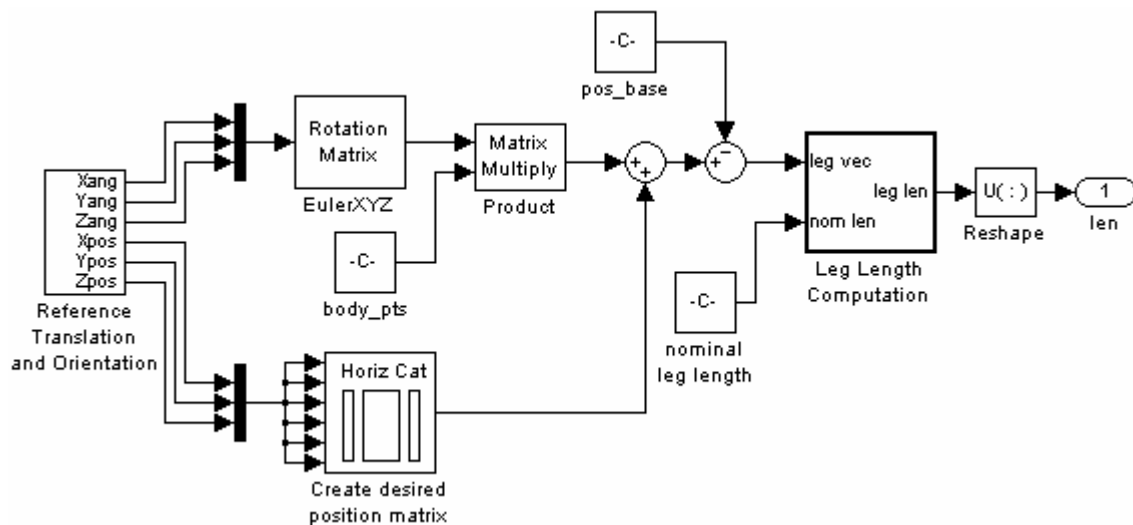
Figure 5.4. Reference trajectory generation for SP simulation
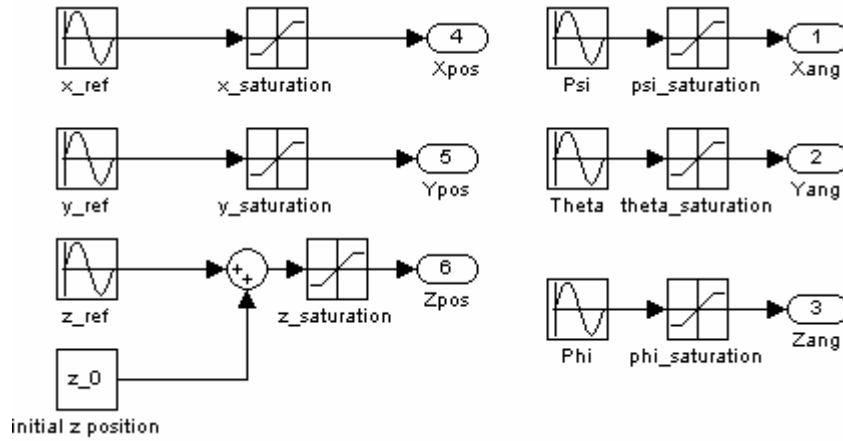
Figure 5.5. Translation and orientation reference blocks

The provided reference uses sinusoidal functions to define the rotational and translational degrees of freedom. It is possible to implement another reference trajectory by replacing these references with other functions or blocks. The saturations calculated in section 3.1.2 are given to the system. The trajectory generation block takes 6 DOF, computes the equivalent rotation and position matrices, and calculates the length vectors for the six legs.

Moreover, it is possible to use space mouse to generate reference trajectory. In other words, it is possible to make the platform track user controlled trajectory in real time. Its block diagram is presented in Figure 5.6.
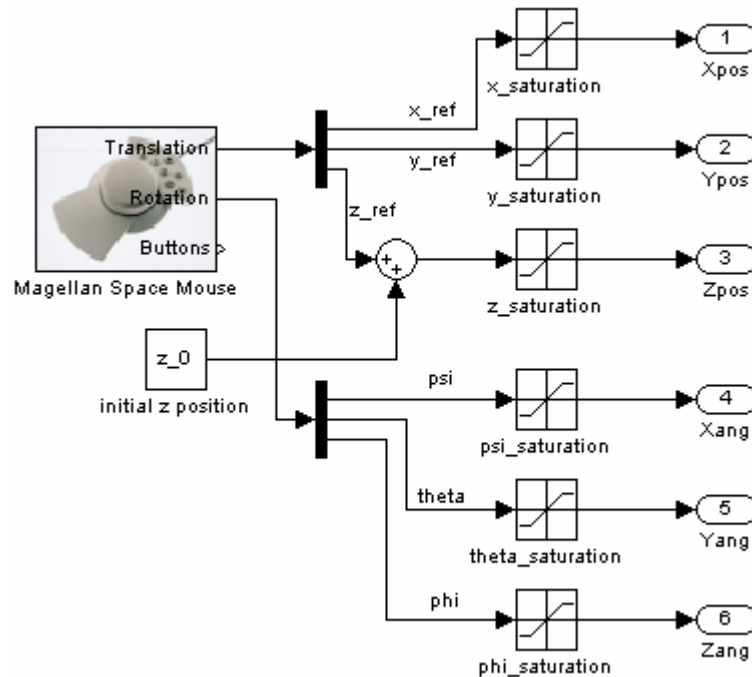
Figure 5.6. References from Magellan space mouse

Space mouse used for the simulation is a high performance motion controller which has advanced 6 DOF optical sensor, and device sensitivity is adjustable to preference [82].

Figure 5.7. Magellan space mouse used for simulation

The actuating force is a function of motion error. Therefore, the input for the control block is the difference between the desired and actual length of the leg.
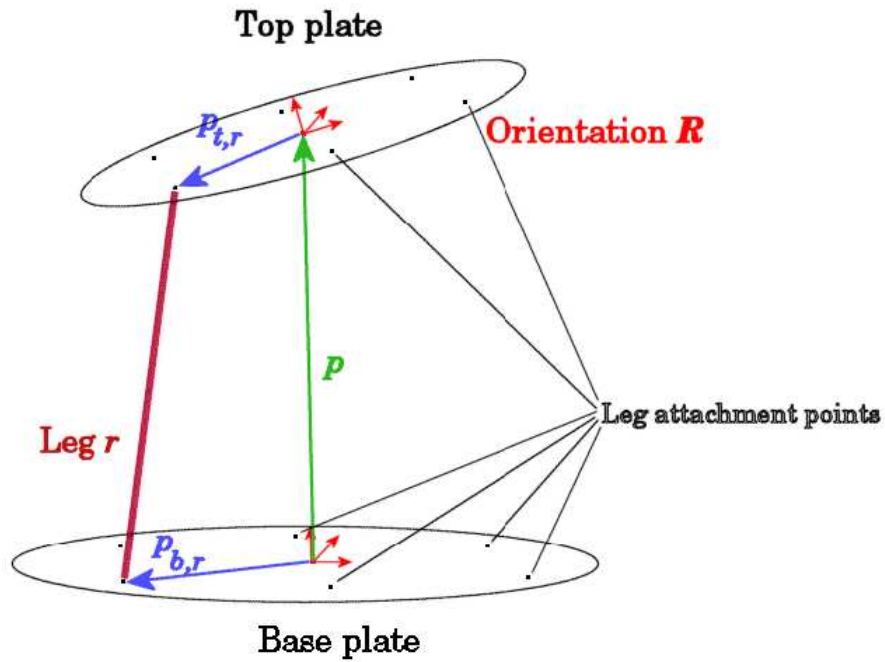
Figure 5.8. Vectors used for reference generation

Control error for each leg length is calculated by:

$$\| (R * p_t + p) - p_b \| - l_n$$

where R is the rotation matrix for the top plate, p is the position of the origin of the top plate, p_t is the leg attachment point at the top plate, p_b is the leg attachment point

at the base, and l_n is the nominal (reference) distance between the top and base attachment points.

In order to compute the control error for each leg, the desired Euler angles are used to generate rotation matrix. p_t and p_b are called back from the m script as 'platform connection points' and 'base connection points' respectively. The difference between the attachment points at base and top plates gives the leg vectors. The lengths of the legs are computed by calculating norm of these vectors. (Detailed information on this subject can be found in Chapter 3 where inverse kinematics solution is explained.)

5.6   Controller Design

The controller is used to control the platform for a predetermined performance. The controller block takes the difference between the desired and actual leg lengths as controller inputs, and generates a response to this leg length error with the force output to actuate the prismatic joints between the lower and upper legs. The controller block accepts leg trajectory, and imposes force on the physical plant by actuating the prismatic joints.

One of the important issues in platform controller design is the selection of the control law. Several models such as proportional, proportional-integral and proportional-integral-derivative controls are considered to select the optimal one.

The proportional control action has very small time constant, and responds to the error instantaneously; however, it has some shortcomings. The main disadvantage of proportional control action is that it results in steady state errors. It can be used only when the gain can be made large enough to reduce errors, and time constant does not require very large actuator output.

The integral control action is used to eliminate the offset error that occurs with proportional control. However, proportional-integral control alone does not give a characteristic equation with enough flexibility to achieve acceptable transient behavior.

Integral action tends to produce a control signal even after the error has vanished. Therefore, the controller should be made aware that the error is approaching zero. One way to accomplish this is to design the controller to react to the rate of change of error

which is derivative action. As a result, PID control and a joint sensor are used in control part of the simulation.

$$F_r = K_p E_r + K_i \int_0^t E_r + K_d \dot{E}_r$$

If E_r is positive, the length of leg is short and F_r is positive (extends)

If E_r is negative, the length of leg is long and F_r is negative (shortens)

If E_r is zero, the length of leg is desired and F_r is zero.

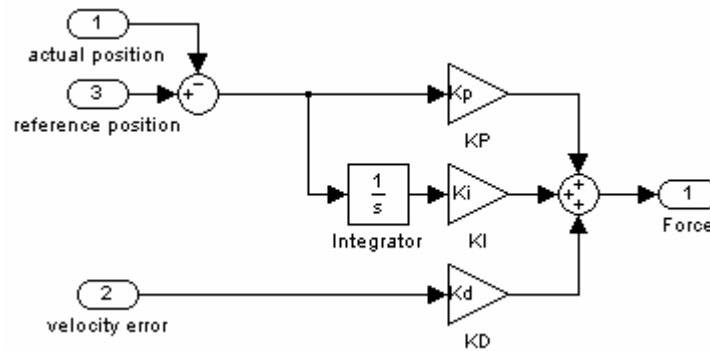The output of the controller F_r is applied to the physical plant as actuating forces.

Figure 5.9. PID controller for the Stewart Platform simulation

In the PID controller, there is no derivative block. Instead, the velocity of the leg vectors is used to avoid negative effects of the derivative action. The velocity of the leg vectors are measured directly from the sensors which are connected at two ends of the prismatic joints.
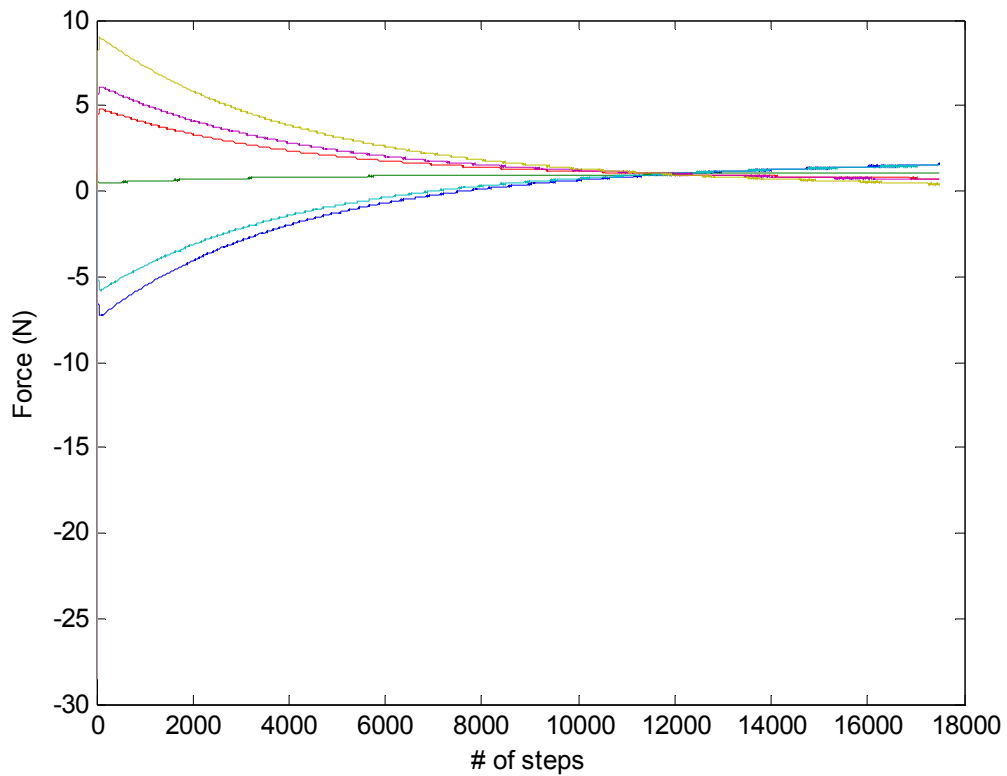
Figure 5.10. Force applied to prismatic joints for simulation (xref: 15, yref: 15, zref: 5, no rotation)

5.7   Initialization of the Platform

When creating physical plant and controller, parameters are defined in the building blocks. Moreover, the geometry, mass properties and inertias are used as variables in these blocks which are defined in m file script. Running this script calls the geometric and mass properties of the initial state. In other words, the model uses this m file as a preload function to initialize with correct values.

The script firstly defines the world coordinate system and basic units. After locating the world coordinate frame to the center of base (stationary) plate, connection points on base and top plates are defined. Moreover, the radii of the base and top plate, their initial position and vectors along the legs are also defined. In other words, the script defines thirteen moving objects' center of gravity and their position vectors.

On the other hand, the script also calculates the mass properties for moving parts of the platform. It computes the inertia tensor, masses of the plates and legs for the

52

given density, their thickness and radii. The other parameters defined in the script are controller parameters. Parameters of the controller K_P, K_I and K_D can be modified for desired characteristics.

5.8   Visualization of the Stewart Platform

The SimMechanics visualization features make it possible to see motion of the platform from different view angles. xz, yz and xy planes are default view options for the visualization window. The window uses the mass and geometric properties which are already defined in m script. The centers of gravity are showed as black circles with a plus inside. As can be seen in Figure 5.11, lower and upper parts of the legs and the upper mobile plate are visualized. The bodies in the platform are shown in red with end points in green-blue color.
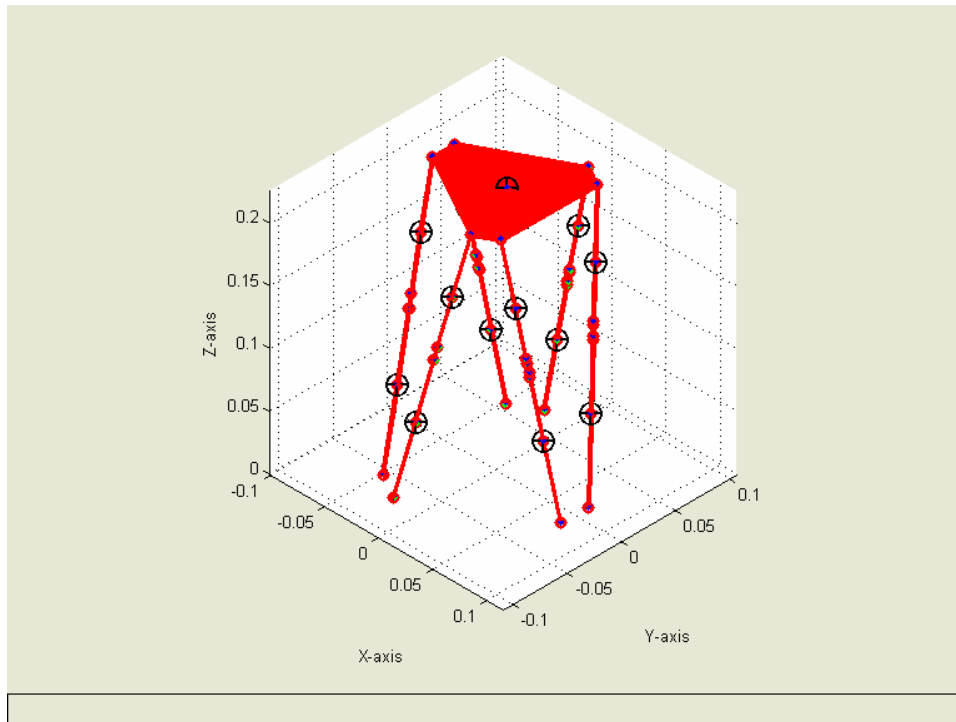
Figure 5.11. 3D view of the simulation
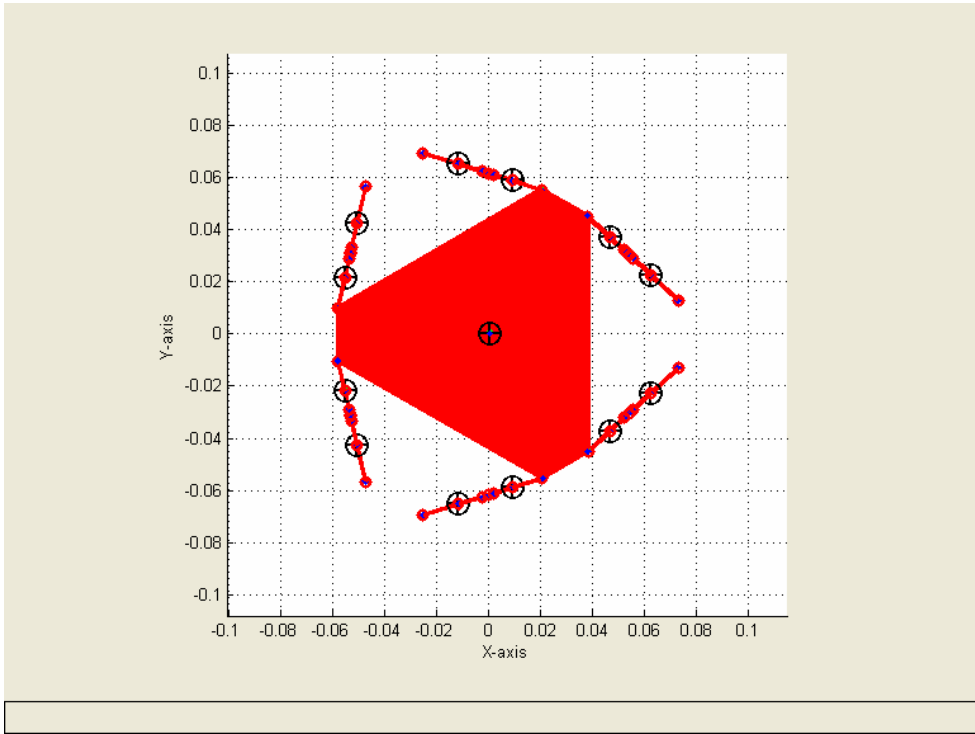
Figure 5.12. View from XY plane
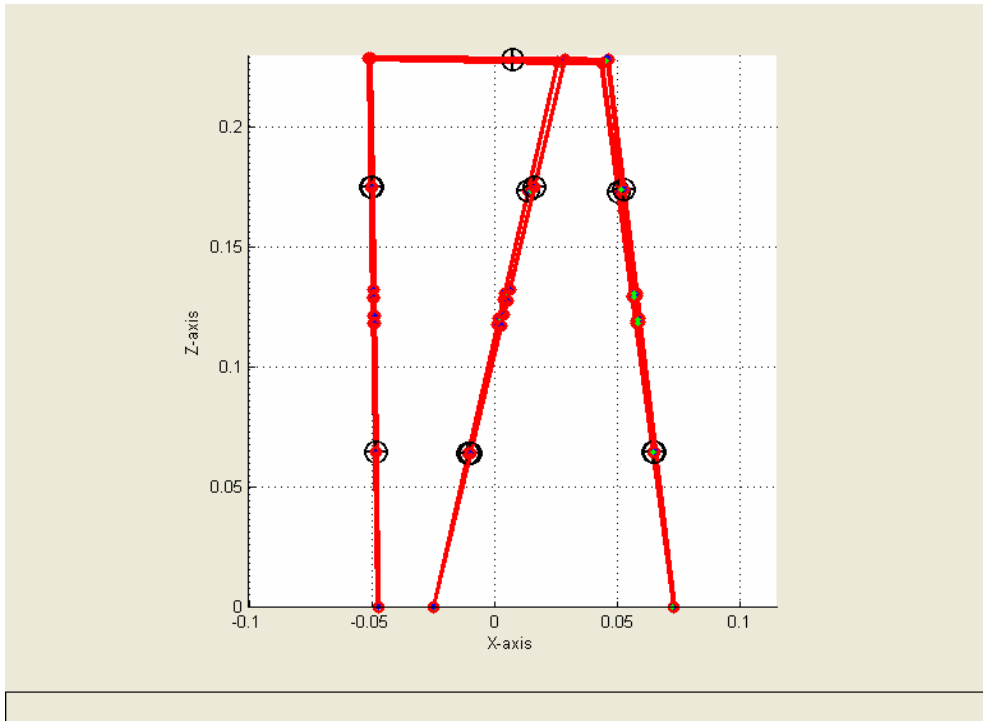
Figure 5.13. View from XZ plane
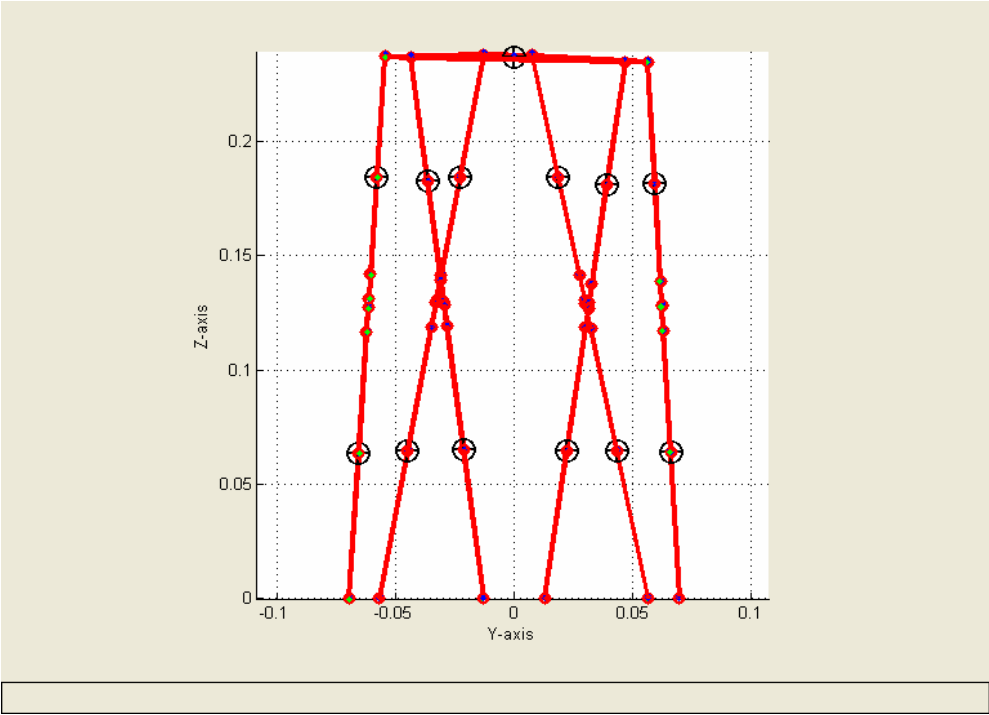
Figure 5.14. View from YZ plane

6   DESIGN

6.1   Overall Design of the Manipulator

In the design of the Stewart Platform PI M-227.25 high resolution DC Mike actuators are used. Travel range of these motors is 25 mm with 0.0035 μm resolution. The motors can handle 40 N push/pull force. As micro level small motion is a desired characteristic, this motor's accuracy would be sufficient with high precision and robust control algorithm. Technical data of selected motors is given in Appendix A [83].
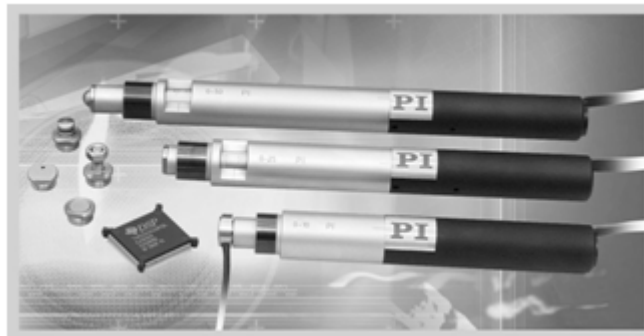
Figure 6.1. PI M-227.25 DC Motors
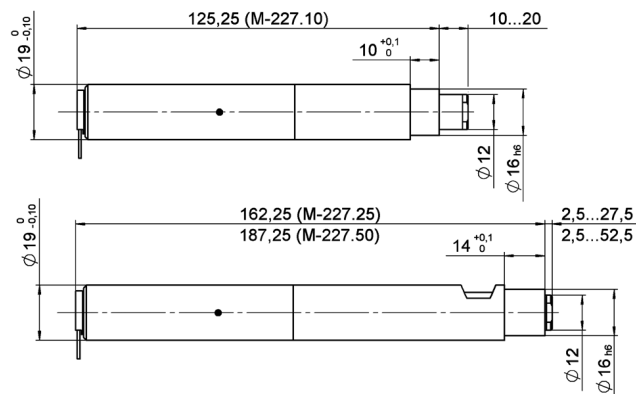
Figure 6.2. Motor drawings

In order to avoid complexities in the design while providing required motion for the system, spherical joints are used to connect the plates with the motors, and magnets are used to provide forces to hold the pieces together.

Magnets are placed with 0.2 mm displacement above and under spherical joints
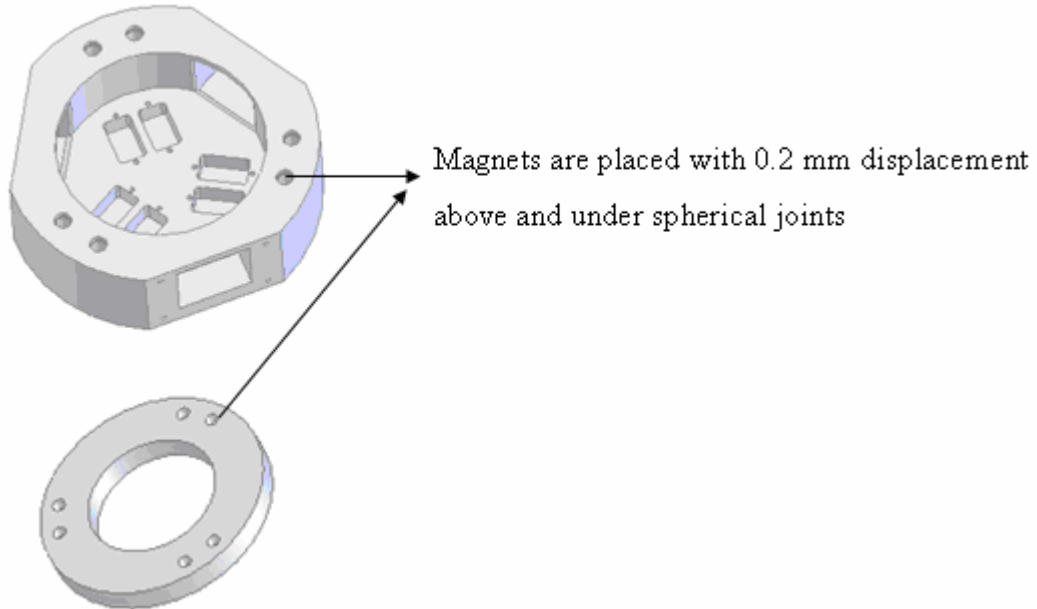
Figure 6.3. Magnet positions in design
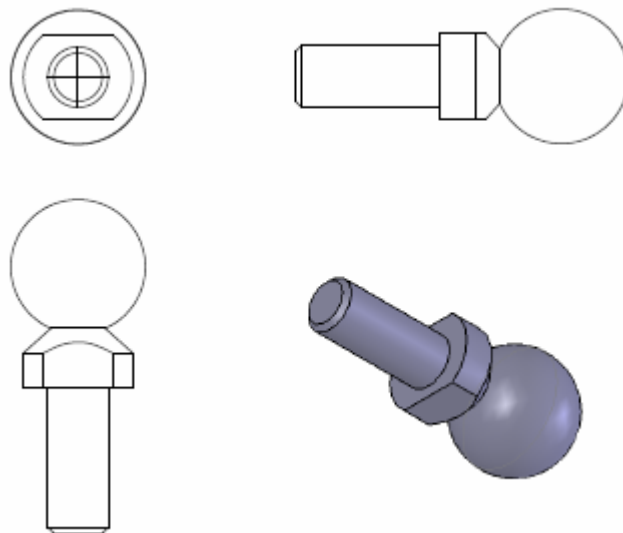
Figure 6.4. Spherical joint used in the design

Joints and motors' connection sections are dimensionally not compatible, and they can not be directly assembled. Therefore, connecting parts between the spherical joints and the motors are needed. Consequently, a ring like part (illustrated in Figure 6.5) is designed for the connection of the motor at the moving platform end.
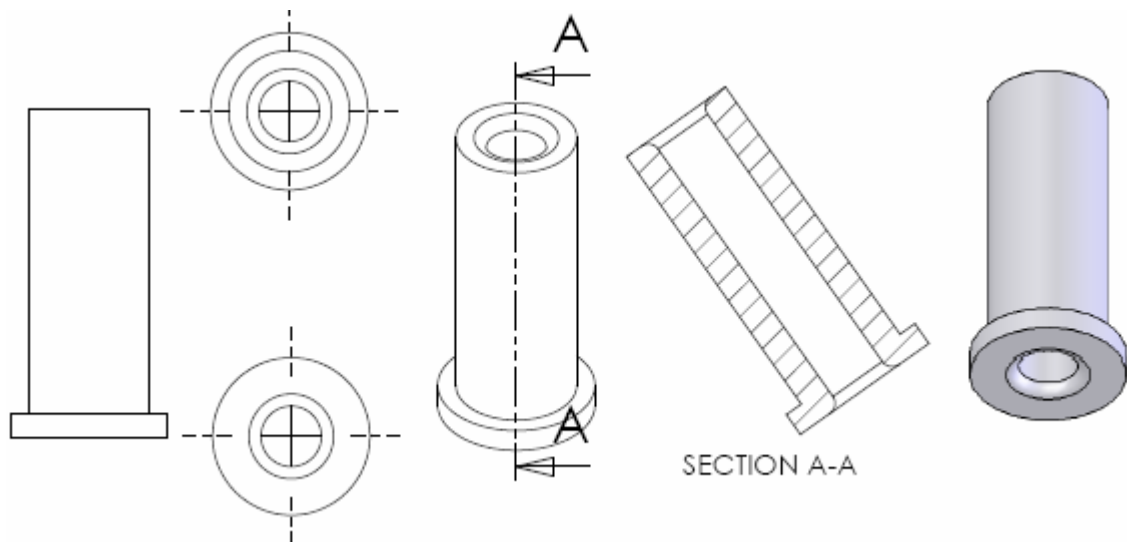
Figure 6.5. Upper connection part

However, for the motor connection at the base plate end, the coupling part must be able to hold the motor in a stable configuration. Therefore, the part is fixed on the motor and does not constraint the spherical joints' movement. There are many problems faced during the design of this part. Due to the motors' extreme sensitivity and vulnerability, utmost care must be given in placing them without sustaining any damage. Therefore, the base that is used to mount the motors is designed very carefully and manufactured with close tolerances. This design provides low weight system with small design using these PI motors.
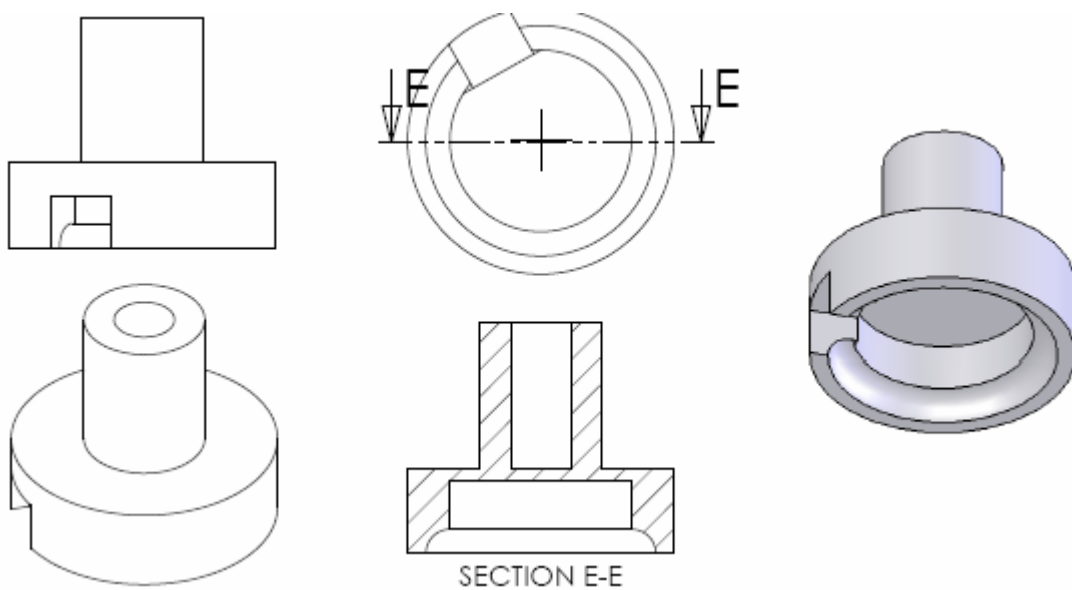
Figure 6.6. Lower connection part
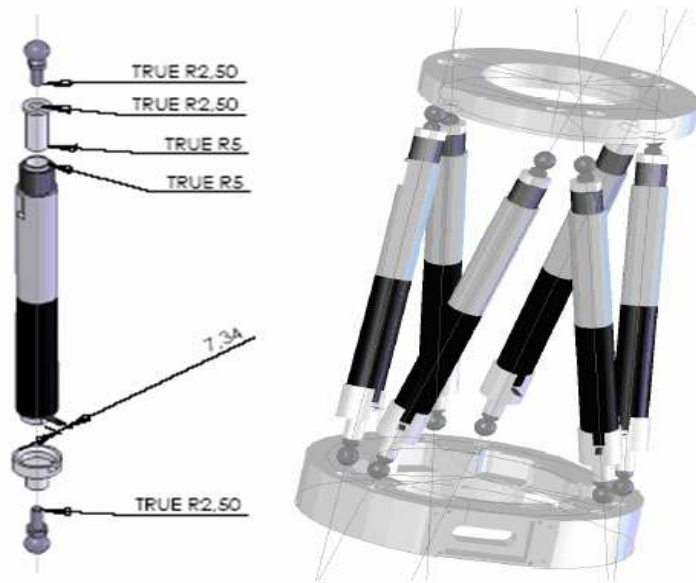
Figure 6.7. CAD model of leg assembly and overall structure
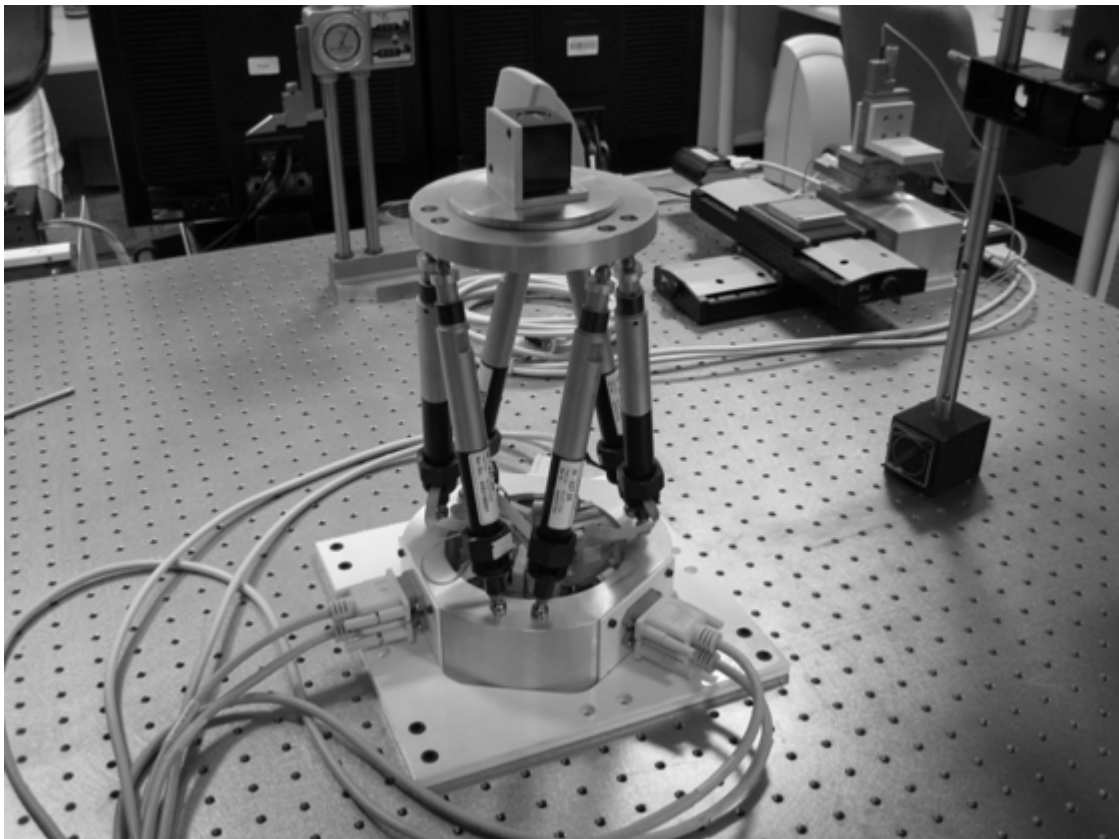
Figure 6.8. Designed Platform

6.2 Flexure Joint Design

For the analysis and optimization of the flexures, COMSOL's FEMLAB Mathematical Modeling Package is used. "COMSOL is a modeling package for simulation of physical processes that can be described with partial differential equations." [84] The flexure geometry is designed using a hyperbolic surface of revolution. Then, it is modeled in COMSOL, the FEM analysis tool. Bezier curves are used to construct hyperbolas. Number of curves used to construct hyperbola is set to 10.

A standard form for the equation of a hyperbola with its center at the origin is given as [85]

$$\frac{x^2}{a^2} - \frac{y^2}{b^2} = 1 \tag{6.1}$$
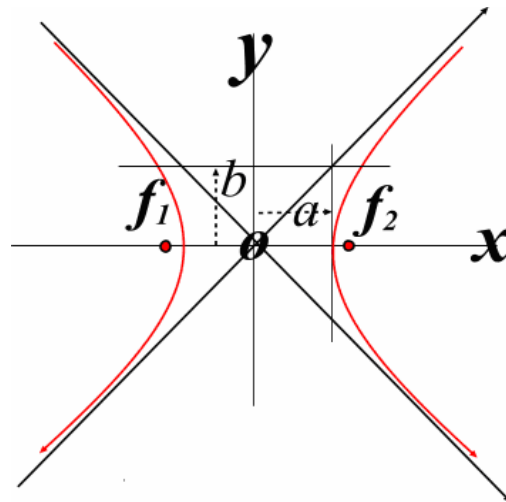
Figure 6.9. Standard hyperbola equation

From (6.1), y can be written as:

$$y = \pm \frac{b}{a}\sqrt{x^2 - a^2} \tag{6.2}$$

$$b = \sqrt{a^2 - c^2} \tag{6.3}$$

$$c = a * e \tag{6.4}$$

where a : the point where hyperbola intersects x axis

b : semi minor axis

c : foci of the hyperbola

e : eccentricity

60
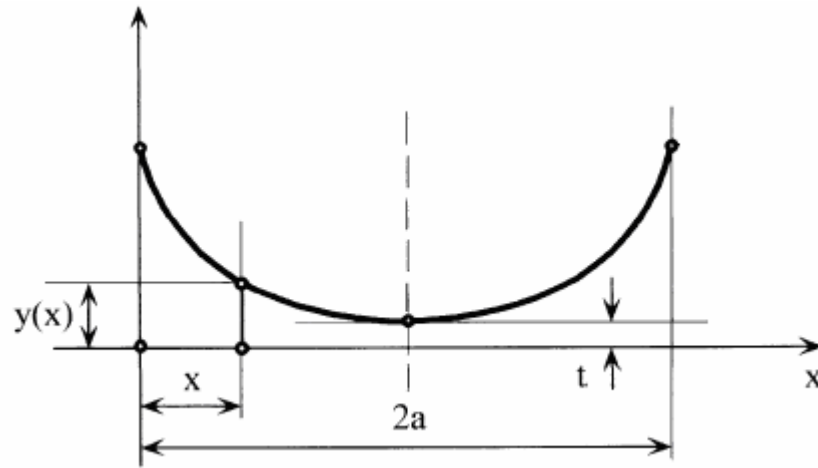
Figure 6.10. Hyperbola used to construct flexure hinge

The shape of the flexure is given in Figure 6.10. However, to construct the flexure as desired, x and y axes have to be exchanged. Besides, parameter 'a' in Equation 6.2 is defined by 't' which denotes thickness. Therefore, after some calculations Equation 6.2 is rearranged as

$$y = \sqrt{\frac{x^2 + t^2(e^2 - 1)}{(e^2 - 1)}} \tag{6.5}$$

After drawing the hyperbola and connecting the lines to x axis to create an enclosed section area, revolving this section around x axis gives the flexure solid model.

6.2.1 Parametric study on optimum flexure design

The parametric search is performed by changing the thickness (T), the length of the flexure (A) and the eccentricity (E) that defines the foci of the hyperbola. There are three boundary sets in the structure. First boundary set, which is surface of the flexure connected to the base of the platform, is fixed in translation and rotation.

First boundary set
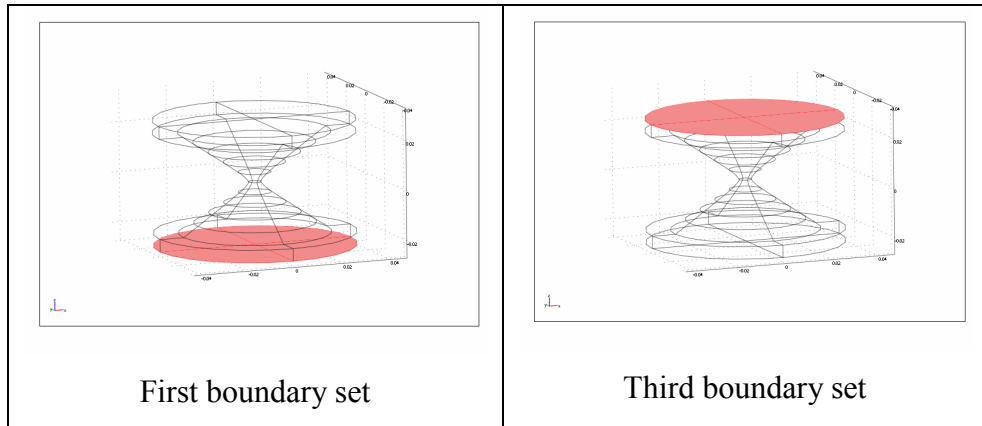
Third boundary set

Figure 6.11. First and third boundary sets

Force is applied along x direction on the third boundary set which is connected to the motors. Calculated maximum stress should not exceed the yield strength of the material. During the search for optimal parameters, while keeping stresses less than the yield strength, deflection that provides maximum allowable motion of the platform should be obtained. Therefore, maximum stress on second boundary set, i.e. the surface of the flexure, deflection in x direction, and angle of the top plane are taken as the output of the search code.
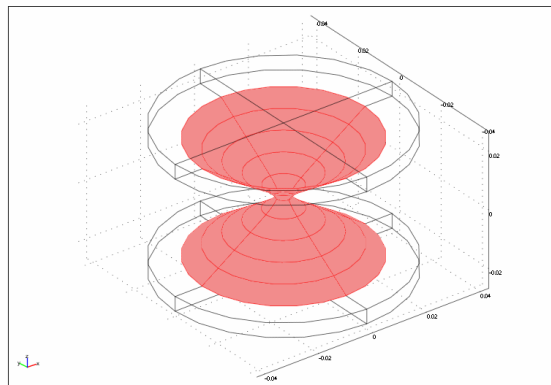
Figure 6.12. Second boundary set

After defining the parameters for search, stress dependence on these parameters are determined as shown in Figure 6.13, 6.14 and 6.15.
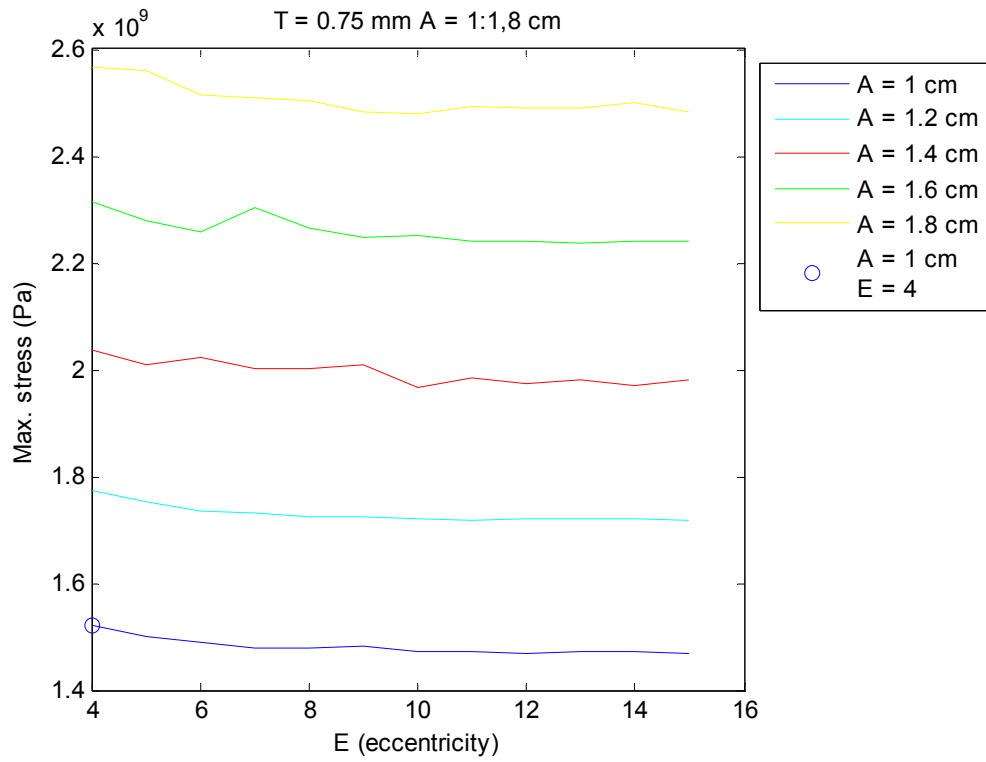
Figure 6.13. Stress dependence on A & E for constant thickness
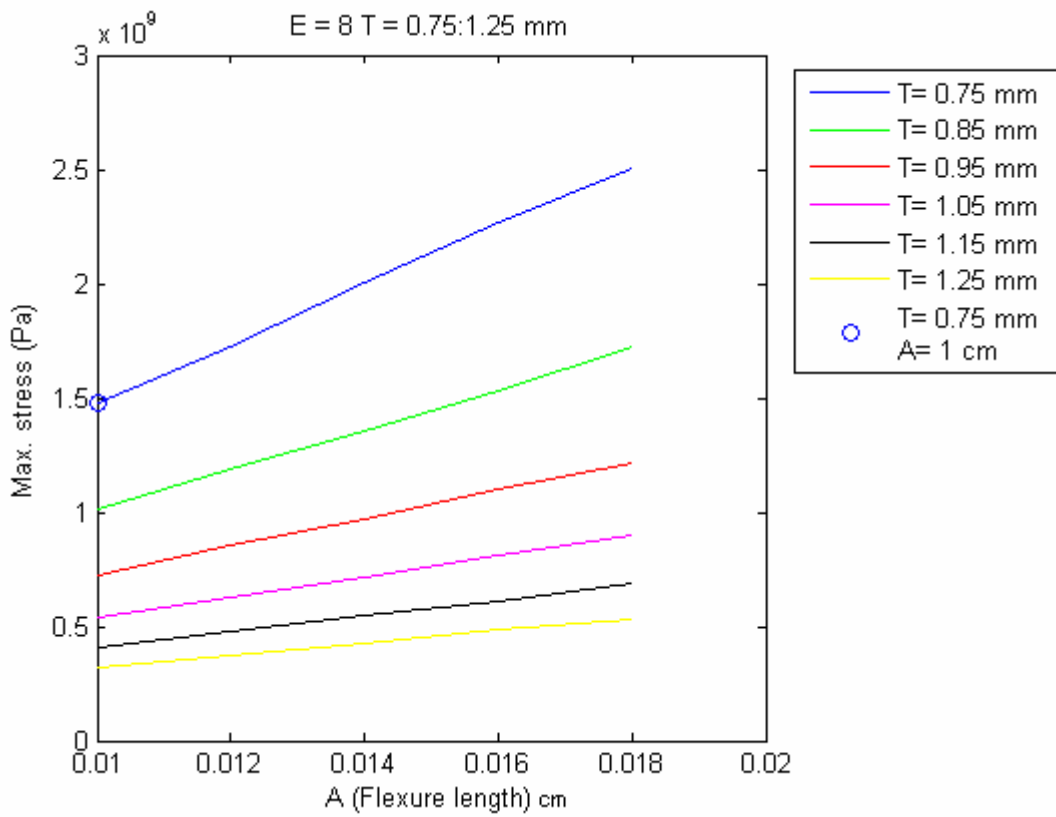
Figure 6.14. Stress dependence on T & A for constant eccentricity

63
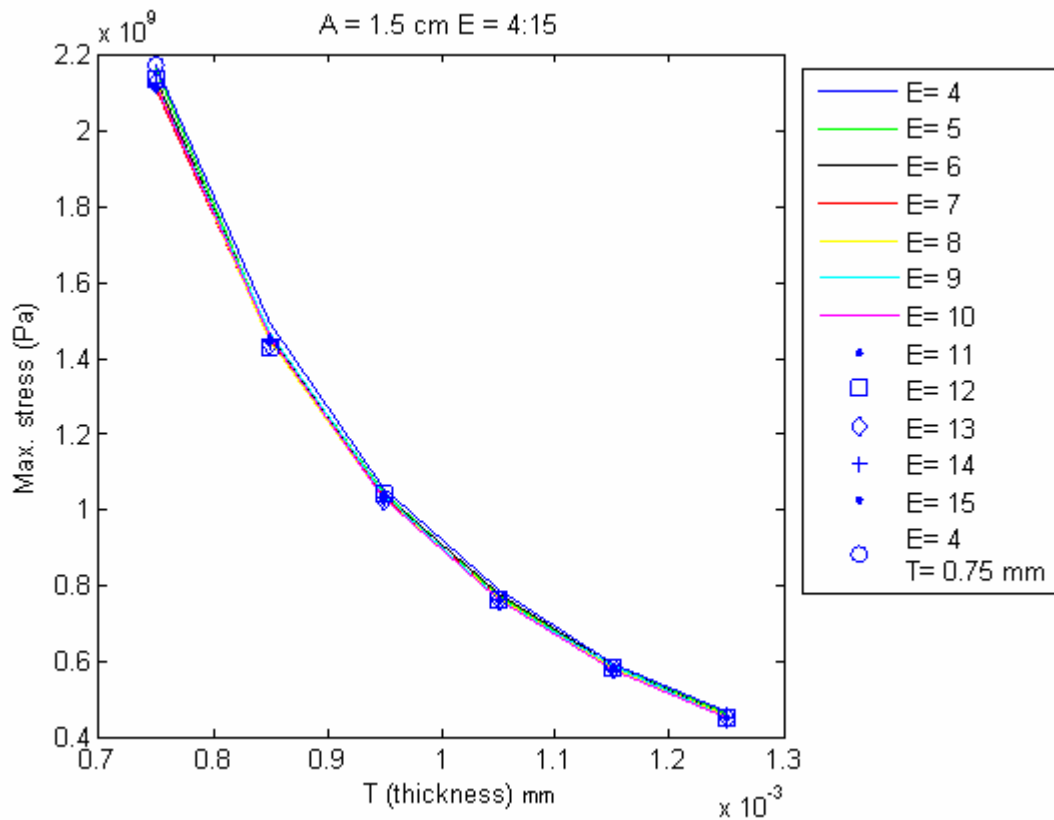
Figure 6.15. Stress dependence on T & E for constant length

6.2.2   Material Selection

Material is selected based on the yield strengths that materials can withstand without permanent deformation. A typical stress-strain curve is shown in Figure 6.16.
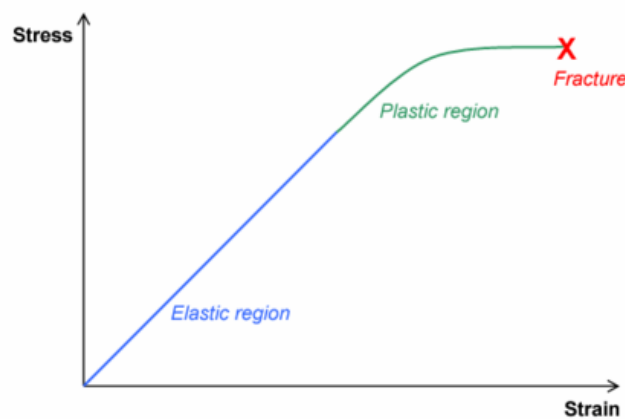
Figure 6.16. Stress-strain curve

Stress vs. Strain curve:

1. Elastic Region
2. Plastic Region
3. Fracture

For stresses below yield strength, all deformation is recoverable, and the material will relax back to its initial shape when the load is removed. For stresses above the yield strength, a portion of the deformation is not recoverable, and the material will not return to its initial shape. This unrecoverable deformation is known as plastic deformation.

Material	Yield strength (MPa)	Ultimate strength (MPa)	Modulus of Elasticity (GPa)
Structural (1020)	207	400	207
Steel (Stainless 201)	301	760	207
Titanium	830	900	105

Table 6.1. Yield/ultimate strengths and elastic modulus of steel and titanium

For many applications plastic deformation is unacceptable, and the yield strength is used as the design limitation [86]. In Table 6.1, it is shown that titanium alloy has high yield strength while its elastic modulus is lower than steel. Titanium has a modulus of elasticity of 105e9 Pa. compared to steel at 207e9 Pa. Therefore, titanium is selected as material for flexures since titanium and its alloys have a high strength to weight ratio as well.

Since titanium has lower modulus of elasticity compared to steel, it has a significantly higher deflection than steel under the same load. Titanium alloys are generally divided into three groups (Alpha, Alpha-Beta and Beta). In analysis, titanium beta-21S is used. The beta alloys have good hardenability. They are slightly denser than other titanium alloys, having densities ranging from 4800 to 5050 kg/m^3, and more importantly, they have yield strength values up to 1345 x 10^6 Pa. [87].

6.2.3 Results

Parametric search and optimization is performed to achieve maximum motion that platform can perform, and at the same time for minimal stress that should not exceed the yield strength of the material selected. From inverse kinematics, maximum angle change between legs' vectors and base plane is calculated as approximately 13.9 degrees. Therefore, the third boundary's orientation allows sufficient change to provide necessary motion for the platform. Besides, stress on second boundary does not exceed 1.345e9 Pa. Maximum stress occurs at z=0, y=0 and x=-t/2 or +t/2. There is a slight stress difference at points x=-t/2 and +t/2. Therefore, stresses at both points are checked and maximum value is considered in the calculations. Parameters' lower and upper boundaries are selected as 1.01 and 25 for eccentricity, 1.5 mm. and 4 mm. for thickness, and 2 cm and 15 cm. for length of the flexure respectively. There are some solutions that satisfy mentioned requirements; however, three of them are worth consideration for their compatibility in the design.

1. T/2 = 1.25 mm 2A= 6.916 cm. E=12
    Maximum stress: 1.0125e9 Pa.
2. T/2 = 1.5 mm. 2A=10 cm. E= 14.6
    Maximum stress: 8.5403e8 Pa.
3. T/2 = 2 mm. 2A=15 cm. E=24.32
    Maximum stress: 5.3371e8 Pa.
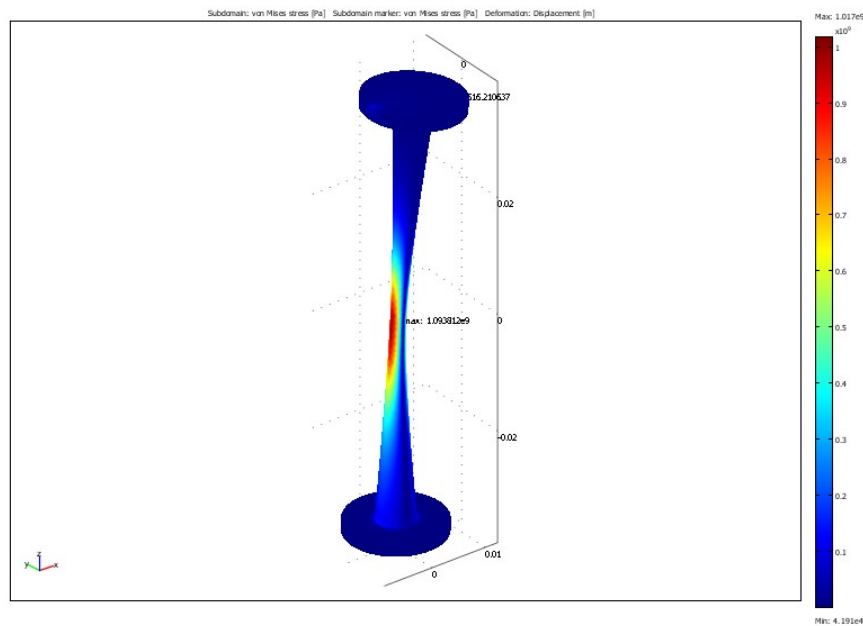
Figure 6.17. T/2 = 1.25 mm 2A = 6.916 cm E = 12, 3D view
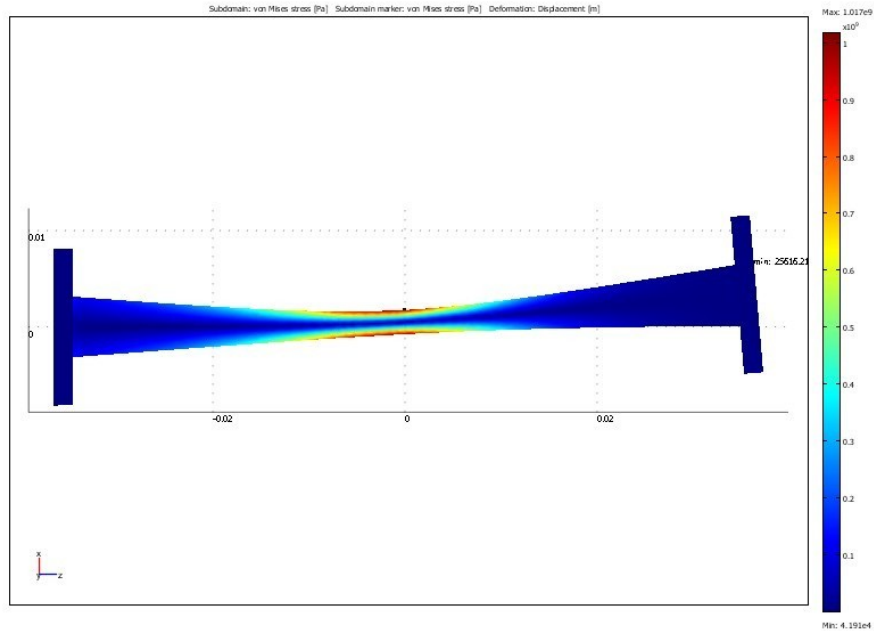
Figure 6.18. T/2 = 1.25 mm 2A = 6.916 cm E = 12, XZ view

Since length scale of the first solution is most suitable one for the design, this solution is applied to the joints of the platform. However, if titanium with high yield strength can not be obtained, other two solutions can be considered. Second and third solutions are given in Figure 6.19 and 6.20.
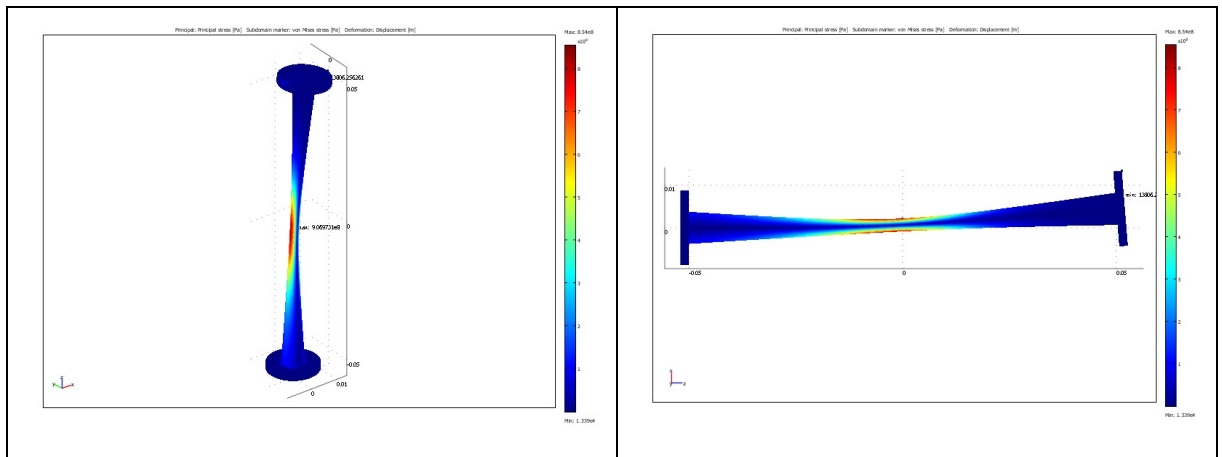
Figure 6.19. T/2 = 1.5 mm 2A = 10 cm E = 14.6
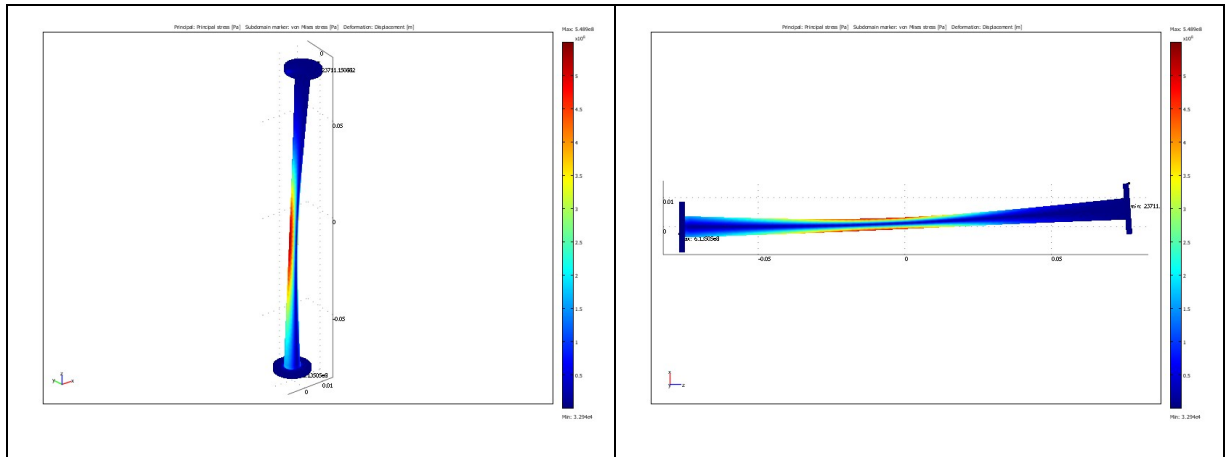
Figure 6.20. T/2 = 2mm 2A = 15 cm E = 24.32

7   CONTROL

Even among the systems which are manufactured for an identical design, differences due to manufacturing processes and tolerances can not be avoided. These parameter variations present uncertainties such as the uncertainty in friction parameters due to time-varying friction characteristics, operating condition changes, load changes, etc. It is highly desired that the same control settings should meet the control specification for all machines of the same type, i.e., without individual tuning. Therefore, it is necessary to find a methodology that produces a robust controller that can be designed by considering only nominal process parameters.

Variable structure control (VSC), which is frequently known as sliding mode control (SMC), is characterized by a discontinuous control action which changes structure upon reaching a set of predetermined switching surfaces. This kind of control may result in a very robust system therefore provides a possibility for achieving the goals of high-precision and fast response.

The most distinctive property of VSS is that the closed loop system is completely insensitive to system uncertainties and external disturbances. However, VSS did not receive wide acceptance among engineering professionals until the first survey paper by Utkin [88]. Since then, and especially during later 80's, the control research community has shown significant interest in VSS. This increased interest is explained by the fact that robustness has become a major requirement in modern control applications.

Due to its excellent invariance and robustness properties, variable structure control has been developed into a general design methodology, and extended to a wide range of systems including multivariable, large-scale, infinite dimensional and stochastic systems. The applications include control of aircraft and spacecraft flight, control of flexible structures, robot manipulators, electrical drives, electrical power converters and chemical engineering systems.

7.1   Sliding-Mode in Variable Structure Systems

Some promising features of SMC are listed below:

- The order of the motion can be reduced.
- The motion equation of the sliding mode can be designed linear and homogenous, despite that the original system may be governed by non-linear equations.
- The sliding mode does not depend on the process dynamics, but is determined by parameters selected by the designer.
- Once the sliding motion occurs, the system has invariant properties which make the motion independent of certain system parameter variations and disturbances. Therefore, the system performance can be completely determined by the dynamics of the sliding manifold.

Consider the system defined below:

$$\dot{x} = f(x,t) + B(x,t)\,u(x,t) \ , \ x \ \in \ \mathbb{R}^n, u \in \mathbb{R}^m$$

where $f(x,t)$ and $B(x,t)$ are assumed continuous and bounded, and the rank of $B(x,t)$ is m. The discontinuous control is given by

$$u = \begin{cases} u^+(x,t) \ if \ \sigma(x) > 0 \\ u^-(x,t) \ if \ \sigma(x) < 0 \end{cases} \tag{7.1}$$

$$\sigma(x)^T = \{\sigma_1(x), \sigma_2(x), ..., \sigma_m(x)\}, \sigma(x) = G(x^r - x) \tag{7.2}$$

where $u^+(x,t)$, $u^-(x,t)$ and $\sigma(x)$ are continuous functions. Since $u(x,t)$ undergoes discontinuity on the surfaces $\sigma_i(x) = 0$, $\sigma_i(x) = 0$ is called the switching surface or the switching hyper plane.

Let $S = x\,|_{\sigma(x)=0}$ be a switching surface that includes the origin $x = 0$. If, for any x_0 in S, $x(t)$ is in S for $t > t_0$, then $x(t)$ is sliding mode of the system in which the motion is determined by the manifold equation only. Therefore, motion order is reduced to the order of control inputs, namely m. The order reduction means that system model of the n_{th} order is decomposed into two modes, one is the so-called "reaching mode" which is defined by a motion of $(n-m)_{th}$ order, and the other is the sliding mode defined by the

motion on the sliding manifold of m_{th} order. Decoupled motion equations of the system could be written as:

$$\dot{x}_1 = f_1(x_1, \sigma(x))$$
$$x_2 = \sigma(x)$$

(7.3)

for $x_1, f_1 \in \mathbb{R}^{n-m}$ and $x_2 \in \mathbb{R}^m$. If $\sigma(x) = 0$ is appropriately designed in such a way that it satisfies the control objectives (e.g. x follows x^{ref}), then SMC is realized.
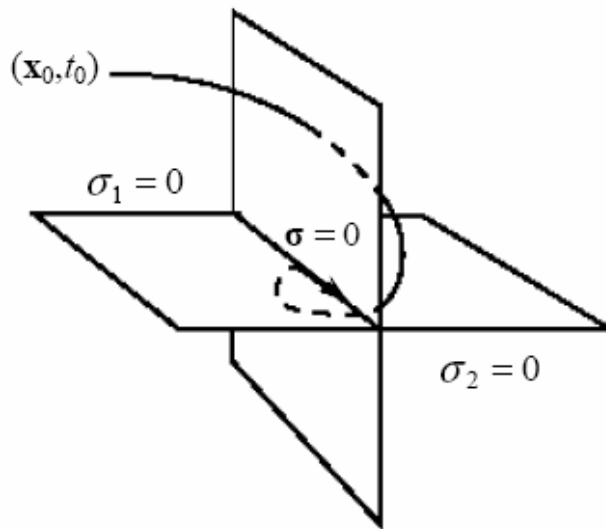
Figure 7.1. Two intersecting switching surfaces

Existence of a sliding mode requires stability of the state trajectory towards the sliding surface $S = x \big|_{\sigma(x)=0}$ at least in the neighborhood of S, i.e., the representative point must approach the sliding surface at least asymptotically. This sufficient condition for sliding mode is called the reaching mode or reaching phase. The largest neighborhood of S for which the reaching condition is satisfied is called the region of attraction.

In order to guarantee the desired behavior of the closed-loop system, the sliding mode controller requires infinitely fast switching mechanism. However, due to physical limitations in real-world systems, directly applying the above mentioned control will always lead to some oscillations in some vicinity of the sliding surface, i.e., the so called chattering problem. Since modern controllers are most likely implemented in digital computers, SMC design in discrete-time should be implemented.

7.2   Sliding-Mode Controller Design and Realization of Discrete-Time Control

The VSS theory was originally developed from a continuous time perspective. It has been realized that directly applying the continuous-time SMC algorithms to discrete-time systems will lead to some unconquerable problems, such as the limited sampling frequency, sample/hold effects and discretization errors. Since the switching frequency in sampled-data systems can not exceed the sampling frequency, a discontinuous control does not enable generation of motion in an arbitrary manifold in discrete-time systems. This leads to chattering along the designed sliding surface, or even instability in case of a too large switching gain.
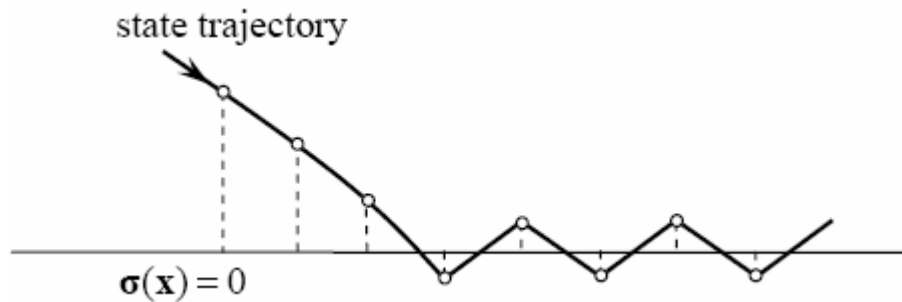
Figure 7.2. Discrete-time system with discontinuous control

The discontinuous sliding-mode controller involves a continuous plant model with a discontinuous right-hand-side due to the switching control function as mentioned above. Due to the problems with the discrete implementation of this discontinuous approach, Drakunov and Utkin [89] introduced a continuous approach to SMC for an arbitrary finite dimensional discrete-time system. This approach implies that for a sampled-data controller, as the system becomes discrete, the controller should be continuous to overcome the sampling frequency limitations of the discontinuous approach. For such continuous implementation of SMC, plant motion is proven to reach the sliding manifold of predefined state trajectory in finite time.

Derivation of the control law starts with the selection of a positive definite Lyapunov function candidate $V(\sigma)$ to satisfy Lyapunov stability criterion as the reaching condition.

$$\dot{V}(\sigma)V(\sigma) < 0 \tag{7.4}$$

Lyapunov function is selected such that it is positive definite.

$$V(\sigma) = \frac{\sigma^T \sigma}{2} \tag{7.5}$$

Hence the derivative of the Lyapunov function is

$$\dot{V}(\sigma) = \sigma^T \dot{\sigma} \tag{7.6}$$

The derivative of the Lyapunov function is selected to be

$$\dot{V}(\sigma) = -\sigma^T D\sigma \tag{7.7}$$

where $D \in \mathbb{R}^{mxm}$ being positive definite symmetrical matrix. The Lyapunov function and its derivative having opposite signs with the aid of control, enforce the system to move to $\dot{V}(\sigma) = V(\sigma) = 0$ and hence, ensure stability.

If (7.6) and (7.7) are combined, the following result is obtained:

$$\sigma^T(\dot{\sigma} + D\sigma) = 0 \tag{7.8}$$

A solution for (7.8) is as follows

$$\dot{\sigma} + D\sigma = 0 \tag{7.9}$$

The derivative of the sliding function combined with (10.2) leads to

$$\dot{\sigma} = G(\dot{x}^{ref} - \dot{x}) + \frac{\partial \sigma}{\partial t} = G\dot{x}^{ref} - Gf + \frac{\partial \sigma}{\partial t} - GBu(t) \tag{7.10}$$

Rewriting (7.10) gives

$$\dot{\sigma} = \left(G\dot{x}^{ref} - Gf + \frac{\partial \sigma}{\partial t} \right) - GBu(t) = GBu_{eq} - GBu(t) = GB(u_{eq} - u(t)) \tag{7.11}$$

If (7.11) is inserted in (7.9), and the result is solved for the control

$$u(t) = u_{eq} + (GB)^{-1} D\sigma \tag{7.12}$$

It can be seen from (7.11) that u_{eq} is difficult to calculate if information about $f(x)$ is not available. Using the fact that u_{eq} is a smooth function, then (7.11) can be written as [90],

$$u_{eq} \cong u(t^-) + (GB)^{-1}\dot{\sigma} = \hat{u}_{eq} \tag{7.13}$$

where

$$t^- = t - \Delta, \Delta \to 0 \tag{7.14}$$

and $\hat{u}_{eq}$ is the estimate of the equivalent control. If (7.13) is inserted back into (7.12), an approximation of the control is obtained.

$$u(t) = u(t^-) + (GB)^{-1}(D\sigma + \dot{\sigma})\big|_{t=t^-} \qquad (7.15)$$

Therefore, the term $(GB)^{-1}(D\sigma + \dot{\sigma})\big|_{t=t^-}$ is used in updating the control in a recursive formula. Note that once on the sliding manifold, $u(t^-)$ becomes the same as the equivalent control.

Although (7.15) is an approximation of (7.11) in discrete-time, it can be used to push σ to zero such that (7.9) is satisfied, and stability is reached. During implementation, the control defined by (7.15) is used with a nominal value of B instead of its exact value since it is difficult to obtain. When actual implementation is done, a tuning term K is introduced before $(GB)^{-1}(D\sigma + \dot{\sigma})\big|_{t=t^-}$ such that the control becomes [91]

$$u(t) = u(t^-) + K(GB)^{-1}(D\sigma + \dot{\sigma})\big|_{t=t^-} \qquad (7.16)$$

For a general system K is a positive diagonal matrix. It is possible to rewrite (7.16) for discrete-time implementation as follows:

$$u((k+1)T_s) = u(kT_s) + K(GB)^{-1}(D\sigma + \dot{\sigma})\big|_{t=t^-} \qquad (7.17)$$

where T_s is the sampling time of the controller. The derivative of the sliding surface is obtained from the backward difference.

$$\dot{\sigma}(kT_s) \approx \frac{\sigma(kT_s) - \sigma((k-1)T_s)}{T_s} \qquad (7.18)$$
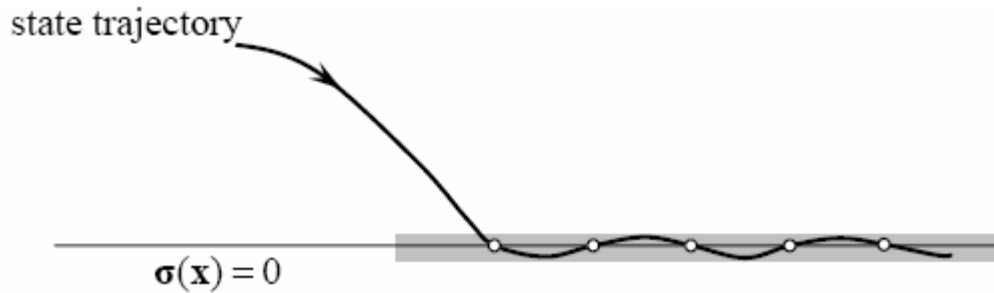
Figure 7.3. Discrete-time sliding mode in sampled-data systems

For a discrete-time system, the discrete sliding mode can be interpreted as that the states are only required to be kept on the sliding surface at each sampling instant. Between the samples, the states are allowed to deviate from the surface within a boundary layer. Note that the control defined by (7.17) is continuous; therefore, chattering is no longer a matter of concern. This is the most striking contrast between discrete-time sliding mode and continuous-time sliding mode. Furthermore, in

continuous-time systems with continuous control, the sliding manifold of state trajectories can be reached only asymptotically, while in discrete time systems with continuous control, sliding motion with state trajectories in some manifold may be reached within a finite time interval [92].

7.3   Control Structure of the System

The control model of the mechanism consists of 'Set Position', 'Trajectory Generation' and 'Strut' subsystems. Trajectory generation subsystem calculates reference leg lengths from position and orientation reference for the center of the moving platform. For controller, position of each leg is obtained from encoders, and error is calculated. Controller subsystem is in leg subsystem. It takes position error value in the leg lengths, and gives current as output. This current value is given to the controller board, and then fed to the motors from the controller.
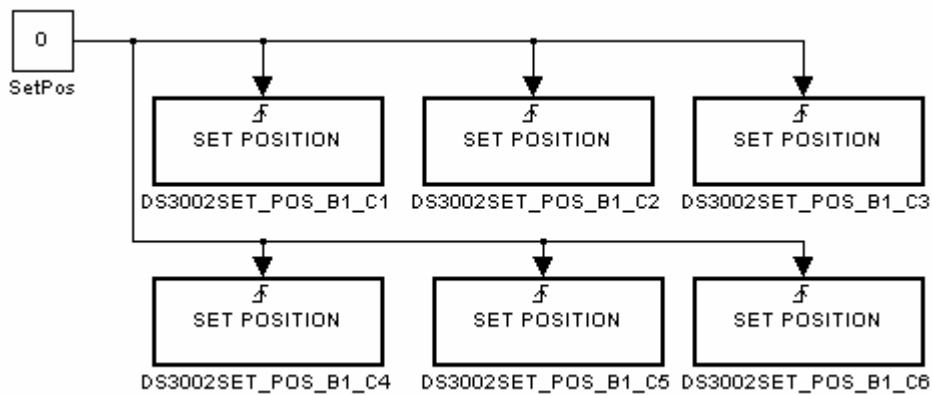
Figure 7.4. Position set subsystem
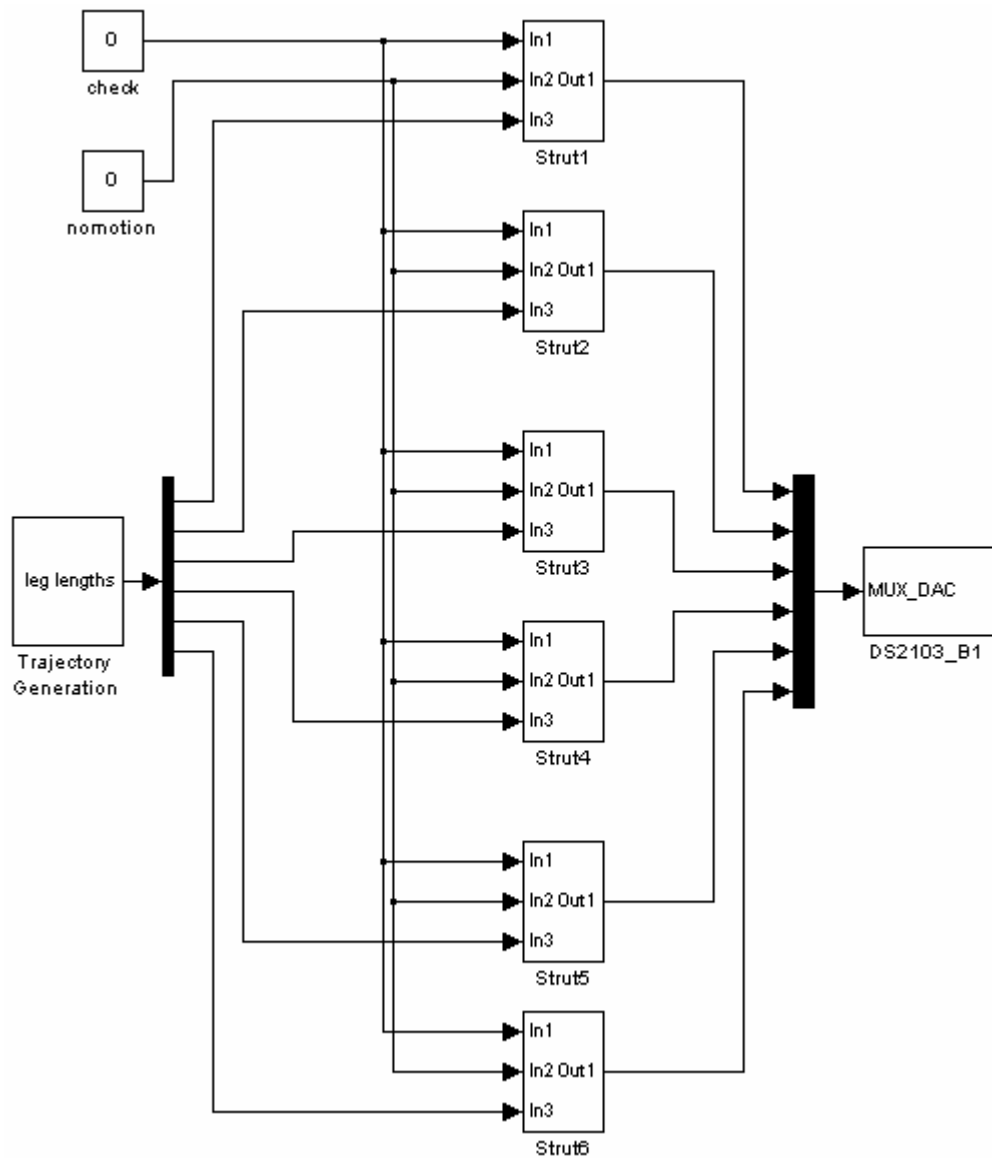
Figure 7.5. Trajectory generation & control
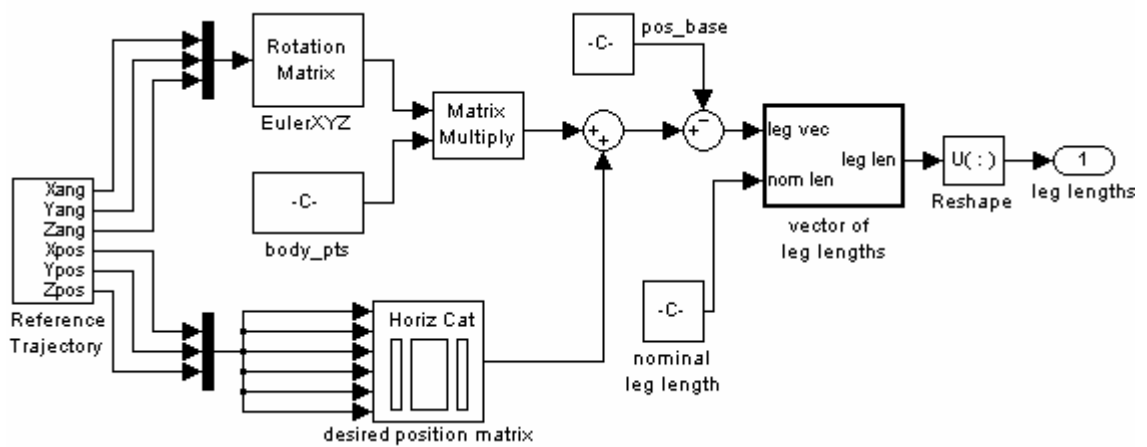
Figure 7.6. Trajectory generation

76

Trajectory generation of the system is the same as presented in the simulation. Detailed calculations are explained in section 3.1.
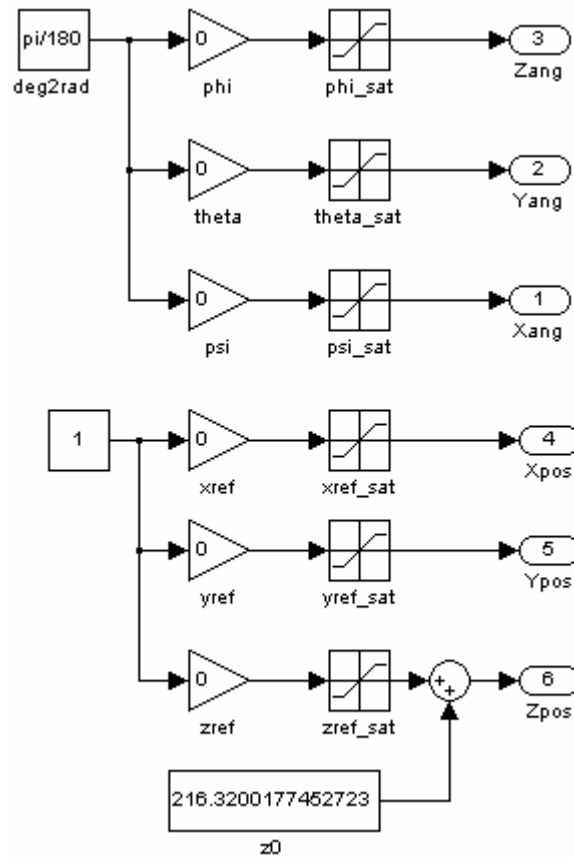
Figure 7.7. Reference trajectory
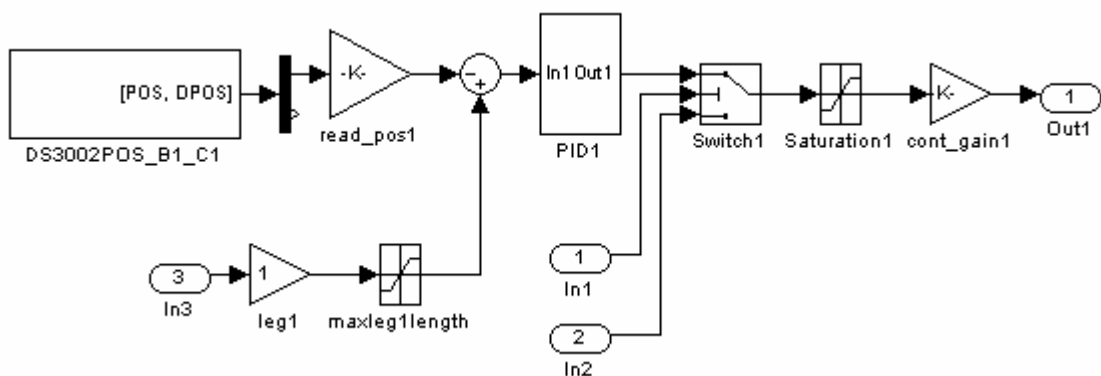
Figure 7.8. Strut subsystem

Strut subsystem reads position of the motor and by taking reference position; it defines the error that is input of the strut controller. The output of the controller is current that satisfies required motion to make the error zero. In order to control the system from dSPACE layout, switch block is used. When the check in the layout is not

set, the controller output is zero. When check button is pressed, controller gives calculated current as output in the strut subsystem.

7.3.1 PID Model
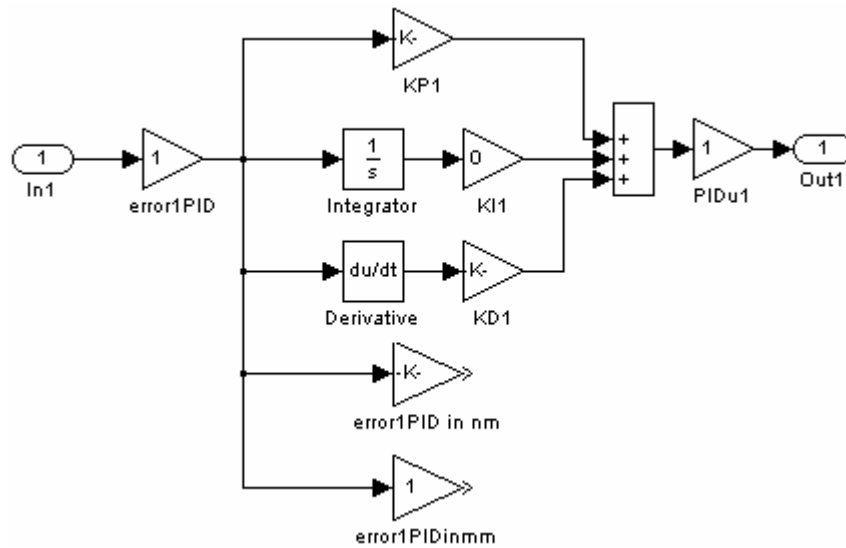
Figure 7.9. PID control model

7.3.2 Sliding Mode Control Structure
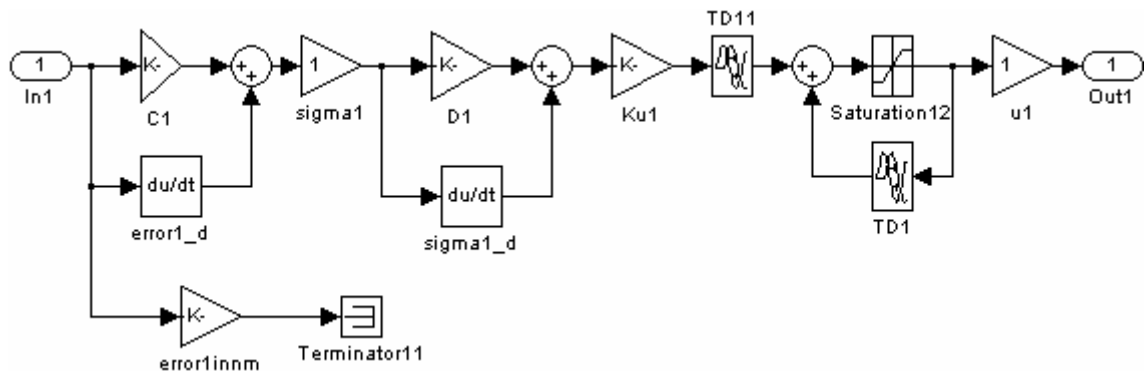
Figure 7.10. SMC model

$$u((k+1)T_s) = u(kT_s) + K(GB)^{-1}(D\sigma + \dot{\sigma})|_{t=t^-} \qquad (7.17)$$

Equation (7.17) is used to control position of the struts in the system. The input is error as in PID control, and output is current that is fed to the controller board.

8   EXPERIMENTS & RESULTS

8.1   Experimental Setup

To control the overall system, the DS1005 board and dSPACE Control Desk Program are used. The DS1005 PPC board is the core of dSPACE's modular real-time systems via the on-board 32-bit PHS-bus interface. All available dSPACE I/O boards can be connected to the DS1005. One processor board can handle up to 16 I/O boards simultaneously [93]. This system allows controlling 6 motors at the same time. This board is equipped with encoder readers, DACs, ADCs etc. It is running on a real time operating system whose frequency can be set by the user. In all of the conducted experiments, sampling interval is set to be 0.001 seconds.

Figure 8.1. DS1005 board

Additionally, to control the motors precisely a special low cost high resolution controller board is used [94]. An amplifier is used in a classical op-amp mode to control the output current on a resistor by measuring the voltage. By setting the suitable resistance, the problem of resolution loss can be avoided.
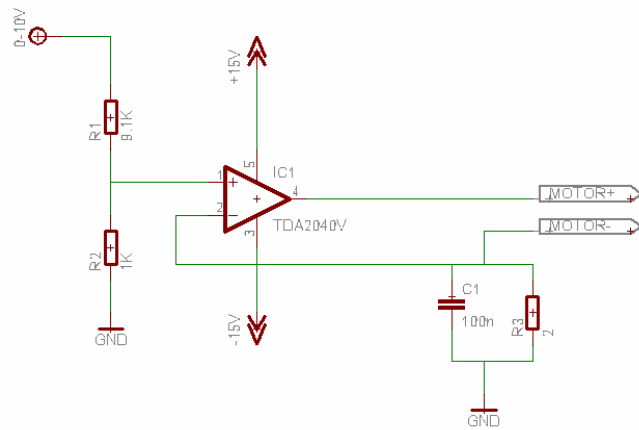
Figure 8.2. Current controller circuit
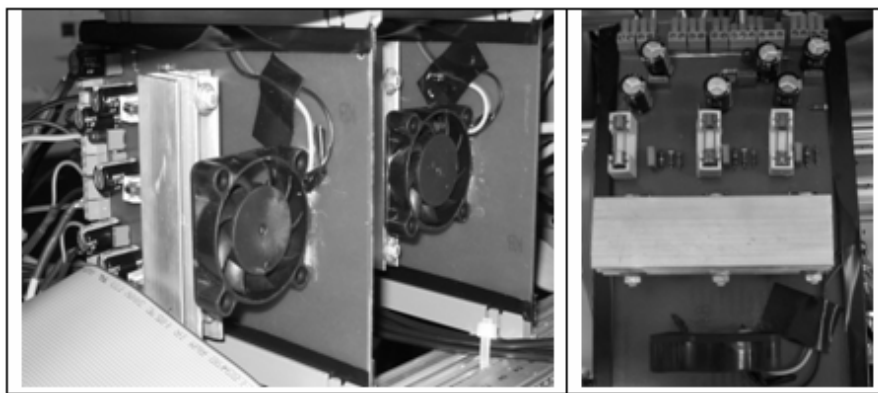
Figure 8.3. High resolution controller board
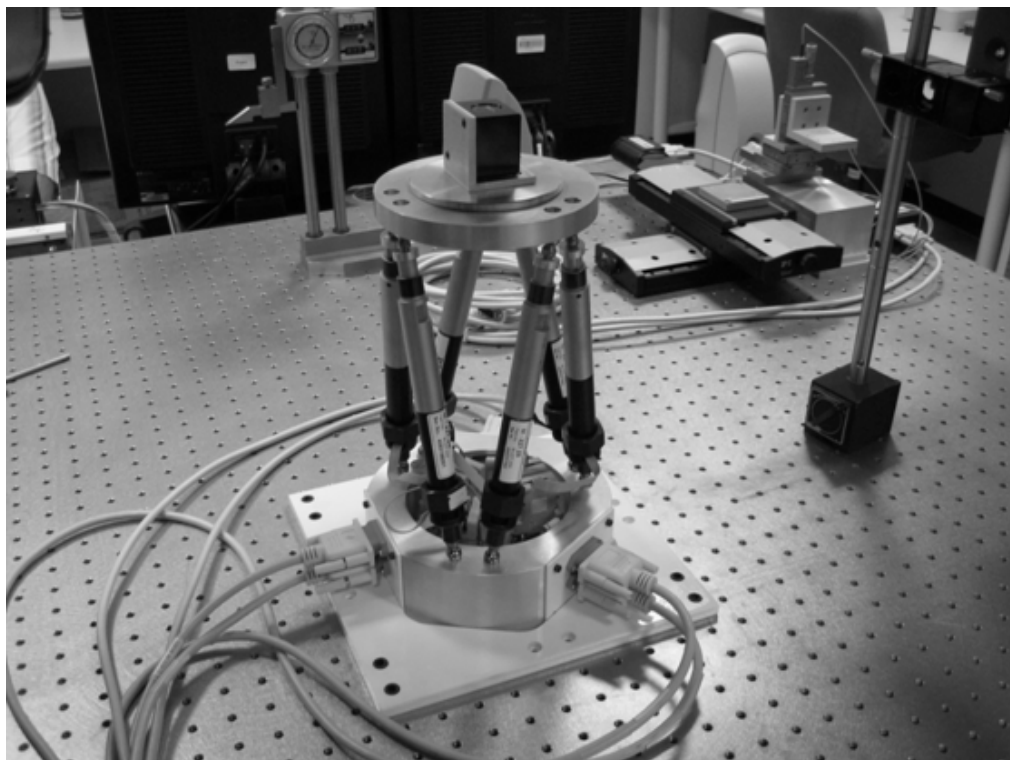
Figure 8.4. Designed Platform

The designed platform and experimental setup is shown in Figure 8.5.
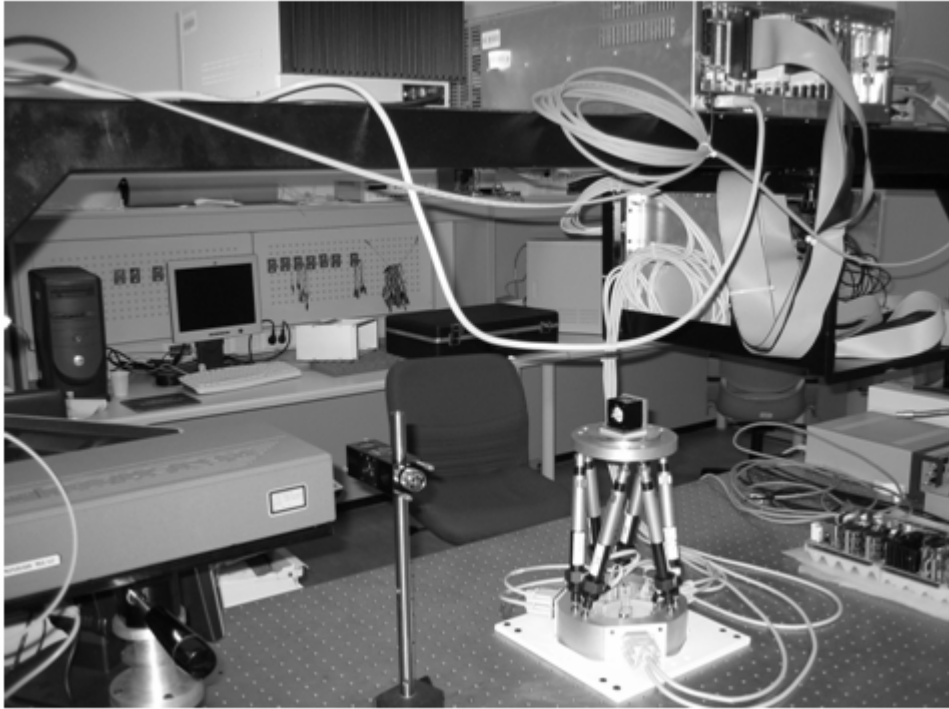
Figure 8.5. Overall system

8.2 PID experiments

After the system setup is completed, PID & sliding mode controllers are used to control the motors. In order to control the system, initial positions of the legs have to be set to 10 mm. since home configuration is defined when all leg lengths are 219.25 mm. Layout of the control is constructed as shown in Figure 8.6. First column of layout represents reference positions of the legs; second one represents positions of the legs read from the encoders.
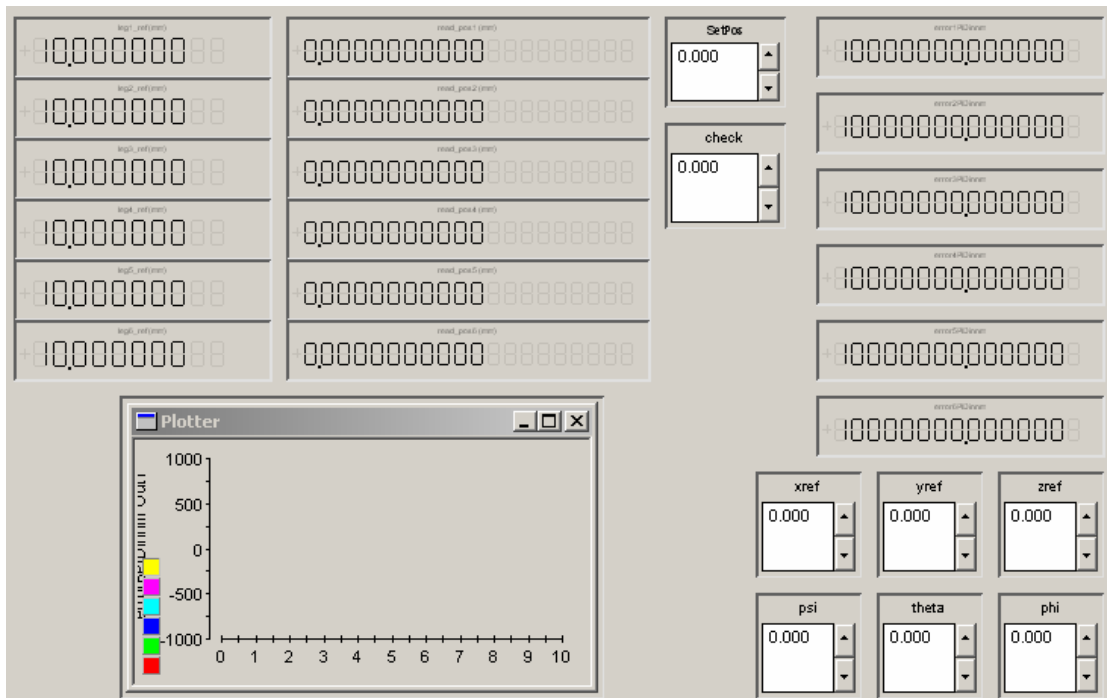
Figure 8.6. dSPACE layout
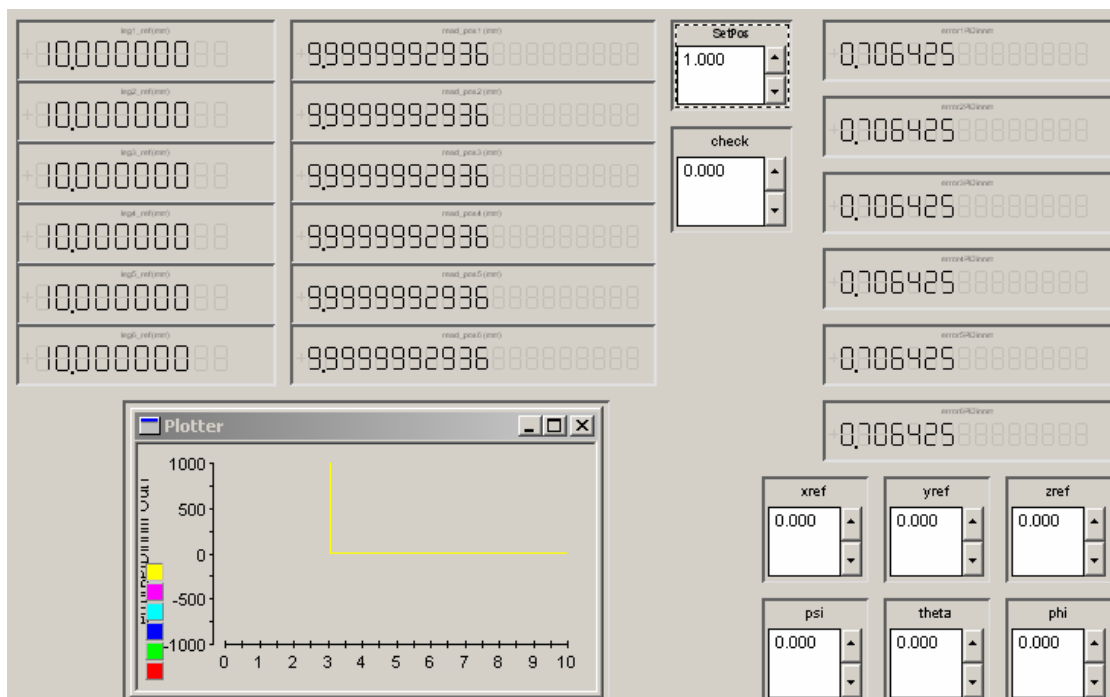
Figure 8.7. Set position for initial configuration

Before giving references, position value has to be set to 1 to provide zero error at home configuration. As a result of this operation Figure 8.7 is obtained. Zero error can not be obtained since there is a constant error which is 0.706425 nm due to encoder resolution.
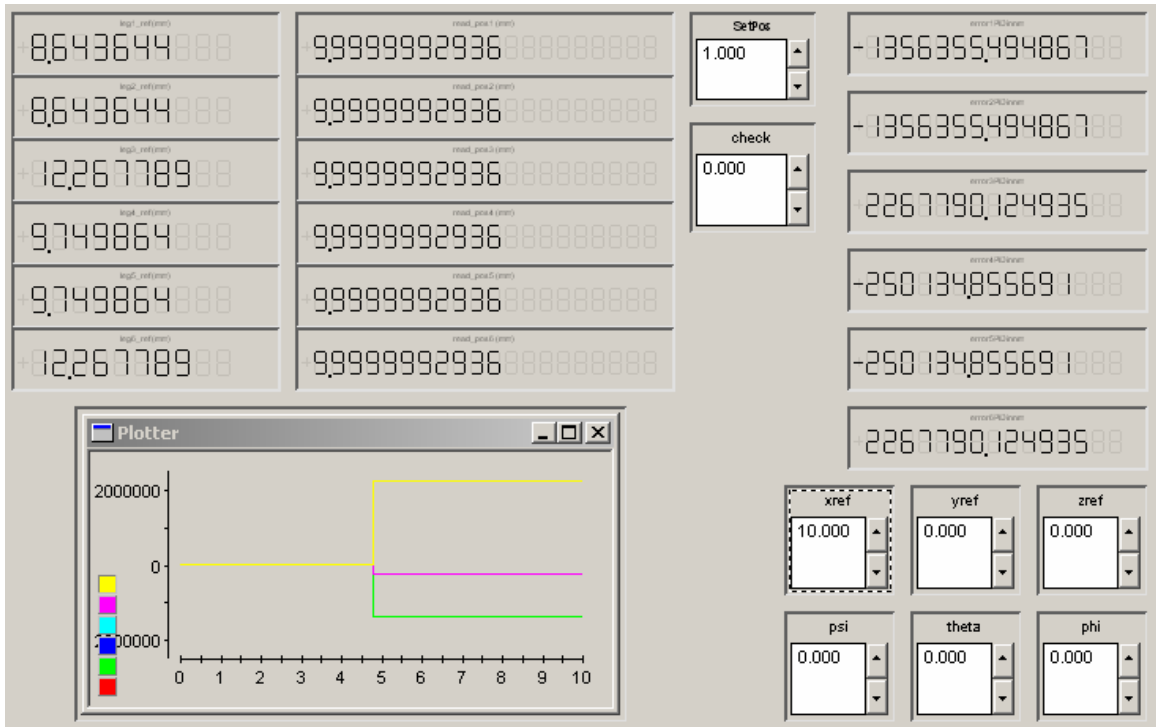
Figure 8.8. 10 mm x reference

Then reference values can be given to the system. When 10 mm. reference in x direction is given to the system, required leg lengths are calculated (see Figure 8.8) from inverse kinematics. Third column represents the error values for each leg in nanometer scale.
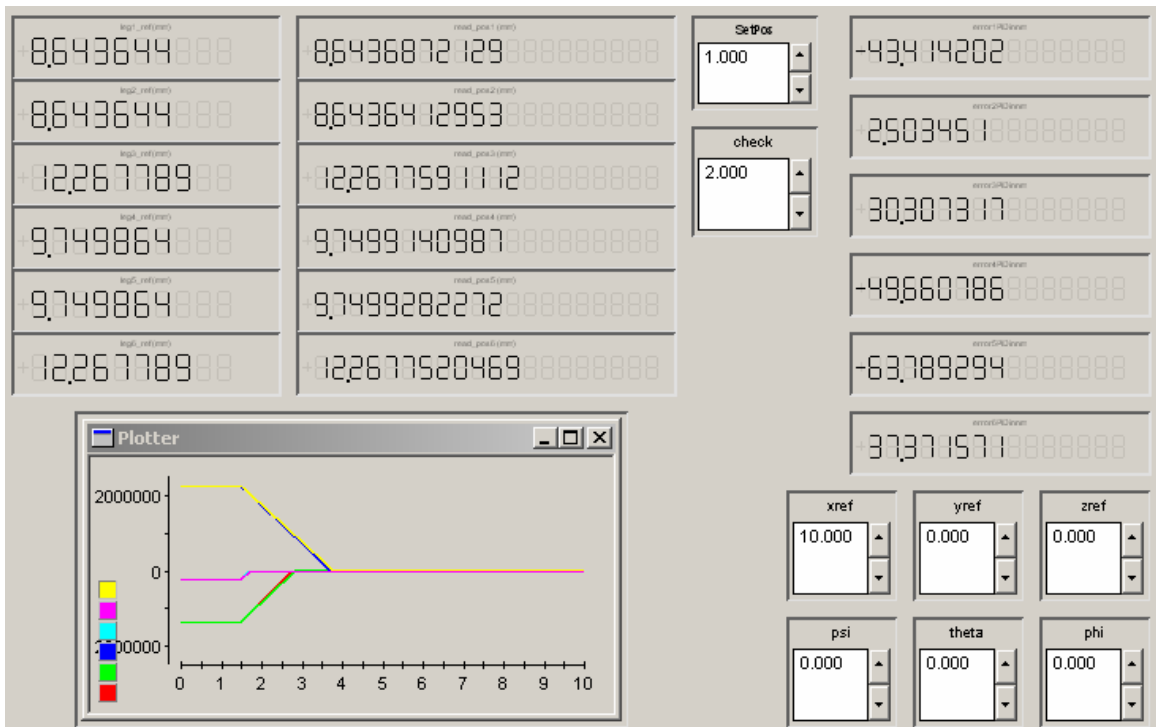
Figure 8.9. Errors at target position, xref : 10 mm (PID)

To initiate control, check value has to be set with a value larger than 1. When check value is set to 2, control gives required current to each motor to make the position error zero.

For PID control, even though same type of motors are used; different control parameters for each motor have to be found to get the desired result from the system. With PID control, approximately 37.83 nm error is acquired which is presented in Figure 8.9, 8.10 and 8.11.
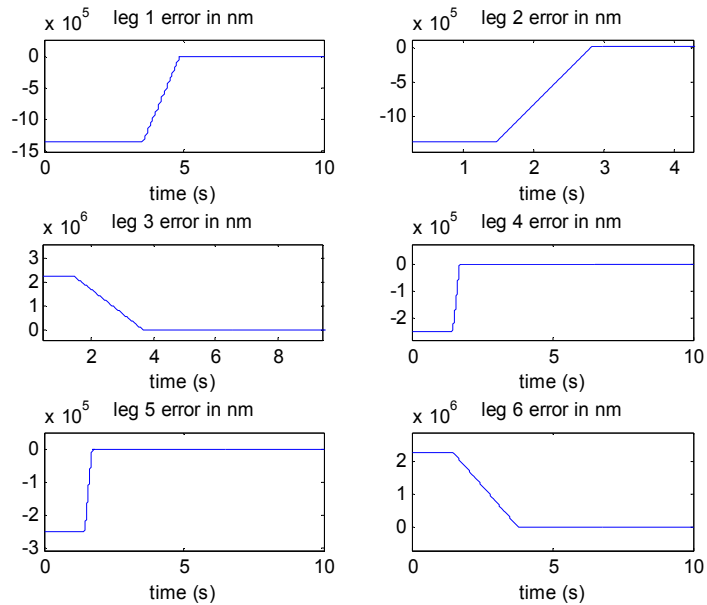
Figure 8.10. Error graphs for each leg for 10 mm xref
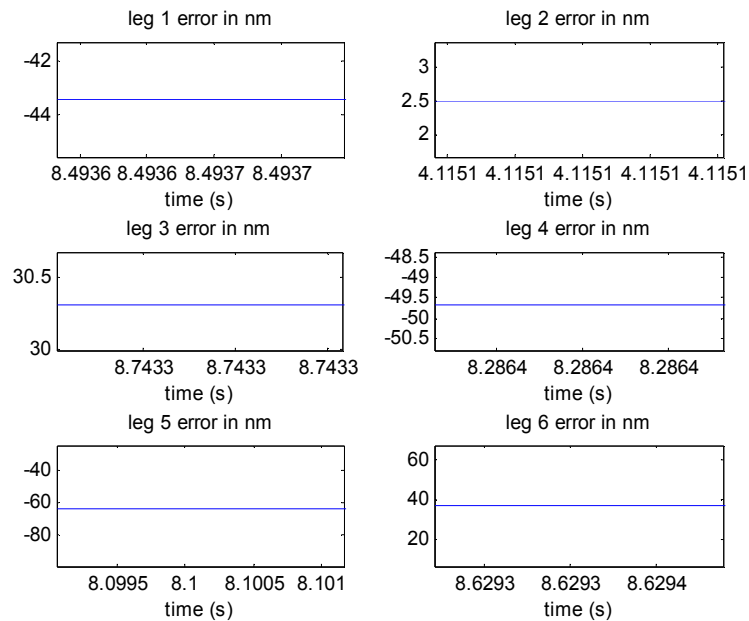
Figure 8.11. Steady-state errors at target position
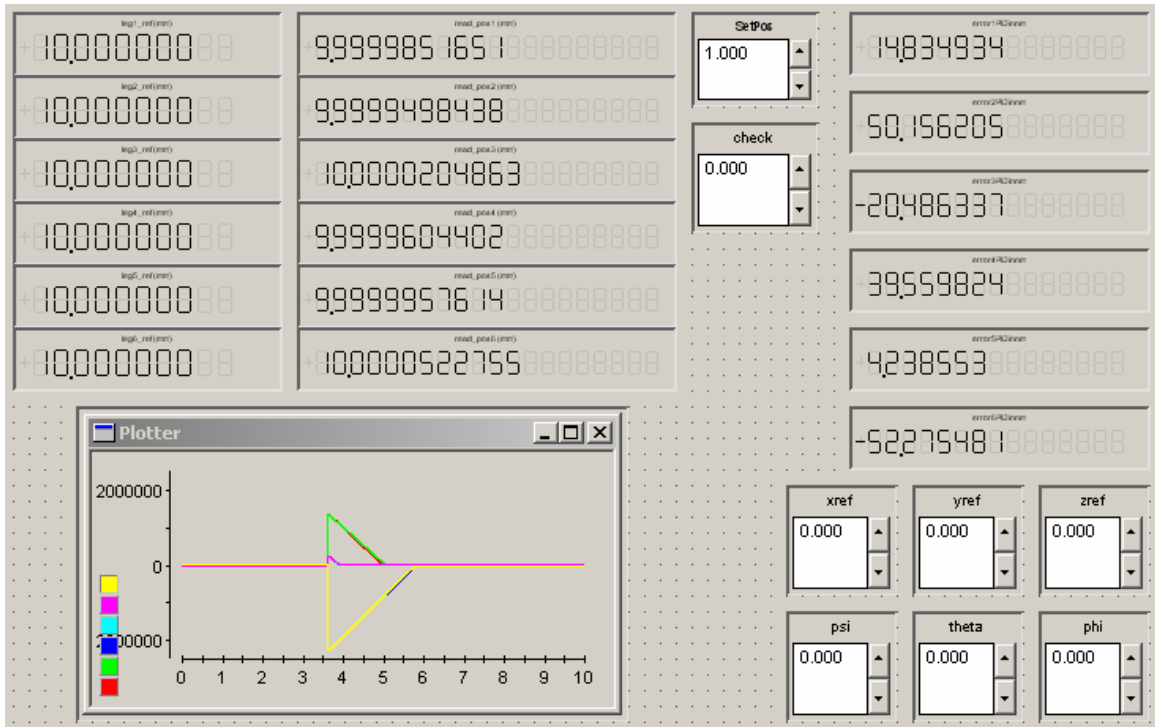
Figure 8.12. Errors at home configuration

When the system reaches desired position, home configuration is given as reference to the system to turn it back to its initial position. Errors at the home configuration are given in Figure 8.12 and Figure 8.13. The average error is 30.25 nm in the leg lengths.
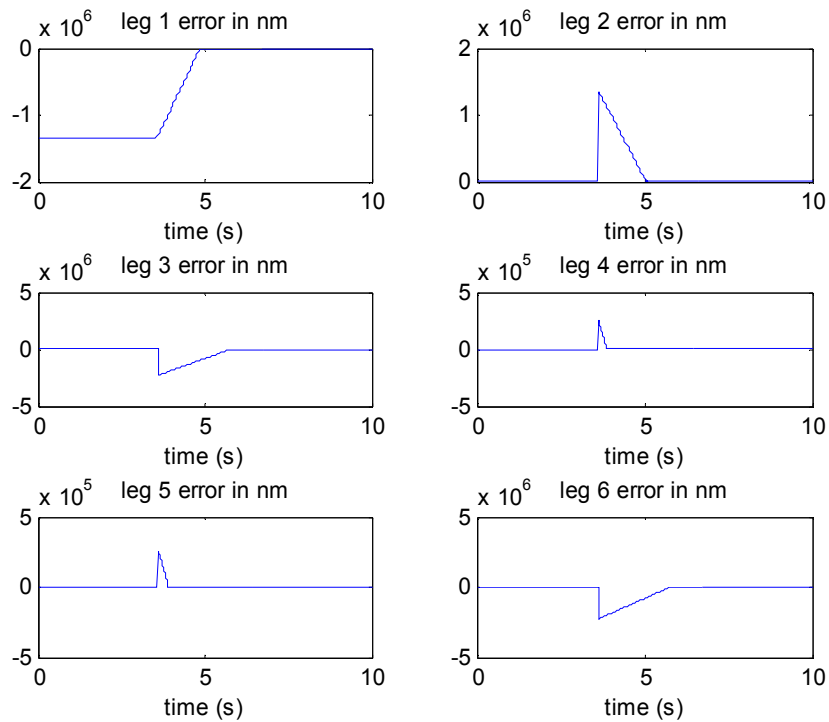
Figure 8.13. Error graphs for each leg for home configuration reference

8.3 SMC Experiments

Layout of the sliding mode control is the same as PID control. Only controller subsystems are changed in the leg subsystems. With sliding mode control the same control settings satisfy the control specification for all motors in the system without individual tuning. Therefore, considering nominal process parameters provides robust control. 10 mm x reference is applied to the system. The layout and error graphs before applying SMC are shown in Figure 8.14 and Figure 8.15.
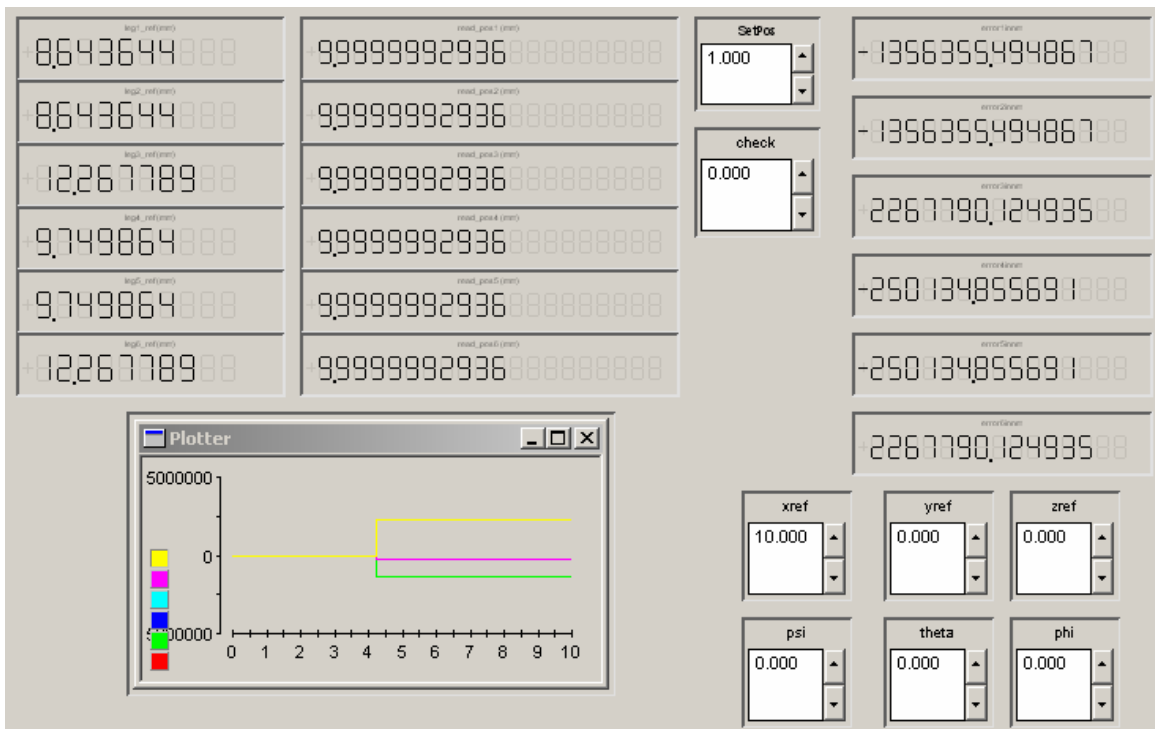
Figure 8.14. Layout for 10 mm x reference when leg positions are set (SMC)
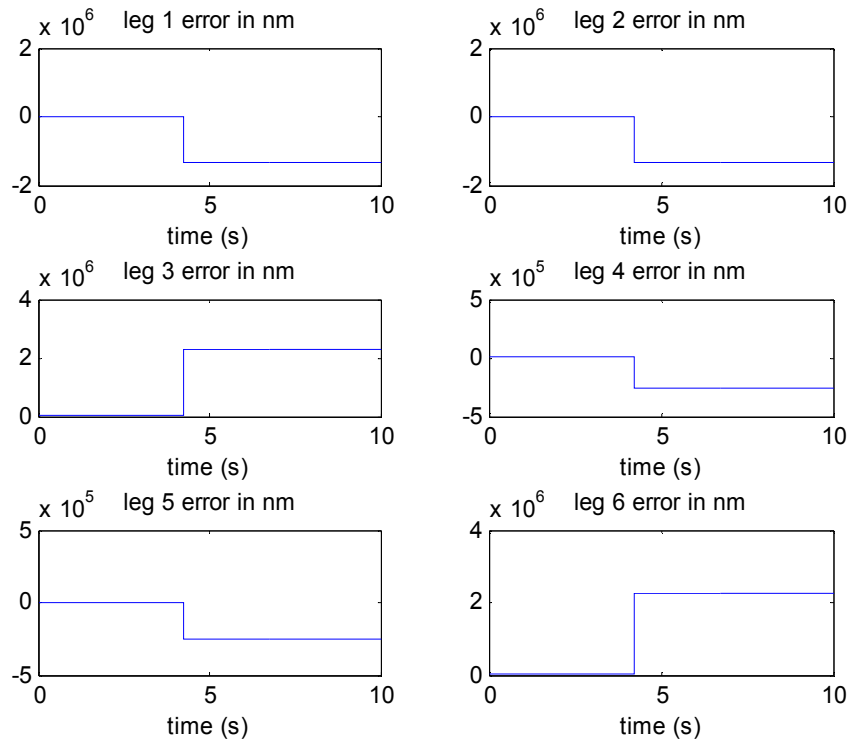
Figure 8.15. Errors in leg lengths when reference is given
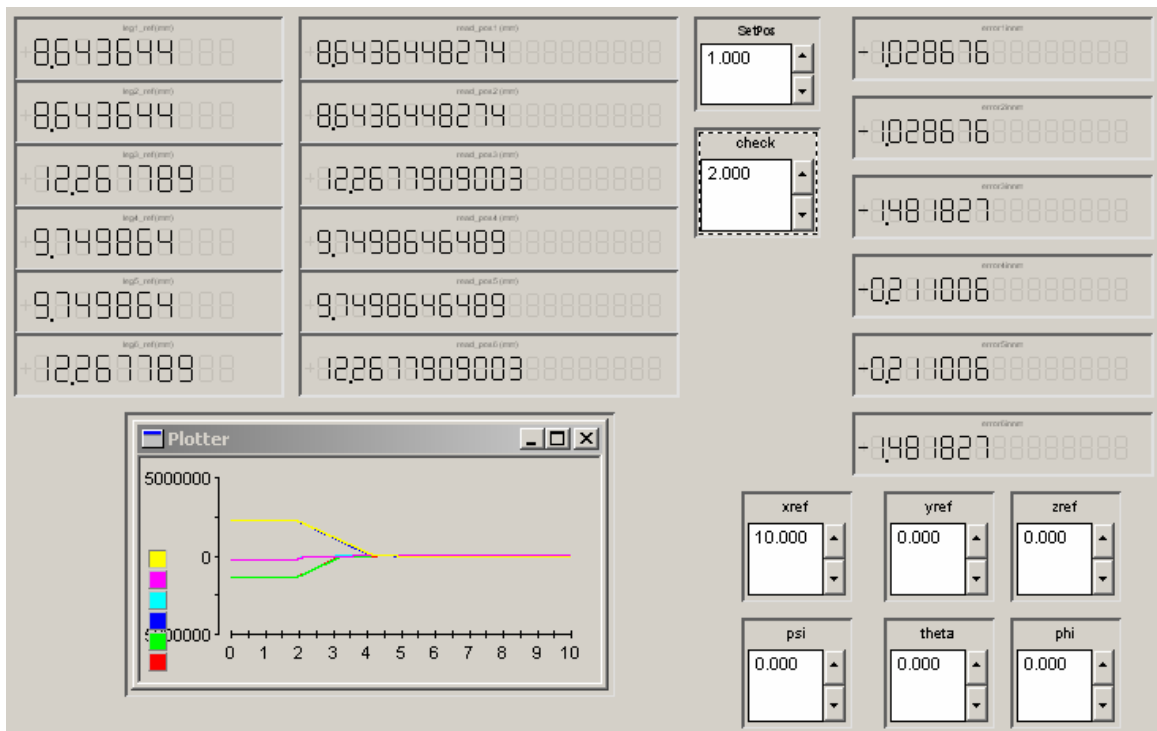
Figure 8.16. Errors at target position, xref : 10 mm

When platform reaches desired position, it has 1 nm. average error value in the leg lengths (Figure 8.16).
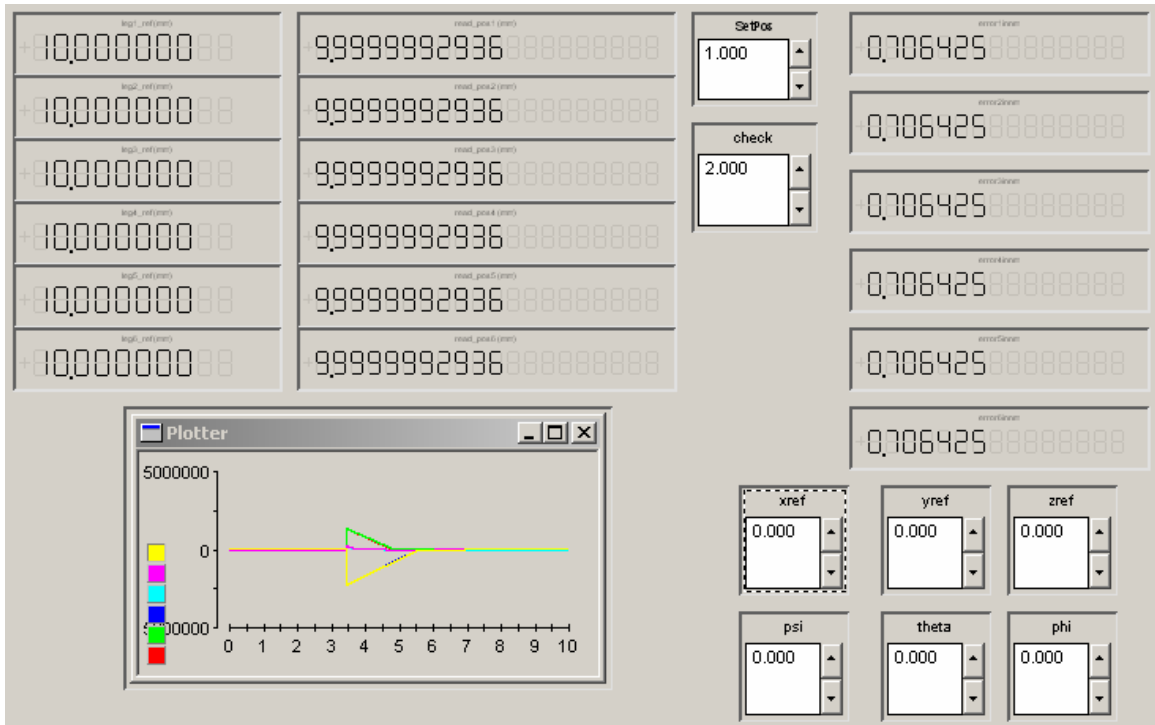
Figure 8.17. Errors when returned to home configuration

Finally, when platform reference is set to initial configuration, it gives minimum possible error value for the leg lengths (Figure 8.17, 8.18 and 8.19).
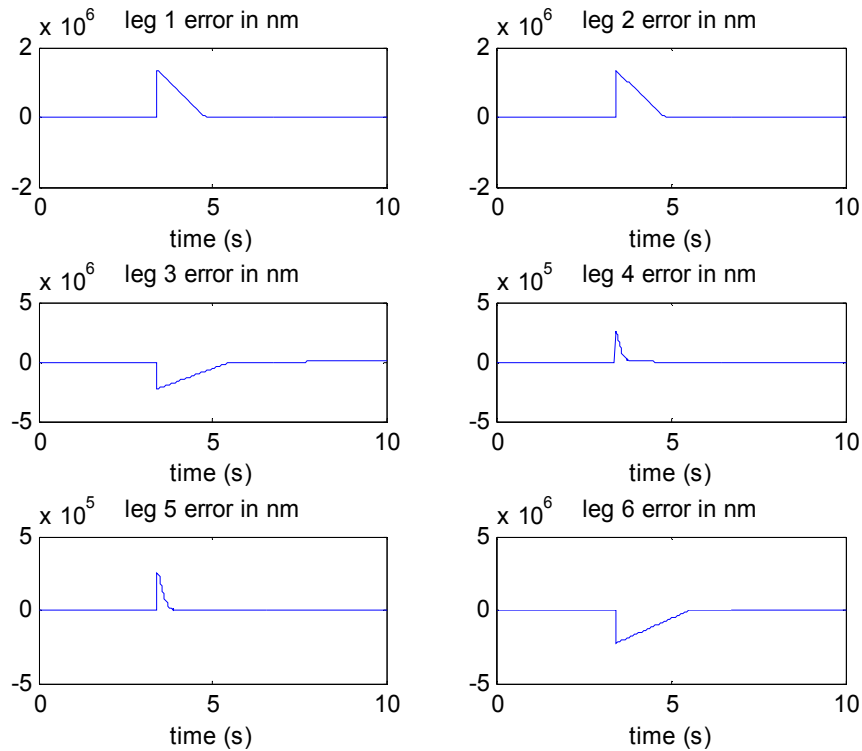
Figure 8.18. Error graphs for each leg for home configuration reference
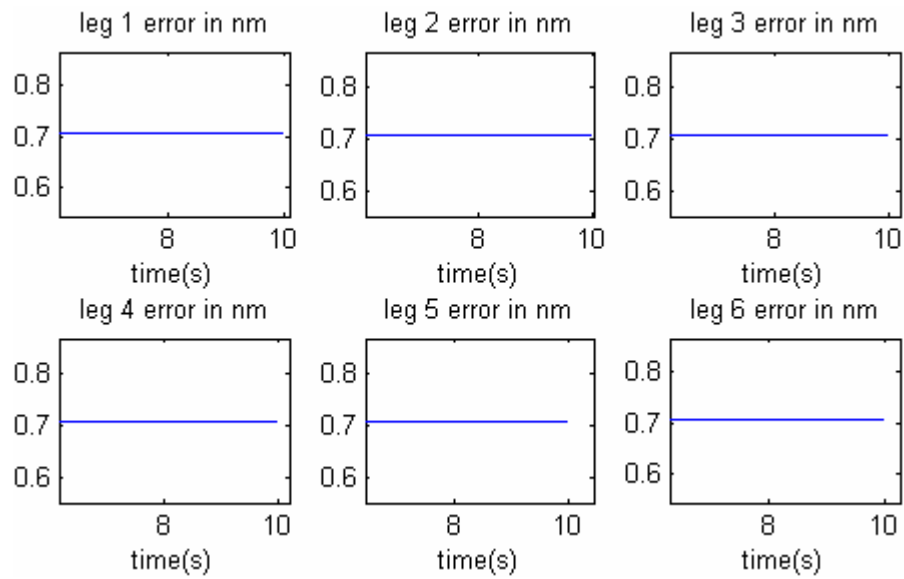
Figure 8.19. Steady-state errors at home configuration

8.4 Laser Measurement

The laser measurement system used in experiments is a Renishaw ML-10 Gold Standard Laser Measurement System. This is one of the most accurate systems available in the market. The system has ±0.7 ppm linear accuracy over its full range [95].

Figure 8.20. The ML-10 gold standard laser measurement system
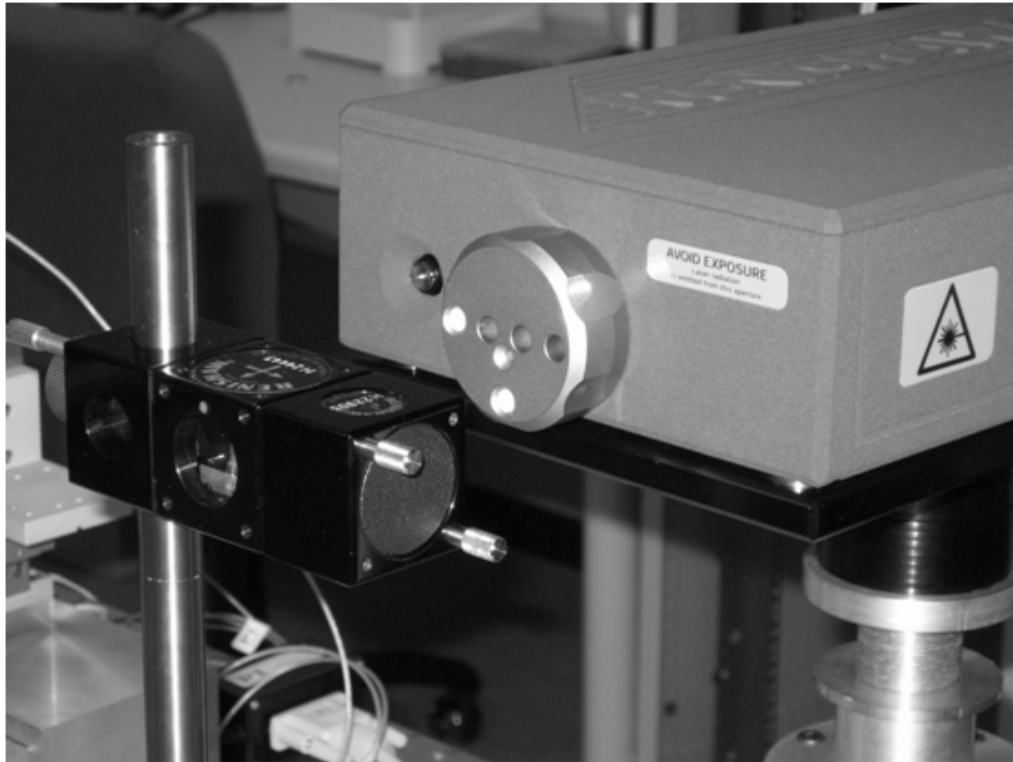
Figure 8.21. Laser measurement system used in the experiments
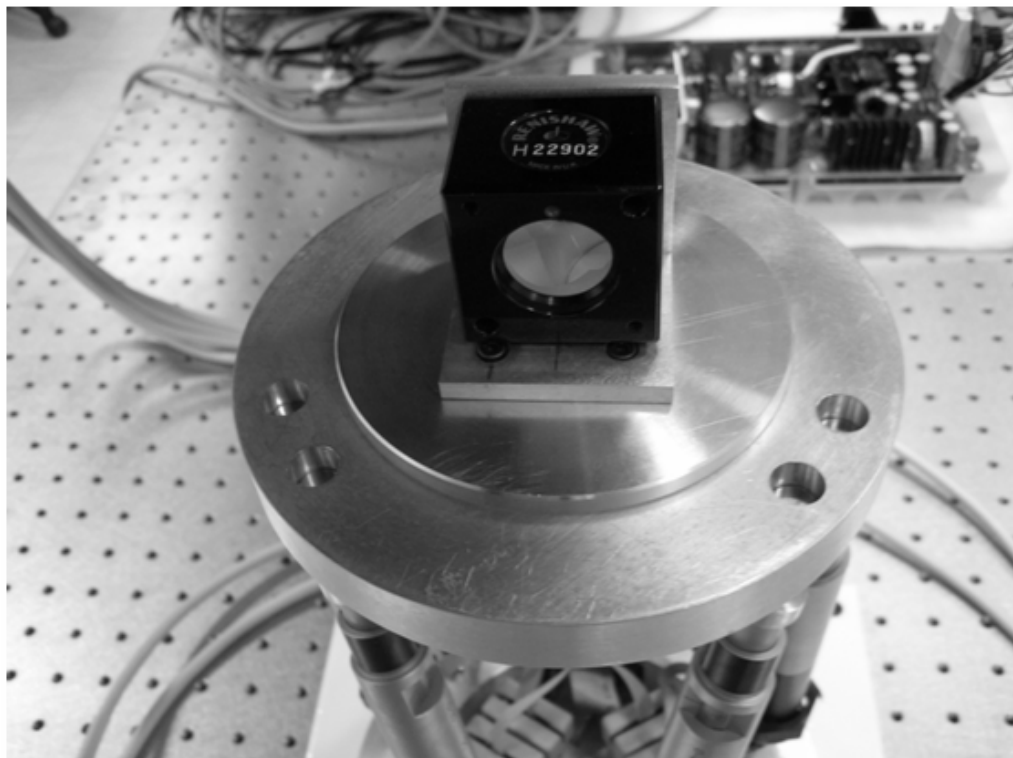
Figure 8.22. Platform apparatus used for laser measurement

After controlling each motor and verifying that desired position can be obtained with nanometer accuracy, overall system behavior is observed using laser

measurements. However, due to misalignment, friction and backlash in the assembly, as well as the fact that the desired tolerances could not be obtained in the manufacturing process, centre position of the upper plate could not be controlled with nanometer accuracy. Laser measurements are applied only in x axis. Error in the system is shown in Figure 8.23 for different reference values.
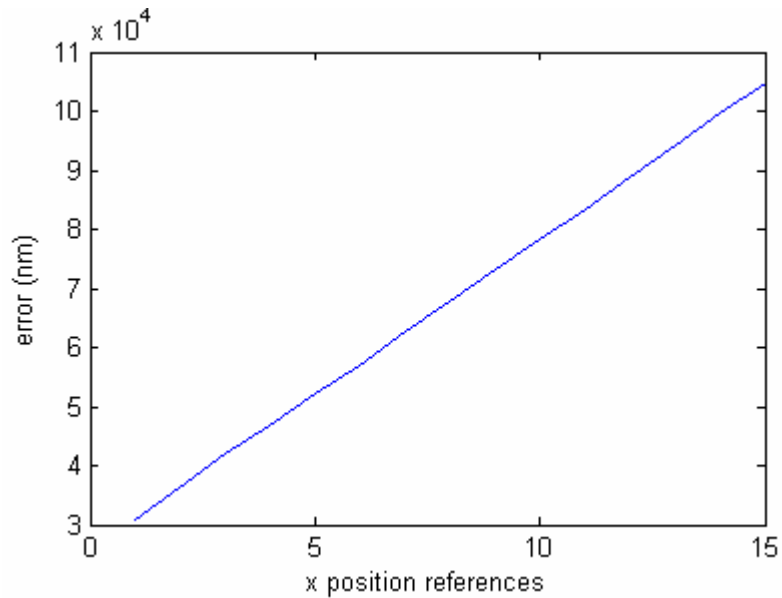
Figure 8.23. Errors for given x references

Error depends on the references almost linearly with some offset value. This linearity of the error can be explained by misalignment of the laser beam direction and platform's x axis (cosine error).
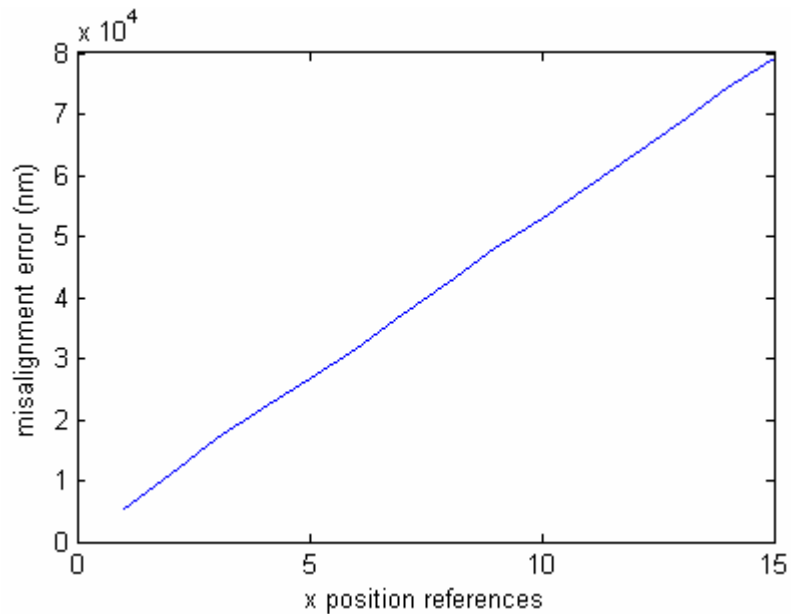
Figure 8.24. Misalignment error

When initial position is given as reference to the platform from the target position; it is expected to get zero error since error is set to zero at initial configuration. Even though, zero error in the leg lengths is read from encoders, laser measurement system measures some errors. This indicates that this error may be due to manufacturing errors, backlash and friction in the system. Even though friction and tolerance errors can not be avoided, backlash can be reduced by applying load to the moving platform since connection parts in the assembly can be modeled as mass-spring-damper systems. In Figure 8.25, for different target positions when load is increased in the system to reduce backlash, errors mainly due to misalignment, friction and manufacturing imperfections are presented.
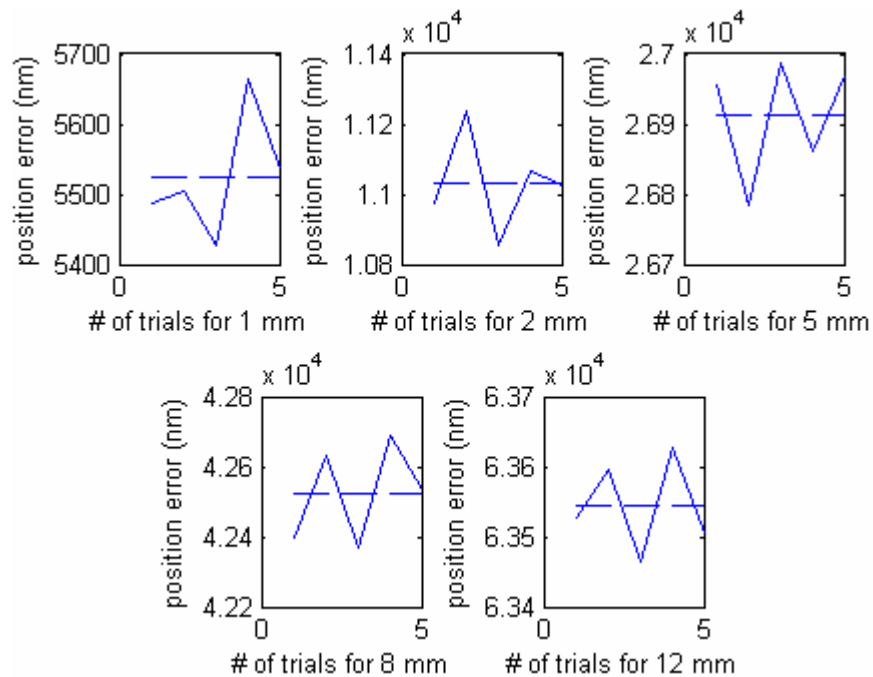
Figure 8.25. Error with reduced backlash for different reference values

Finally, actual performance of the system can be determined by also removing misalignment error from the result presented above. Experiment results (see Figure 8.26) show that the error bound is reduced below 500 nm which is better than the target performance value.
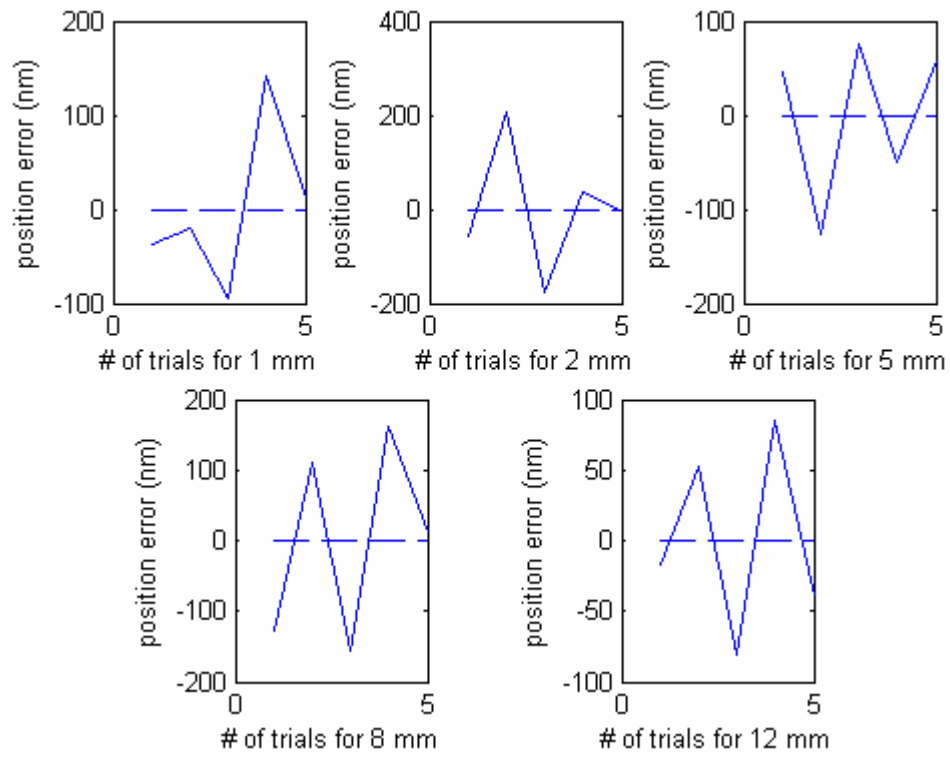
Figure 8.26. Repeatability of the system

9   CONCLUSION

Stewart Platform manipulators have better precision, stiffness, and smaller overall dimensions than equivalent conventional serial-link manipulators. In this work, a Stewart Platform utilizing spherical joints with magnets has been developed. The analysis results have demonstrated the superior performance of a Stewart Platform as micro-nano positioning mechanism. Relations for the inverse kinematics and methods to obtain forward kinematics have been presented. Since the subject problems are in the order of micro and nanometer scales, typical small workspace of the Stewart Platform is sufficient to carry out any required motion. The simplicity of its inverse kinematics makes it well suited for real time trajectory calculations. Simulations have shown that the calculated dimensions are valid for the required workspace. In addition, practical aspects of building such a challenging system have been addressed. It has been shown that the required 500 nm motion can be achieved using readily available actuators. A discussion on experimental setup errors has also been included.

Analytical results indicate that use of flexure hinges and other promising features will allow better performance. To increase performance of the manipulator through reduction of errors due to nonlinear friction behavior and the backlash, further flexure joint analysis and measurements are needed. Positional measurement accuracy can be increased by overcoming cosine error (misalignment of the laser beam and platform x axis). Although singularities of the platform behavior have been studied, and precautions have been embedded in the software, free path planning can be used to avoid singularities that exist in the manipulator workspace. Finally, as a future work, it is worthwhile to consider the manipulator motion control using the feedback from laser measurement.

APPENDIX A. SPECIFICATIONS OF MOTORS AND LASER SYSTEM

Specifications of PI M-227.25

Travel range (mm)	25
Design resolution (µm)	0.0035
Min. incremental motion (µm)	0.05
Unidirectional repeatability (µm)	0.1
Backlash (µm)	2
Max. velocity (mm/s)	1
Max. push/pull force (N)	40
Max. lateral force (N) at tip	0.1
Encoder resolution (counts/rev.)	2048
Drivescrew pitch (mm/rev.)	0.5
Gear ratio	69.12:1
Nominal motor power (W)	2
Motor voltage (V)	12
Weight (kg)	0.22

Specifications of Renishaw ML-10 Gold Standard Laser Measurement System

Length (mm)	335
Width (mm)	176
Height (mm)	75
Weight (g)	4500
Range	40m (1600 in)
Laser Source	Helium Neon (HeNe) laser tube (CLASS II)
Laser Power	<1 mW
Vacuum Wavelength	632.990577 nm (nominal)
Laser Frequency Accuracy	+/- 0.05ppm (parts per million)
Outputs	RS485 from 5 pin 'Datalink'
Power Supply	Nominal voltage rating is 100-240 VAC, 50/60 Hz, autosensing (limit rating 85-265 VAC)
Operating Temperature	0-40°C (32-104 °F)
Operating Humidity	0-95% non condensing

APPENDIX B. FORWARD KINEMATICS SOLUTION USING NEWTON-RAPHSON METHOD

Base (lower plate) and platform (upper plate) points have to be given in base and platform coordinates respectively to construct the model of the Stewart Platform. Designed platform's base plate radius is 74 mm. and moving platform radius is 59 mm. and with these radius values and offset angles that define angle between connection point pairs, the connection points in the plates are calculated.

(Offset angles: $Theta_b = 20*180/pi$ and $Theta_p = 20*180/pi$)

$base\_angles = \pi *[0 \quad 0 \quad 1/2 \quad 1/2 \quad 3/2 \quad 3/2]$
$platform\_angles = \pi *[3/2 \quad 1/2 \quad 1/2 \quad 1 \quad 1 \quad 3/2]$
$offset\_base = Theta_b *[-1/2 \quad 1/2 \quad 1 \quad 2 \quad -2 \quad -1]$
$offset\_platform = Theta_p *[2 \quad -2 \quad -1 \quad -1/2 \quad 1/2 \quad 1]$

Table B.1. Connection points' main and offset angles

In order to calculate connection angles, base and platform angles are added to their corresponding offset values:

$Lambda_b = base\_angles + offset\_base$
$Lambda_p = platform\_angles + offset\_platform$

Table B.2. Connection points' angles

connection angles	1	2	3	4	5	6
$Lambda_b$	350°	10°	110°	130°	230°	250°
$Lambda_p$	310°	50°	70°	170°	190°	290°

Table B.3. Connection angles of the base and moving platform in degrees

Base and platform points' calculation is given in Table B.4

$$
base = \begin{bmatrix} R_b * \cos(Lambda_b) \\ R_b * \sin(Lambda_b) \\ zeros(1,6) \end{bmatrix} \qquad platform = \begin{bmatrix} R_p * \cos(Lambda_p) \\ R_p * \sin(Lambda_p) \\ zeros(1,6) \end{bmatrix}
$$

Table B.4. Base and platform points' calculation

where R_b and R_p are base and platform radii.

Base points					
72.8758	72.8758	−25.3095	−47.5663	−47.5663	−25.3095
−12.85	12.85	69.5373	56.6873	−56.6873	−69.5373
0	0	0	0	0	0
Platform points					
37.9245	37.9245	20.1792	−58.1037	−58.1037	20.1792
−45.1966	45.1966	55.4419	−10.2452	10.2452	−55.4419
0	0	0	0	0	0

Table B.5. Base and platform points' coordinates of designed platform

Third rows in Table B.5 are zero because the connection points of the designed platform are given in their coordinate frame.

After defining point coordinates and model of the platform, estimated solution (guess) is given for forward kinematics solution of the platform. Using inverse kinematics, leg lengths of estimated configuration of the platform are calculated. Then homogenous transformation matrix is constructed for the given translation and rotations.

From error found from estimated leg lengths and actual ones, using Newton-Raphson method, error is decreased to zero iteratively and actual configuration of the platform is obtained. Leg lengths depend on x, y, z translation parameters and Euler angles. A function X is defined that depends on leg lengths and describes the configuration of the platform. Leg lengths can be estimated by making function $X(leg\_lengths(xyzeuler))$ linear around initial value of the leg lengths. The error is difference between the actual leg lengths and estimated leg lengths that are found from given estimated xyzeuler vector. Therefore finding function X's derivative with respect to xyzeuler vector provides to calculate $\Delta xyzeuler$.
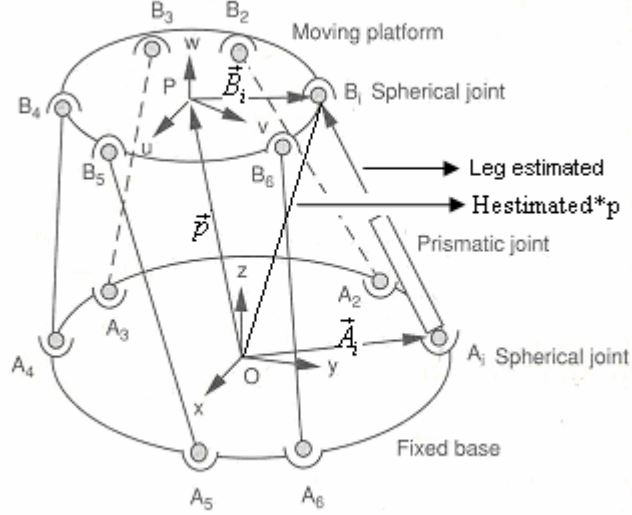
Figure B.1. Numerical forward kinematics solution

$$Leg\_actual \ = \ Leg\_estimated \ + \ (\ dX \ / \ dxyzeuler\ )\ \Delta xyzeuler \qquad \text{(B.1)}$$

(B.1) can be written in another form using chain rule.

$$Leg\_actual \ = \ Leg\_estimated \ + \ (\ dX \ / \ d\ leg\_lengths)\ (\ d\ leg\_lengths \ / \ dxyzeuler\ )\ \Delta xyzeuler$$
$$\text{(B.2)}$$

From estimated transformation matrix, estimated leg lengths are found:

$$Leg\_estimated \ = Hestimated * p \ - \ b \qquad \text{(B.3)}$$

where *Hestimated* is estimated transformation matrix, and p and b are platform and base connection points respectively.

$$H = \begin{bmatrix} \cos\phi\cos\theta & -\sin\phi\cos\psi+\cos\phi\sin\theta\sin\psi & \sin\phi\sin\psi+\cos\phi\sin\theta\cos\psi & x \\ \sin\phi\cos\theta & \cos\phi\cos\psi+\sin\phi\sin\theta\sin\psi & -\cos\phi\sin\psi+\sin\phi\sin\theta\cos\psi & y \\ -\sin\theta & \cos\theta\sin\psi & \cos\theta\cos\psi & z \\ 0 & 0 & 0 & 1 \end{bmatrix}$$

The homogeneous transformation matrix H is obtained by rotation ψ angle in x axis (yaw), θ angle in y axis (pitch) and ϕ angle in z axis (roll) performed in given order. (Rotation about fixed axes is used.) After rotation, translation is performed and resulting homogeneous transformation matrix is obtained from the estimate values.

(B.3) can also be expressed as:

$$leg\_lengths = H(xyzeuler) * platform\_points - base\_points \qquad (B.4)$$

Since

$$(d\ leg\_lengths\ /\ dxyzeuler) = dH\ /\ dxyzeuler \qquad (B.5)$$

Therefore (B.2) can be written as:

$$Leg\_actual = Leg\_estimated + (dX\ /\ d\ leg\_lengths)(dH\ /\ d\ xyzeuler)\Delta xyzeuler$$
$$(B.6)$$

from which error is calculated as:

$$error = (dX\ /\ d\ leg\_lengths)(dH\ /\ d\ xyzeuler)\Delta xyzeuler = leg\_lengths - estleglength$$
$$(B.7)$$

where '$leg\_lengths$' describes actual leg lengths and '$estleglength$' describes estimated leg lengths calculated at each iteration until error is smaller than user defined permissible error that satisfies nanometer error in translation and orientation to achieve mentioned specifications in section 1.1.

$$estleglength = sqrt(sum(Leg\_estimated^2)) \qquad (B.8)$$

After error is calculated, $\Delta xyzeuler$ has to be found. After finding $\Delta xyzeuler$, Leg_actual can be calculated with the following equation:

$$Leg\_actual = Leg\_estimated + G * \Delta xyzeuler \Rightarrow \Delta xyzeuler = inv(G) * (error)$$
$$(B.9)$$

where $G = (dX\ /\ d\ leg\_lengths)(dH\ /\ dxyzeuler)$.

In order to calculate $\Delta xyzeuler$, $dH\ /\ dxyzeuler$ has to be calculated first. $dH\ /\ dxyzeuler$ is constructed by taking derivative of the transformation matrix with respect to x, y, z, ψ, θ and ϕ.

$$dH\ /\ dx = \begin{bmatrix} 0 & 0 & 0 & 1 \\ 0 & 0 & 0 & 0 \\ 0 & 0 & 0 & 0 \\ 0 & 0 & 0 & 0 \end{bmatrix} \quad dH\ /\ dy = \begin{bmatrix} 0 & 0 & 0 & 0 \\ 0 & 0 & 0 & 1 \\ 0 & 0 & 0 & 0 \\ 0 & 0 & 0 & 0 \end{bmatrix} \quad dH\ /\ dz = \begin{bmatrix} 0 & 0 & 0 & 0 \\ 0 & 0 & 0 & 0 \\ 0 & 0 & 0 & 1 \\ 0 & 0 & 0 & 0 \end{bmatrix}$$

$$dH\ /\ d\phi = \begin{bmatrix} -\sin\phi\cos\theta & -\cos\phi\cos\psi - \sin\phi\sin\theta\sin\psi & \cos\phi\sin\psi - \sin\phi\sin\theta\cos\psi & 0 \\ \cos\phi\cos\theta & -\sin\phi\cos\psi + \cos\phi\sin\theta\sin\psi & \sin\phi\sin\psi + \cos\phi\sin\theta\cos\psi & 0 \\ 0 & 0 & 0 & 0 \\ 0 & 0 & 0 & 0 \end{bmatrix}$$

$$dH / d\theta = \begin{bmatrix} -\cos\phi\sin\theta & \cos\phi\cos\theta\sin\psi & \cos\phi\cos\theta\cos\psi & 0 \\ -\sin\phi\sin\theta & \sin\phi\cos\theta\sin\psi & \sin\phi\cos\theta\cos\psi & 0 \\ -\cos\theta & -\sin\theta\sin\psi & -\sin\theta\cos\psi & 0 \\ 0 & 0 & 0 & 0 \end{bmatrix}$$

$$dH / d\psi = \begin{bmatrix} 0 & \sin\phi\sin\psi + \cos\phi\sin\theta\cos\psi & \sin\phi\cos\psi - \cos\phi\sin\theta\sin\psi & 0 \\ 0 & -\cos\phi\sin\psi + \sin\phi\sin\theta\cos\psi & -\cos\phi\cos\psi - \sin\phi\sin\theta\sin\psi & 0 \\ 0 & \cos\theta\cos\psi & -\cos\theta\sin\psi & 0 \\ 0 & 0 & 0 & 0 \end{bmatrix}$$

Aim is to make the error zero by changing translation and Euler angle values iteratively. If error is not small enough Newton - Raphson method is used to find actual result from estimation. For that purpose, derivative of a transformation matrix with respect to translation and roll-pitch-yaw angles is calculated.

$$dR = Hderiv(xyzeuler) \tag{B.10}$$

$$dq = dR * p \tag{B.11}$$

(B.11) gives change of the pose of the platform, and besides this, $dX / d\ leg\_lengths$ has to be calculated which determines the change of the directions of the platform points.

$$dX / d\ leg\_lengths = leg\_estimated ./ [\ estleglength;\ estleglength;\ estleglength;\ estleglength] \tag{B.12}$$

From (B.9)

$$G = (dX / d\ leg\_lengths) * dq \tag{B.13}$$

As the last step, parameters have to be corrected.

$$d\ xyzeuler = G \backslash error\ \ where\ \ d\ xyzeuler = inv(G) * error$$
$$xyzeuler = xyzeuler + d\ xyzeuler \tag{B.14}$$

(Since $G*d\ xyzeuler = error$, left matrix divide is used to find $d\ xyzeuler$).

From calculated xyzeuler vector, new transformation matrix is calculated.

$$Hestimated = transEuler\_H(xyzeuler) \tag{B.15}$$

If error is still not smaller than given tolerance value, this procedure is repeated until actual configuration is found. At each iteration error becomes close to zero.

APPENDIX C. FORWARD KINEMATICS SOLUTION BASED ON GEOMETRIC CONSTRAINTS

Starting with an initial estimate for the first two direction cosines d_{1x} and d_{1y}, third one can be calculated from

$$d_{1z} = \pm\sqrt{1 - d_{1x}{}^2 - d_{1y}{}^2} \tag{C.1}$$

Only positive solution is considered because the mirror images are not required. Then the location of the first platform point is given by

$$\underset{\sim}{p_1}' = \underset{\sim}{b_1} + \underset{\sim}{S_1} = \begin{bmatrix} b_{1x} \\ b_{1y} \\ 0 \end{bmatrix} + S_1 \begin{bmatrix} d_{1x} \\ d_{1y} \\ d_{1z} \end{bmatrix} \tag{C.2}$$
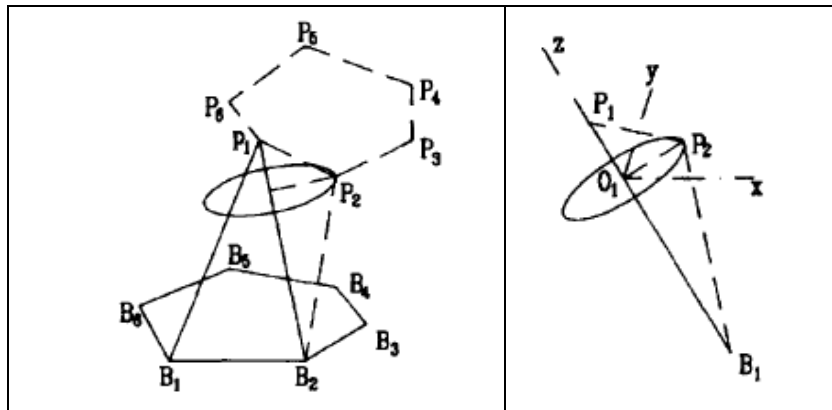
Figure C.1. Second platform point calculation

Now, a triangle $B_1\hat{B}_2 P_1$ can be constructed since all the edges are known.

$$B_2 P_1 = \mid \underset{\sim}{p_1}' - b_2 \mid$$
$$B_2 P_2 = S_2 \tag{C.3}$$

$B_2 P_2$ is constraining the platform point P_2 to rotate in a circle (Figure C.1).

Let r_1 be the radius of this circle with center O_1 and $O_1 P_2 = r_1$ which can be found from the equations:

$$\cos \alpha_1 = \frac{B_2 P_1^2 + B_2{}^2 P_2^2 - P_1 P_2^2}{2 B_2 P_1 * B_2 P_2} \tag{C.4}$$

$$B_2 O_1 = B_2 P_2 \cos \alpha_1$$
$$r_1 = O_1 P_2 = B_2 P_2 \sin \alpha_1 \tag{C.5}$$

The position vector of the center O_1 can be obtained by (C.6) and (C.7).

$$\widehat{B_2 P_1} = \text{ unit vector of } B_2 P_1 \tag{C.6}$$

$$o_1 = b_2 + B_2 O_1 = b_2 + B_2 O_1 \widehat{B_2 P_1} \tag{C.7}$$

To determine the rotation of the r_1 and P_2 in the circle, a triad is needed. The direction $O_1 P_1$ and the direction parallel to the base plane can be taken as Z and X axis respectively for the triad. Since X and Z axes are known, Y could be derived from the cross product of these two vectors.

$$\Im = [k \times B_2 P_1 \quad B_2 P_1 \times (k \times B_2 P_1) \quad B_2 P_1] \tag{C.8}$$

In the case of parallel $B_2 P_1$ to the base Z axis, the rotation matrix will be an identity matrix.

The platform point $p_2{}'$ can be found after a rotation of θ_1 about its Z axis:

$$p_2{}' = o_1 + \Im [r_1 \cos \theta_1 \quad r_1 \sin \theta_1 \quad 0]^T \tag{C.9}$$

The direction of cosines for the second leg can be determined from the difference between the platform and base point:

$$\begin{bmatrix} d_{2x} \\ d_{2y} \\ d_{2z} \end{bmatrix} = \frac{1}{S_2} \begin{bmatrix} p_{2x}{}' - b_{2x} \\ p_{2x}{}' - b_{2y} \\ p_{2z}{}' \end{bmatrix} \tag{C.10}$$

Now, there exists a second triangle $P_1 P_2 P_3$ which rotates about $P_1 P_2$. P_3 becomes an intersection point of a circle and a sphere.
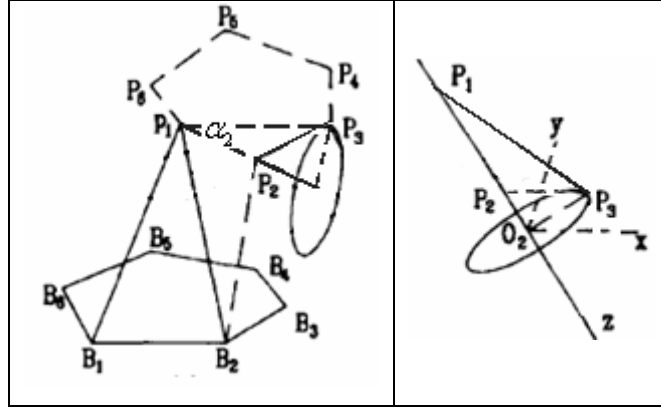
Figure C.2. Third platform point calculation

$\alpha_2(\widehat{P_2 P_1 P_3})$ can be obtained from law of cosines

$$\cos \alpha_2 = \frac{P_1 P_2^2 + P_1 P_3^2 - P_2 P_3^2}{2 P_1 P_2 \times P_1 P_3}$$

$$P_1 O_2 = P_1 P_3 \cos \alpha_2 \qquad \text{(C.11)}$$

$$r_2 = O_2 P_3 = P_1 P_3 \sin \alpha_2$$

$$\underset{\sim}{o_2} = \underset{\sim}{p_1}' + P_1 O_2 \underset{\sim}{P_1 P_2}$$

A similar triad $\Im'$ can be constructed for determining the rotation of P_3 around o_2. There are two possible positions for the location of P_3. X axis can be taken in the direction of $O_2 P_3$ and θ_2 is rotation angle about the Z axis of the triad.

$$\Im' = [k \times \underset{\sim}{P_1 P_2} \quad \underset{\sim}{P_1 P_2} \times (k \times \underset{\sim}{P_1 P_2}) \quad \underset{\sim}{P_1 P_2}] \qquad \text{(C.12)}$$

After fitting a triad for the rotation, P_3 could be found from the following equations:

$$\underset{\sim}{p_3}' = \underset{\sim}{o_2} + \Im'[r_2 \cos \theta_2 \quad r_2 \sin \theta_2 \quad 0]^T$$

$$\underset{\sim}{p_3}' - \underset{\sim}{b_3} = \underset{\sim}{S_3} \qquad \text{(C.13)}$$

$$|\underset{\sim}{p_3}' - \underset{\sim}{b_3}| = S_3^2$$

which gives the leg length S_3. However, θ_2 is an unknown that can be obtained from the orthogonality of the rotation matrix $\Im'$

$$\Im'^2_{11} + \Im'^2_{12} + \Im'^2_{13} = 1$$

$$\Im'^2_{12} + \Im'^2_{22} + \Im'^2_{32} = 1 \qquad \text{(C.14)}$$

$$\Im'_{11} \Im'_{12} + \Im'_{21} \Im'_{22} + \Im'_{31} \Im'_{32} = 0$$

where

$$(o_{2x} - b_{3x})^2 + (o_{2y} - b_{3y})^2 + o_{2z}{}^2 + r_2{}^2 - S_3{}^2$$
$$+ 2r_2[\Im'_{11}(o_{2x} - b_{3x}) + \Im'_{21}(o_{2y} - b_{3y}) + \Im'_{31} o_{2z}]\cos\theta_2 \qquad \text{(C.15)}$$
$$+ 2r_2[\Im'_{12}(o_{2x} - b_{3x}) + \Im'_{22}(o_{2y} - b_{3y}) + \Im'_{32} o_{2z}]\sin\theta_2 = 0$$

Using trigonometric equations

$$\cos\theta_2 = \frac{1 - \tan^2(\theta_2/2)}{1 + \tan^2(\theta_2/2)} \quad \text{and} \quad \sin\theta_2 = \frac{2\tan(\theta_2/2)}{1 + \tan^2(\theta_2/2)} \qquad \text{(C.16)}$$

a univariate quadratic equation is obtained

$$C_1 \tan^2(\theta_2/2) + C_2 \tan(\theta_2/2) + C_3 = 0 \qquad \text{(C.17)}$$

with the coefficients:

$$C_1 = [(o_{2x} - b_{3x})^2 + (o_{2y} - b_{3y})^2 + o_{2z}{}^2 + r_2{}^2 - S_3{}^2]$$
$$\quad - 2r_2[\Im'_{11}(o_{2x} - b_{3x}) + \Im'_{21}(o_{2y} - b_{3y}) + \Im'_{31} o_{2z}]$$
$$C_2 = 4r_2[\Im'_{12}(o_{2x} - b_{3x}) + \Im'_{22}(o_{2y} - b_{3y}) + \Im'_{32} o_{2z}] \qquad \text{(C.18)}$$
$$C_3 = [(o_{2x} - b_{3x})^2 + (o_{2y} - b_{3y})^2 + o_{2z}{}^2 + r_2{}^2 - S_3{}^2]$$
$$\quad + 2r_2[\Im'_{11}(o_{2x} - b_{3x}) + \Im'_{21}(o_{2y} - b_{3y}) + \Im'_{31} o_{2z}]$$

There are two roots for the solution of this quadratic equation. Therefore, both solutions for the position of P$_3$ should be considered. During iterative steps, in the case of complex roots, current set of the given values will be eliminated and the algorithm will start with new values of d_{1x}, d_{1y}, θ_1.

Once the third platform point is found, the platform is fully determined. From these points, the transformations between base frame and platform frame can be determined as follows

$$\underset{\sim}{p_i}{}' = \underset{\sim}{t} + \Re \underset{\sim}{p_i} \qquad \text{(C.19)}$$

Let $\Re$ rotation matrix maps the matrix V to the matrix W. In order to find these V and W frames, $\underset{\sim}{p_1}$ and $\underset{\sim}{p_1}'$ can be taken as origins; $(\underset{\sim}{p_2} - \underset{\sim}{p_1})$ and $(\underset{\sim}{p_2}' - \underset{\sim}{p_1}')$ as X axes; perpendicular to $(\underset{\sim}{p_2} - \underset{\sim}{p_1})$, $(\underset{\sim}{p_3} - \underset{\sim}{p_1})$ and to $(\underset{\sim}{p_2}' - \underset{\sim}{p_1}')$, $(\underset{\sim}{p_3}' - \underset{\sim}{p_1}')$ as Z axes respectively.

$$V = [\underset{\sim}{p_2} - \underset{\sim}{p_1} \quad ((\underset{\sim}{p_2} - \underset{\sim}{p_1}) \times (\underset{\sim}{p_3} - \underset{\sim}{p_1})) \times (\underset{\sim}{p_2} - \underset{\sim}{p_1}) \quad (\underset{\sim}{p_2} - \underset{\sim}{p_1}) \times (\underset{\sim}{p_3} - \underset{\sim}{p_1})]$$
$$W = [\underset{\sim}{p_2}' - \underset{\sim}{p_1}' \quad ((\underset{\sim}{p_2}' - \underset{\sim}{p_1}') \times (\underset{\sim}{p_3}' - \underset{\sim}{p_1}')) \times (\underset{\sim}{p_2}' - \underset{\sim}{p_1}') \quad (\underset{\sim}{p_2}' - \underset{\sim}{p_1}') \times (\underset{\sim}{p_3}' - \underset{\sim}{p_1}')] \qquad \text{(C.20)}$$

$$W = \Re V$$
$$\Re = W V^{-1} = W V^{T}$$
(C.21)

$$\underset{\sim}{t} = \underset{\sim}{p_1}' - \Re \underset{\sim}{p_1}$$
(C.22)

After the rotation and translation matrices are found, the remaining platform points could be obtained and the error between the given and obtained leg lengths could be calculated:

$$\underset{\sim}{E} = \begin{bmatrix} dS_4 \\ dS_5 \\ dS_6 \end{bmatrix} = \begin{bmatrix} S_4' - S_4 \\ S_5' - S_5 \\ S_6' - S_6 \end{bmatrix}$$
(C.23)

$$E = |\underset{\sim}{E}|$$
(C.24)

The norm of the error is used as a feedback to find the number of positions in allowed tolerance. After some sets of d_{1x} and d_{1y} are offered to the algorithm, a number of predictions are chosen within a predetermined tolerance. In order to find all the solutions, in the ranges of d_{1x}, d_{1y}, θ_1, a three dimensional scan is executed. Although the absolute range for d_{1x} and d_{1y} is -1 to 1 and 0 to 2π for θ_1, it is not possible in the real case due to physical constraints. Therefore some validity checks are needed to continue the search.

One of the validity checks is to eliminate the mirror images about the base plane because the assembly configurations of the Stewart Platform occur in pairs over and below the base plate. Therefore, negative signed direction cosines along the Z axis are pre-eliminated for economizing the computation.

The other check is introduced to see whether the distances satisfy the closure requirements for the triangles $P_2 P_i B_i$:

$$P_2 B_i \leq P_2 B_i + B_i P_i \text{ and } P_2 B_i \geq |P_2 B_i - B_i P|$$
(C.25)

for $i = 1, 3, 4, 5, 6$

If the conditions do not satisfy the closure, the corresponding set is rejected before the error estimation.

REFERENCES

[1]   D. Stewart. *A Platform with Six Degrees of Freedom*. Proceedings of the Institute of Mechanical Engineering. Vol. 180, Part 1, No. 5, pp. 371-386, 1965

[2]   http://www.parallemic.org/Reviews/Review007.html

[3]   B. Dasgupta, T.S. Mruthyunjaya. *The Stewart Platform manipulator: a review*. Mechanism and Machine Theory 35 (2000) 15-40, December 1998

[4]   K.H. Hunt. *Structural kinematics of in-parallel-actuated robot-arms*. ASME J. Mech., Trans. Automat. Des., vol. 105, pp. 705–712, 1983

[5]   http://www.mathworks.com/products/simmechanics

[6]   N. Smith and J. Wendlandt. *Creating a Stewart Platform Model Using SimMechanic*s. The MathWorks - MATLAB Digest, Volume 10, Number 5, September 2002

[7]   M. Griffis and J. Duffy. *A forward displacement analysis of a class of Stewart Platforms*. J. Robot. Sys., 6(6), pp. 703-720, 1989

[8]   W. Lin, M. Griffis and J. Duffy. *Forward displacement analysis of the 4-4 Stewart Platform*. ASME J. of Mechanical Design, 114(3):444-450, September 1992

[9]   W. Lin, C.D. Crane and J. Duffy. *Closed-Form Forward Displacement Analysis of the 4-5 In-Parallel Platforms*. Trans. of the ASME, Journal of Mechanical Design, Vol. 116, pp. 47-53, 1994

[10]   C. Innocenti and V. Parenti-Castelli. *Direct position analysis of the Stewart Platform mechanism*. Mechanism and Machine Theory, 25(6):611-621, 1990

[11]   P. Nauna, K.J. Waldron and V. Murthy. *Direct kinematic solution of a Stewart Platform*. IEEE. Trans. Robotics Automat. 6 (4), 438-444, 1990

[12]   V. Murthy and K. J. Waldron. *Position kinematics of the generalized lobster arm and its series-parallel duality. ASME J. of Mechanical Design*, 114(3):406-413, September 1992

[13]   J. P. Merlet. *Direct kinematics and assembly modes of parallel manipulators*. Int. J. of Robotics Research, 11(2):150-162, 1992

[14]   N. X. Chen and S. M. Song. *Direct position analysis of the 4-6 Stewart Platform*. ASME J. of Mechanical Design, 116(1):61-66, 1994

[15]   Q. Liao, L. D. Seneviratne and S.W.E. Earles. *Forward kinematic analysis for the general 4-6 Stewart Platform*. Intelligent Robots and Systems, IROS '93. Proc. of the IEEE/RSJ International Conference, Volume 3, pp. 1659-1665, July 1993

[16] C. Innocenti. *Direct kinematics in analytical form of the 6-4 fully parallel mechanism*. ASME J. of Mechanical Design, 117(1):89-95, 1995

[17] C. Innocenti and V. Parenti-Castelli. *Analytical form solution of the direct kinematics of a 4-4 fully in-parallel actuated six-degree-of-freedom mechanism*. Ninth CISM-IFToMM Symposium on Theory and Practice of Robots and Manipulators, Udine, Italy, Sept. 1-4, 1992

[18] C. Innocenti and V. Parenti-Castelli. *Closed-form direct position analysis of a 5-5 parallel mechanism*. ASME J. of Mechanical Design, 115(3), 515-521, 1994

[19] C. Innocenti and V. Parenti-Castelli. *Echelon form solution of direct kinematics for the general fully-parallel spherical wrist*. Mechanism and Machine Theory, 28(4):553-561, 1993

[20] M. Husain and K.J. Waldron. *Direct position kinematics of the 3-1-1-1 Stewart Platform*. ASME J. of Mechanical Design, 116(4):1102-1108, 1994

[21] C-D. Zhang and S.M. Song. *Forward kinematics of a class of parallel (Stewart) platforms with closed-form solutions*. IEEE Int. Conf. on Robotics and Automation, pp. 2676-2681, Sacramento, 1991

[22] W. Guozhen. *Forward displacement analysis of a class of the 6-6 Stewart Platforms*. ASME DE v 45, Robotics, Spatial Mechanisms and Mechanical Systems, pp. 113-117, Scottsdale, 1992

[23] S. V. Sreenivasan, K.J. Waldron and P. Nanua. *Closed-form direct displacement analysis of a 6-6 Stewart Platform*. Mechanism and Machine Theory, 29(6):855-864, 1994

[24] R. Nair and J. H. Maddocks. *On the Forward Kinematics of Parallel Manipulators*. Int. J. Robotics Res. 13(2): 171-188, 1994

[25] J.C. Faugere and D. Lazard. *The combinatorial classes of parallel manipulators*. Mechanism and Machine Theory, 30(6):765-776, August 1995

[26] C.C. Nguyen, Z.L. Zhou, S.S. Antrazi and C.E. Campbell Jr. *Efficient Computation of Forward Kinematics and Jacobian Matrix of a Stewart Platform-Based Manipulator*. Proc., IEEE Southeastcon '91, Williamsburg, Virginia, pp. 869-874, April 1991

[27] L.C. T. Wang and C.C. Chen. *On the numerical kinematic analysis of general parallel robotic manipulators*. IEEE Trans. on Robotics and Automation, 9(3):272-285, 1993

[28] C. Innocenti and V. Parenti-Castelli. *A New Kinematic Model for the Closure Equations of the Generalized Stewart Platform Mechanism*. Meccanica, 26, pp. 247–252, 1991

[29] C. Innocenti and V. Parenti-Castelli. *A Novel Numerical Approach to the Closure of the 6-6 Stewart Platform Mechanism*. ICAR'91, Fifth International Conference on Advanced Robotics, June 19–22, 1991, Pisa, Italy, pp. 851–855, 1991

[30] M. Ait-Ahmed and M. Renaud. *Polynomial representation of the forward kinematics of a 6 d.o.f. parallel manipulator*. Int. Symp. on intelligent robotics, 1993

[31] C. Innocenti and V. Parenti-Castelli. *Forward Kinematics of the General 6-6 Fully Parallel Mechanism: An Exhaustive Numerical Approach Via a Mono-Dimensional Search Algorithm*. ASME J. Mech. Des., 115, pp. 932–937, 1993

[32] B. Dasgupta and T.S Mruthyunjaya. *A Constructive Predictor-Corrector Algorithm for the Direct Kinematics Problem for a General 6-6 Stewart Platform*. Mech. Mach. Theory 31(6), 799-811 (1996)

[33] M. Raghavan. *The Stewart Platform of General Geometry has 40 Configurations*. ASME J. Mech. Des., 115, pp. 277–282, 1993

[34] A. Morgan. *Solving Polynomial Systems using Continuation for Engineering and Scientific Problems*. Prentice-Hall, Inc. (1987)

[35] S.V. Srinivasan and P. Nanua. *Solution of the direct position kinematics problem of the general Stewart Platform using advanced polynomial continuation*. 22nd Biennial Mechanisms Conf., pages 99-106, Scottsdale, 1992

[36] A. Dhingra, D. Kohli and Y.X. Xu. *Direct kinematic of general Stewart Platforms*. 22nd Biennial Mechanisms Conf., pp. 107-112, Scottsdale, 1992

[37] C. de Zang and S.M. Song. *Forward Position Analysis of Nearly General Stewart Platforms*. ASME J. Mech. Des., 116, pp. 54–60, 1994

[38] B. Dasgupta and T.S Mruthyunjaya. *A Canonical Formulation of the Direct Position Kinematics Problem for a General 6-6 Stewart Platform*. Mechanism and Machine Theory, Vol. 29, No. 6, 819-827, 1994

[39] F. Wen and C. Liang. *Displacement Analysis of the 6-6 Stewart Platform Mechanisms*. Mechanism and Machine Theory, Vol. 29, No. 4, pp. 547-557, 1994

[40] K. Hunt and E. J. F. Primrose. *Assembly configurations of some in-parallel actuated manipulators*. Mechanism and Machine Theory, 28(1):31-42, 1993

[41] C.W. Wampler. *Forward Displacement Analysis of General Six-In-Parallel SPS (Stewart) Platform Manipulators Using Soma Coordinates*. Mech. Mach. Theory, 31, No. 3, pp. 331–337, 1996

[42] M. L Husty. *An Algorithm for Solving the Direct Kinematics of the Stewart-Gough Platforms*. Mech. Mach. Theory, 31, No. 4, pp. 365-380, 1996

[43] L. Baron and J. Angeles. *The Decoupling of the Direct Kinematics of Parallel Manipulators Using Redundant Sensors*. Proc. IEEE Int. Robotics and Automation Conf., May 8–13, San Diego, CA, pp. 974–979, 1994

[44] L. Baron and J. Angeles. *The measurement subspaces of parallel manipulators under sensor redundancy*. ASME Design Automation Conf., pp. 467-474, Minneapolis, 11-14, 1994

[45] L. Baron and J. Angeles. *The isotropic decoupling of the direct kinematic of parallel manipulators under sensor redundancy*. IEEE Int. Conf. on Robotics and Automation, pp. 1541-1546, Nagoya, 25-27, 1995

[46] Z. Geng and L. Haynes. *Neural network for the forward kinematics problem of a Stewart Platform*. IEEE Int. Conf. on Robotics and Automation, pp. 2650-2655, Sacramento, 11-14, 1991

[47] L.W. Tsai. *Solving the inverse dynamics of a Stewart–Gough manipulator by the principle of virtual work*. J. Mech. Design (122):3-9, 2000

[48] B. Dasgupta, and T.S. Mruthyunjaya. *A Newton–Euler formulation for the inverse dynamics of the Stewart Platform manipulator*. Mech. Mach. Theory, 33(8):1135-1152, 1998

[49] C.C. Nguyen and F.J. Pooran. *Dynamic analysis of a 6 DOF CKCM robot end-effector for dual-arm telerobot systems*. Robot. Autom. Syst., 5, 377-394, 1989

[50] G. Lebret, K. Liu, and F.L. Lewis. *Dynamic analysis and control of a Stewart Platform manipulator*. J. Robot. Syst., 10(5):629-655, 1993

[51] J.D. Lee and Z. Geng. *A dynamic model of a flexible Stewart Platform*. Comput. Struct., 48(3):367-374, 1993

[52] J. Gallardo, J.M. Rico, D. Checcacci, and M. Bergamasco. *Dynamics of parallel manipulators by means of screw theory*. Mech. Mach. Theory, 38(11):1113-1131, 2003

[53] J.G. Wang and C.M. Gosselin. *A new approach for the dynamic analysis of parallel manipulators*. Multibody Syst. Dyn., 2, 317-334, 1998

[54] S.H. Koekebakker, P.C. Teerhuis, A.J.J. Van der Weiden. *Alternative parameterization in modelling and analysis of a Stewart Platform*. Sel. Topics Ident. Model. Contr., 9, 59–68, 1996

[55] M.J. Liu, C.X. Li and C.N. Li. *Dynamics analysis of the Gough-Stewart Platform manipulator*. IEEE Trans. Robot. Autom., 16(1):94-98, 2000

[56] L. Meirovitch. *Methods of analytical dynamics*. McGraw Hill, New York, 1970

[57] Z.M. Ji. *Dynamics decomposition for Stewart Platforms*. J. Mech. Design, 116, 67-69, 1994

[58] H.B. Guo and H.R. Li. *Dynamic analysis and simulation of a six degree of freedom Stewart Platform manipulator*. Proc. IMechE Vol. 220 Part C: J. Mechanical Engineering Science

[59] L. L. Howell. *Compliant Mechanisms*. New York: Wiley, 2001

[60] S. T. Smith. *Flexures: Elements of Elastic Mechanisms*. New York: Gordon and Breach, 2000

[61] H.K. Byoung, T.W. John, G. D. Nicholas and J.G. Jason. *Analysis and Design of Parallel Mechanisms With Flexure Joints*. IEEE Transactions on Robotics, vol 21, no 6, April 2004

[62] W. Dong, Z. Du, L. Sun. *Conceptional design and kinematics modeling of a wide-range flexure hinge-based parallel manipulator*. IEEE Int. Conf. on Robotics and Automation, pp. 4042-4047, Barcelona, 2005

[63] G.M. Chen, J-Y. Jia, and Z-W. Li. *On Hybrid Flexure Hinges*. IEEE Transactions on Robotics, July 2005

[64]   J.M. Paros and L. Weisbord. *How to design flexure hinges*. Mech. Des. vol. 3*7*, pp. 151-156, Nov. 1965

[65]   T. Smith, V.G. Badami, J.S. Dale, and Y. Xu. *Elliptical flexure hinges*. Rev. Sci. Instrum. vol. 68. pp. 1474-1483, March 1997

[66]   N. Lobontiu, J.S.N. Paine, E. Garcia, M. Goldfarb. *Comer-filleted flexure hinges*. ASME Trans. J. Mech. Des., vol. 123, pp. 346-352, Sept. 2001

[67]   N. Lobontiy I.S.N. Paine, E. O'Malley, M. Samuelson. *Parabolic and hyperbolic flexure hinges: flexibility, motion precision and stress characterization based on compliance closed-form equations*. Precis. Eng, vol. 26, 183-192, 2002

[68]   N. Lobontiu , E. Garcia. *Two-axis flexure hinges with axially-collocated and symmetric notches*. Sibley School of Mechanical and Aerospace Engineering, Cornell University, 258 Upson Hall, Ithaca, NY14850, USA, January 2003

[69]   N. Lobontiu , J. S.N. Paine , E. Garcia ,M. Goldfarb. *Design of symmetric conic-section flexure hinges based on closed-form compliance equations*. Mechanism and Machine Theory, 37, pp. 477-498, 2002

[70]   F.C. Park and J.W. Kim. *Singularity Analysis of Closed Kinematic Chains*. Trans. ASME J. Mech. Des., 121:32-38, March 1999

[71]   K.H. Hunt. *Kinematic Geometry of Mechanisms*. Oxford, Great Britain : Oxford University Press, 1978

[72]   E.F. Fitcher. *A Stewart Platform-Based Manipulator: General Theory and Practical Construction*. Int. J. of Robotics Research, Vol5 No 2 pp 157-182, 1986

[73]   J.P. Merlet. *Singular Configurations of Parallel Manipulators and Grassmann Geometry*. Technical Report No 791, INRIA, France, 1988

[74]   D. Kim and W. Chung. *Analytic Singularity Equation and Analysis of Six-DOF Parallel Manipulators Using Local Structurization Method*. IEEE Transactions on Robotics and Automation, Vol. 15, No. 4, August 1999.

[75]   J. Sefrioui and C.M. Gosselin. *Singularity analysis and representation of planar parallel manipulators*. Robot. Autom. Syst., vol. 10, pp.209-224, 1993

[76]   B. Mayer St-Onge, and C.M. Gosselin, "Singularity Analysis and Representation of Spatial six-DOF Parallel Manipulators", Recent Advances in Robot Kinematics, Kluwer Academic Publishers, pp. 389-398, 1996

[77]   C.M. Gosselin and J. Angeles. *Singularity analysis of Closed-loop Kinematic Chains*. IEEE Trans. Robot. Automat., vol. 6, pp. 281-290, June 1990.

[78]   O. Ma and J. Angeles. *Architecture singularities of platform manipulators*. IEEE Int. Conf. Robot. Automat., pp. 1542-1547, 1991

[79]   Y.X. Su, C.H. Zheng and B.Y. Duan. *Singularity Analysis of a 6 DOF Stewart Platform Using Genetic Algorithm*. Systems, Man and Cybernetics, 2002 IEEE International Conference, vol. 7, 6-9, 2002

[80]   D.C.H. Yang and T.W. Lee. *Feasibility Study of a Platform Type of Robotic Manipulators from a Kinematic Viewpoint*. Journal of Mechanisms, Transmissions, and Automation in Design, 106(2):191-198, 1984

[81]   L., Zoran. *Feasibility of a Stewart Platform with Fixed Actuators as a Platform for CABG Surgery Device*. Master Thesis, Department of Bioengineering, Columbia University, 1997

[82]   http://www.3dconnexion.com/products/3a3.php

[83]   http://www.physikinstrumente.com/en/products/prdetail.php?VID=icShBZg06iPvHY4V &sortnr=703300

[84]   http://www.comsol.com/

[85]   http://www.tpub.com/math2/18.htm

[86]   http://en.wikipedia.org/wiki/Tensile_strength

[87]   http://www.roymech.co.uk/Useful_Tables/Matter/Titanium.html

[88]   V. I. Utkin. *Variable Structure Systems with Sliding-Modes*. IEEE Transactions on Automatic Control, vol. 22, no. 2, pp. 212-222, 1977

[89]   S. V. Drakunov, V. Utkin. *A Semigroup Approach to Discrete-Time Sliding Modes*. Proceedings of the American Control Conference, June 1995

[90]   Y-F. Li. *High Precision Motion Control Based on a Discrete-time Sliding Mode Approach*. Doctoral Thesis, Royal Institute of Technology, Sweden, Dec. 2001

[91]   K. Abidi. *Sliding-Mode Control for High-Precision Motion Control Systems*. Master Thesis, Department of Engineering and Natural Sciences, Mechatronics Program, Sabanci University, 2004

[92]   V. I. Utkin. *Sliding mode control in discrete-time and difference systems*. Variable Structure and Lyapunov Control, Alan S.I. Zinober (Ed.) Springer-Verlag London Limited, pp. 87-107, 1994

[93]   http://www.dspaceinc.com/ww/en/inc/home/products/hw/modular_hardware_introductio n/processor_boards/ds1005.cfm

[94]   E. Deniz. *Haptic Device for Micro Parts Handling*. Master Thesis, Department of Engineering and Natural Sciences, Mechatronics Program, Sabanci University, 2006

[95]   http://www.renishaw.com/client/product/UKEnglish/PRD-3.shtml